Predicting the printability of concrete structures

The influence of temperature on the mechanical properties of fresh concrete and numerical modelling of the 3D printing process

M. Schuur

Movares
adviseurs & ingenieurs

TU Delft Delft University of Technology

bruil®

Predicting the printability of concrete structures

The influence of temperature on the mechanical properties of fresh concrete and numerical modelling of the 3D printing process

By

M. Schuur

To obtain the degree of Master of Science
at the Delft University of Technology
to be defended publicly on Friday January 10, 2020 at 16:00.

Student number:	4299019
Project duration:	November 2018 – January 2020
Thesis committee:	Prof. Dr. ir. E. Schlangen, TU Delft, supervisor
	Dr. ir. M. Hendriks, TU Delft
	Dr. ir. H.R. Schipper, TU Delft
	Dr. ir. H. Stuit, Movares
	T. Voogd, Bruil

This thesis is confidential and cannot be made public until January 10, 2023.

TU Delft Delft University of Technology

Preface

This thesis marks the end of my graduation project on 3D printing of concrete structures. It is the final part of the master Civil Engineering, track Structural Engineering at the TU Delft.

This project was part of a fruitful collaboration between engineering firm Movares and concrete manufacturer Bruil. I would like to express my gratitude to both companies to provide me the opportunity to graduate on such an innovative topic. The resources that were at my disposal throughout the project have been of tremendous value for this thesis.

I would like to thank Theo Voogd for his trust in letting me conduct the extensive material research at the printing facility of Bruil. The ability to conduct research on such a large scale has given me the opportunity to develop new skills and gain a unique experience with concrete printing. I would especially like to thank the people that helped me prepare and conduct the experiments and the fruitful discussions on concrete printing: Elise Buiter, Stephano Sabandar, Eric Barendse, Robert Huitema, Benno van Dijk and Joost Mink. It has been a long two weeks of testing, printing and not to forget: demolishing. It was worth it.

Additionally, it would like to thank the people of the Dynamics department of Movares that helped me with scripting and processing the large amounts of data. A special thanks to Olivier Louis, who guided me throughout the project and Herke Stuit for his critical eye and feedback during the project.

I would like to thank my supervisors from the TU Delft, Erik Schlangen, Roel Schipper and Max Hendriks for their feedback during the meetings and their support throughout the project.

Finally, I would like to thank my friends and family that have supported me throughout the course of my studies and making my time at the TU Delft very joyful.

M. Schuur
De Meern, January 2019

Summary

3D concrete printing provides the engineering and construction industry with new possibilities to create complex-shaped geometries without the need of labour-intensive formwork. Currently, the cement and concrete industry has a large environmental impact and is considered conservative in the adoption of novel techniques. With 3D concrete printing the sustainability of the industry can be improved by reducing material usage. The decreased material usage and the possibility to create complex shapes at no extra cost can make 3D concrete printing a technology that can both compete with the traditional concrete manufacturing industry as well as enhance it with new possibilities in automated design and manufacturing.

In this thesis a parametric finite element model has been developed to predict the printability of concrete structures of arbitrary geometries. The model can be used to effectively explore design and process parameters to optimize printed objects. In addition, the model can be used to improve the reliability of the printing process, reduce the number of failures during production and enhance the production capabilities of complex geometries.

A state-of-the-art literature review has been conducted to explore the properties of printed concrete in both its fresh state, and their influence on the hardened state. Experimental procedures to determine the mechanical properties of fresh concrete and numerical methods to analyse the printing process have been studied. Based on the results of the literature review it was concluded that in order to build finite element models that can successfully simulate the printing process at Bruil, the material properties of the fresh concrete used in their printing process had to be fully characterised.

Before conducting the experimental programme, finite element models had been developed in ANSYS to analyse the stability and deformational behaviour of prints during the printing process. A parametric APDL script was built to incorporate the evolution of material properties during printing. The models were compared to literature and proved to be able to produce similar results as found in literature. Hence, they were deemed suitable to predict the printability of arbitrary geometries.

A comprehensive experimental programme was designed in which uniaxial compression tests have been performed to determine the development of the mechanical properties of the concrete during the printing process. A novel method was created by which test samples could be extracted directly from printed concrete in order to incorporate the influence of the full printing process on the properties of the concrete. Moreover, from both literature and the valuable experience in printing of Bruil it was known that the temperature of the concrete mix can have a major influence on the mechanical properties of concrete. Therefore, the performance of the concrete under elevated temperatures was included in the research too. On top of that, printing experiments were conducted in which two geometries were printed multiple times to characterize the reliability of the printing process, and to verify the finite element models with.

The uniaxial compression tests showed that the mechanical properties of the concrete used in the printing process of Bruil evolve exponentially over a period of three hours. When the concrete is stored at a temperature of 35°C before testing, the mechanical properties severely enhanced. After 90 minutes, the concrete at stored at 35°C was able to reach strengths three times as high as similar concrete stored at room temperature. However, mechanical properties of concrete at room temperature and heated concrete of ages under 45 minutes can be considered equal.

Large variations are observed between the measurements of the mechanical properties at different ages. Similar variations in printing of objects were observed too, as prints that remained stable on one day could collapse on other days, even though they had been printed at the same speed and otherwise similar parameters. Importantly, a relation between the measurements of the uniaxial compression test and the printed objects was found as relatively many prints collapsed on days at which mechanical properties of samples were measured to be relatively low.

The developed numerical models were then used to simulate the prints printed during the experiment with the material properties obtained from the uniaxial compression tests. The models were able to

accurately describe the behaviour of prints during printing. Predictions of collapsing of prints showed good correspondence with the experimental results. To improve the reliability of the printing process it is proposed to adopt lower bound material properties in modelling. By adopting lower bound material properties in the model, safe predictions of printability can be made that lead to a decrease in failure rate and an improved production process.

The research has contributed to the better understanding of the influence of temperature on the development of mechanical properties of concrete during printing. By extracting samples directly from printed concrete, the influence of the total printing process on the mechanical properties of the concrete over time was captured. By the knowledge of the writer this method of extracting samples has not been used before. It has been shown that the mechanical properties are influenced by the printing process itself. Concrete that was extracted from the printer after it had already been running for several hours generally has a higher uniaxial compressive strength and Young's modulus than concrete that is extracted at the start of a printing session. Until now, these effects had not been quantified. Also, a direct relation between mechanical properties derived from uniaxial compression tests and objects printed at the same time had not yet been presented in literature.

Contents

1 Introduction

In the western society the demand for a more sustainable built environment is growing. In most EU member countries, the highest demand for resources is from construction projects. 82.7% of all waste produced by economic activities in the EU is generated by construction activities [1]. Moreover, focussing on specifically the concrete industry, the production of cement is responsible for 8% of the global CO_2 emissions [2]. At the same time, cement is expected to play a vital role in the expansion of the built environment, especially in emerging economies. Rapid urbanization and economic development in regions such as Southeast Asia and sub-Saharan Africa will increase demand for new buildings, and thus for concrete and cement.

To accommodate the increasing demand in a sustainable way, the concrete construction industry has to reduce the use of cement. The use of novel cement types, such as geopolymers, can reduce emissions up to 90% [3]. Concrete demand and consumption can be reduced as well by taking new design approaches, increasing the share of concrete that is reused and recycled, and by improving production techniques and material efficiency.

Additive manufacturing of concrete structures, often referred to as 3D concrete printing (3DCP), can especially accommodate the latter by providing a solution for the material efficiency of concrete structures. 3DCP creates the possibility to only apply material where it is required. Solid and massive structures are no longer needed and the demand for concrete, and coherently cement, can be drastically reduced. Combining the use of novel cement types with 3DCP technology can potentially steer the concrete construction industry to a net-zero CO_2 emission industry.

The construction industry has traditionally relied on 2D drawings to convey material properties, performance details and location information. Developments in digital design, structural optimization, additive manufacturing and robotics have introduced new processing routes for the industry, increasing the possibilities to construct iconic buildings dominated by curved surfaces, complex geometries and minimized material usage. The application in practice is however limited due to limitations of traditional production techniques.

A major cost associated with concrete construction is the formwork. This was demonstrated by cost estimates for construction of a concrete wall in a multi-storey building in the Central Business District of Sidney. Here, formwork contributed to approximately 80% of the total costs [4]. Considerable savings can potentially be made by eliminating the use of formwork. However, the costs of advanced robotic manufacturing and development of printable concretes can be significant.

Moreover, creating shapes with complex geometries, such as double curved surfaces, require custom made moulds. These products are often ‘one-offs’, meaning that after production the moulds are useless and considered waste. As formwork is not needed in 3DCP, construction waste can be greatly reduced and decrease the ecological footprint of the concrete industry. Besides that, as high costs for bespoke formwork disappear, complex organic shapes and curved geometries become accessible to a larger part of the building industry and geometrical freedom for architects is increased.

1.1 Printing technology

Different 3DCP technologies have been developed in recent years. These technologies are either extrusion-based or powder-based. The most widely adopted 3DCP technique is based on extrusion and Bruil, the collaborating partner in this thesis, also uses a printing process based on extrusion. Powder-based techniques will therefore not be discussed.

Extrusion-based 3DCP is the process of extruding a continuous filament, pumped through a nozzle which is mounted to a gantry or robotic arm that places the material on the desired position during the printing process. Figure 1 shows a typical setup for extrusion-based 3D printing with a robotic arm. Although the basic principles of extrusion based 3DCP are the same, different strategies to produce concrete elements with 3DCP are being adopted by the industry.

Extrusion-based printing is sometimes used to build a vertical formwork and is also referred to as Contour Crafting (CC). Once the extruded formwork is completed, concrete is manually poured to fill the mould. Structurally the formwork can be considered as a loss. As CC still uses formwork and creates solid objects it does not contribute to the reduction of materials in the concrete industry. It does however contribute to the practical use of 3DCP. Formwork can be easily created by printing without skilled labour and integral components such as reinforcement, pipes and ducts can be easily installed.

To fully realize the potential of 3DCP, manufacturers as Bruil aim for the creation of complex geometries without the use of temporary or permanent formwork. Although the used technique is similar to CC, the approach is fundamentally different. Structurally optimized objects are being created in which the printed geometry is the final product. To create such objects, ultra-high-performance concrete (UHPC) has to be used to provide excellent structural performance both during printing as well as in the final stage. This approach to 3DCP will be subject of study in this thesis.

The aforementioned approaches are mostly limited to off-site printing as it has to be done in a controlled environment and focussed on separate building elements. It is worth mentioning that also on-site printing methods are being developed based on extrusion. CONPrint3D is currently being developed at the TU Dresden in Germany which intends to bring concrete printing directly into building sites. It focuses on large scale applications such as printing entire houses.

1.2 Recent projects

Over the last years an exponential growth in the applications of 3DCP have been observed. Many academic and industrial parties have successfully realised full-scale structures. Limitations in the current codes of practice to evaluate their structural integrity have however resulted in most of these structures not being guaranteed as safe for public use. Accordingly, they are deemed as test prototypes for display purpose only. A couple of projects that demonstrate the viability of concrete printing and its potential as a new processing route for builders, engineers and architects will be highlighted here.

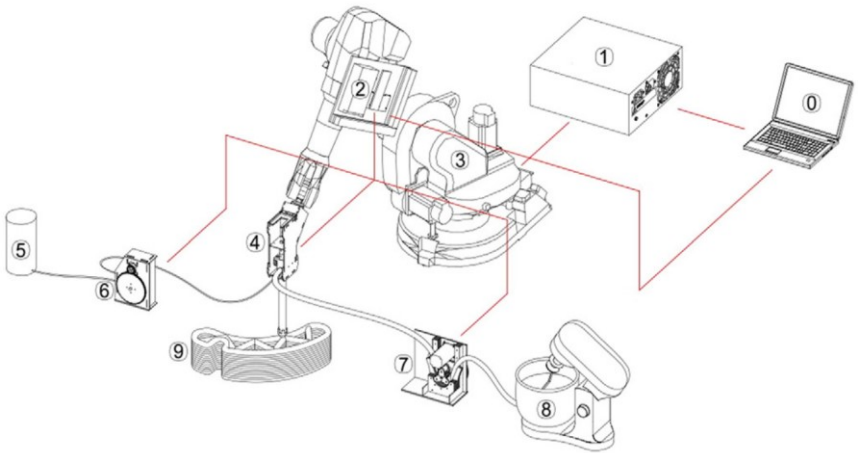

Figure 1: typical 3D printing setup: 0) System command; 1) Robot controller; 2) Printing controller; 3) Robotic arm; 4) Printhead; 5) Accelerating agent; 6) Pump for accelerating agent; 7) Pump for premix; 8) Premix mixer; 9) 3D printed object [44].

1.2.1 Bicycle bridge

In 2017, in the village Gemert in the Netherlands the first structural application of 3DCP certified as safe for public use was realised with the print facility of the Eindhoven University of Technology [5]. A bicycle bridge was constructed based on the concept of 'Design by Testing' as codes to test the structural properties of printed concrete do not exist.

The bridge has a span of 6.5 m and a width of 3.5 m and crosses a small local canal. To benefit from the printer and optimise the cross-section of the bridge, the bridge was printed in multiple elements that had to be assembled. After printing the segments, they were rotated by 90° and pressed together by post-tensioned prestressing tendons. The prestressing tendons were placed in the openings of the cross-section, stressed and anchored at concrete blocks at the beginning and end of the bridge. The elements where stressed to a level that only compression remains in the section, meaning that no additional passive reinforcement was required. The uncertainty regarding the tensile strength of the interfaces of the filaments was therefore made irrelevant too.

Reinforcement cables that may act as stirrups were embedded in the printing process. Their presence was however not accounted for in determining the shear resistance of the bridge as their performance had not been established. Instead, the shear strength of the concrete was derived from the tensile and compression strength, based on a Mohr-Coulomb failure criterion.

During design of the bridge, 1:2 scale test were adopted to determine the structural properties and load capacity of the bridge. Finally, a full-scale test was performed in situ to guarantee the bridge to be structurally safe. The process of printing, in situ testing and final use are shown in Figure 2.

Figure 2: From left to right: printing of an element of the bridge, full scale test before final use, finished bridge. Reproduced from [5].

1.2.2 Water taxi stop

A 3D printed water taxi stop is to be realised in Rotterdam in the Netherlands by the Dutch company Bruil in collaboration with Movares, Studio RAP and the municipality of Rotterdam (see Figure 3). As a result of the complex shape and surface, the design would be very expensive to cast in concrete as it would require complex formwork. The design of the cantilevering water taxi stop therefore aims to push the limits of the printing technology to its limits [6]. The main shape is based on a hypar-shell that has the properties of a ruled surface, which makes it possible to apply straight steel prestressing cables in a double curved object. In this way the shape is both structurally as aesthetically integrated into the object.

As printing of an object with such a cantilever is impossible due to limitations of the material the water taxi stop had to be produced by an assembly of different elements, similar to the bicycle bridge mentioned previously (see the right picture in Figure 3). Although the water taxi stop was printed in several segments, the elements put the 3D printer of Bruil seriously to the test. Due to the slenderness and cantilevering of the segments the prints were prone to failure during the printing process. Multiple iterations were necessary to print the desired geometries.

Moreover, the project demonstrates that the design, engineering and manufacturing of 3D printed objects is an integrated approach and requires adaptation of all parties to a new design process. Methods of production, specific printer specifications, shape, architecture and mechanics are all closely related.

At the moment research into the constructability is still on-going.

Figure 3: Left: render of the water taxi stop. Right: printed segments.

1.2.3 Other projects

Other interesting projects, showing the potential use of 3DCP have been conducted. At the moment new project are presented on a regular basis. Some noteworthy projects showing the variable use of concrete printing will be listed below and are shown in Figure 4:

- Single storey office building in Dubai, UAE, measuring 250 m^2, constructed in 2016 by the Chinese company WinSun. Due to the applied surface finishing the layered structure, characteristic for 3D printing, is not visible anymore and therefore the building does not appear to be printed. For more details reference is made to [7].
- XtreeE printed a complex truss-shaped pillar supporting a roof. The pillar was created by printing formwork in several segments and pouring of concrete. After hardening, some of the formwork could be removed as it was considered a temporary support. The rest of the structure was smoothly finished by covering of the line pattern with a coating [8].
- Costanzi et al. demonstrated the possibility of 3D printing on a temporary freeform surface by creating a partially printed and partially cast shell structure. This work was achieved by combining the Flexible Mould technology developed at TU Delft and the 3DCP at the TU Eindhoven [9].

Figure 4: Several projects completed with the by 3DCP. From left to right: Office building in Dubai by Winsun [7], truss-shaped pillar in France by XtreeE [8] , freeform shell structure by TU Delft and TU Eindhoven [9].

2

Research design

While the advantages of 3DCP are clear, its application in practice can still be considered limited. Although many new project initiatives are being undertaken, until now only few serious applications have been demonstrated as was shown in the previous section. As the relations between the printed objects, printable material and printing strategy are not well known, 3DCP manufacturing processes are currently inconsistent and unreliable. Reinforcement principles, material compositions and assembly strategies will have to be reinvented to comply with the new process requirements of 3D printing.

The robustness of 3DCP is essential to the commercial viability of the technology. As the conformity to the design geometry is what gives the printed shape its value, this thesis focusses on the printing phase. Research into material properties, shape instability and process parameters will be conducted. If 3DCP is to become common practice in the construction industry, deep understanding is needed on how to design structures that are manufactured from printed materials.

This thesis will be a partial follow-up on the work of Joost Mink. His work is an exploration into predicting the stability of 3D-printed structures. Material characterization and mechanical modelling have been the main focus of his research. Partly based on his findings and recommendations a new research plan has been devised.

2.1 Objectives

Understanding the relationship between all aspects involved in the 3DCP process is essential to allow full control of the technology and utilize its potential to revolutionize the building industry. Even more so when high quality applications, where Bruil and Movares aim for, are considered. These high standards can only be obtained when the influence of each process parameter is known.

At Bruil, the printability of an object is currently mainly determined by trial-and-error: an object is printed several times with different printing speeds, layer heights or slight geometrical changes. Based on experience of the operators those changes are applied and tested until a successful print is realized. Another issue the operators encountered in printing was the unreliability and repeatability of successful prints. Sometimes when an object was successfully printed, meaning without collapse or significant deformations, this could not be repeated.

The repeatability of successful prints and the reliability of the printing process is a key aspect of successfully adopting 3DCP techniques. A method to analyse a print geometry in terms of printability and conformity to end-product requirements and expectations beforehand is therefore a must-have for a manufacturer as Bruil. To perform such analyses, models need to be developed that can accurately simulate the printing process of any object. These models have to take into account the time dependent mechanical properties of the print material, while also considering the speed of material deposition and geometric built-up over time.

The main goal of this thesis is to create a numerical model which can accurately analyse any geometry for printability. This includes an analysis of the failure mechanisms and deformations occurring during printing. A sub-goal is to generate an optimized printing protocol directly from the requirements of the end product: Ideally, an object is imported into the model and is subsequently analysed and optimised for printing with the optimised geometry and/or printing strategy (e.g.: print speed) as output.

The main research objective of the thesis is:

To create a model that can accurately predict the printability of any geometry, specifically tailored to the process requirements of the printing facility of Bruil and the design process at Movares.

The following sub-objective is to be achieved:

To optimize an object for 3D printing without compromising the intended geometry and provide optimal parameters as input for the printing process.

2.2 Methodology

A preliminary literature study into the state-of-the-art of concrete printing was performed to map out the major barriers encountered in 3D printing of concrete and design an efficient research approach and strategy. The approach is described here.

It has been proven that the mechanical behaviour of straight 3D printed walls can be analysed by means of an analytical model [10]. However, this analytical model is solely intended for the analysis of straight walled structures. As 3D printing offers the possibility to produce any possible geometry, it's likely that it will mainly be utilized for the creation of complex and curved geometries. Less complex geometries are expected to remain in the domain of the conventional prefab industry. Therefore, for practical applications the developed analytical model is limited in its use and an approach applicable to any desired geometry will be developed.

To accomplish the main objective of this thesis, a combination of computer programming and existing analyses tools will be adopted. Finite element modelling (FEM) will be used, as it was demonstrated by Wolfs et al. [11] that satisfactory results can be achieved. The FEM programme should be capable of: a) Implementing time dependent material parameters; b) Geometrical and physical non-linear analysis; c) Implementation of geometrical imperfections; d) Modelling layered deposition of concrete filaments over time.

To achieve the sub-objective an iterative process has to be arranged in which an initial geometry is analysed for printability. The output of the process must be either optimized printing parameters (e.g.: building rate and material output) or an improved geometry, that does not compromise the intended initial geometry, including optimized printing parameters.

To verify the model, printing experiments will be executed at the printing facility of Bruil. At the moment of writing this research methodology, Joost Mink has not yet finished his thesis. The accuracy of the FE model is largely dependent on the accuracy of the obtained material properties in his work. Verification of the model might therefore prove to be difficult or even impossible. This can have two implications for the research. Firstly, the intended goal of the research, to *accurately* predict the printability of any geometry, and be able to find the limits of what is printable at Bruil will have to be let go. A model will be created that can be used as soon as material parameters are known. Or secondly, material research has to be conducted to find the mechanical properties of the material used at Bruil. A major downside would be that organizing an experimental programme and analysing the forthcoming data is time consuming. Within the considered timeframe of this thesis that means that it might affect the quality of the numerical model and some aspects of implementing optimization strategies might not be explored.

To further explore the critical aspects of 3DCP an extensive literature study will be conducted in which both the requirements of the fresh- and final stage of the printed concrete, as well as the printing process itself, will be mapped out. From this study conclusions will be drawn on how to proceed to achieve the main objective of this thesis.

3

State of the art

Despite the advantages, 3D-printing technology is still in its infancy and requires more fundamental research. If the technology is to become common construction practice, designers and engineers will need to understand how to design structures to be manufactured with printed materials, leading to new design codes and standardised methods of testing. The state of the art of research into the properties of fresh concrete, hardened concrete and methods to predict the printability are presented here. Additionally, first-hand experience with 3D printing at Bruil and the research performed by Joost Mink is described.

3.1 Fresh state concrete

In ordinary production processes of concrete elements concrete is poured into formwork. Under the effect of gravity, the concrete adopts the shape of the mould and forms the final structural element. The role of formwork is however not only limited to imposing the shape of the concrete elements. It also protects the concrete from drying in its early age before being removed once the material has set. The absence of a mould poses different requirement to the fresh concrete used in 3DCP. The consequences on the requirements of the fresh concrete properties will be discussed below.

3.1.1 Rheology

Printable materials can be compared to visco-plastic Bingham materials. Only when submitted to shear stresses higher than its yield stress, the material will flow. As it flows, the material displays a viscous behaviour and the shear rate is proportional to the stress in excess of the yield stress through a constant that is termed the plastic viscosity [12]. However, materials used for 3DCP are only flowing through the relatively short pumping and mixing phases of the process after which they must be at rest. Therefore, their elasto-plastic behaviour can be considered more important than their visco-plastic behaviour as this determines whether the material can retain its shape during a printing process.

The ability of these materials to build up an internal structure at rest (referred to as thixotropy) is a key feature for printing applications. When the material exits the nozzle of the printer it has an initial yield stress, an initial critical strain and an initial elastic modulus. With rest the yield stress and elastic modulus increase over time, but the yield/critical strain decreases with time at rest [11]. Therefore, the material does not only become stronger, but also more rigid as it has a higher elastic modulus. The speed of which the yield stress and elastic modulus increase was determined to be linear by Wolfs et al. [11]. Lecompte and Perrot [13] observed an exponential relationship between resting time and yield stress.

When looking at a microstructural level, cementitious materials have the ability to form flocs and to nucleate early hydrates between cement grains in the flocculated structure formed by the cement grains [14]. This allows the cementitious material to display a yield stress and build up a structure at rest. Figure 5 schematically shows this process: (a) cement particles are dispersed at the end of the mixing phase; (b) within a few seconds, cement particles form flocs and form a network of interacting particles (darker particles) that are able to resist stress and develop an elastic modulus; (c) At the same time, at the pseudo contact points between particles within the network, nucleation of CSH occurs (black and white dots) even though the material is still in its dormant period. This nucleation locally changes the weak colloidal interactions between cement particles into the stronger CSH bridges. Consequently, the strength and elastic modulus increases. After several tens of seconds, a percolation path of particles

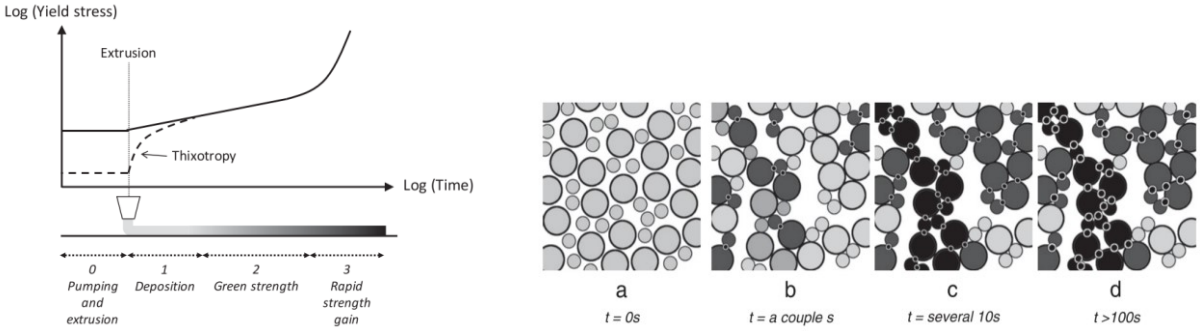

Figure 5: Left: Evolution of static yield stress over time (log-scale). A part of stage 0 and 1 is represented by a solid and a dashed line, where the solid line represents a system without thixotropy [15]*. Right: Build-up of strength and elasticity on a microscopic level during the dormant period.*

interacting purely through CSH bridges appears (black particles); (d) An increase in the size and numbers of CSH bridges between the cement particles lead to a further development of the elastic modulus and yield stress.

During the phases described above, in which hydration reactions are considered slow, the resulting percolation is still reversible as long as the mixing power can break the CSH bridges [14]. However, after the so-called induction period, an onset of massive precipitation of CSH occurs, which leads to the general setting and hardening of the cement [15].

3.1.2 Assessment of mechanical properties of fresh concrete

As a print progresses and grows in height, stresses on the bottom layer increase due to gravitational loads of the above layers. Consequently, these gravity-induced stresses could lead to yielding and print failure when the yield stress of the bottom layer is reached before the print has been finished [16]. Failure of a print might also be driven by a loss of stability. This instability failure mechanism is mainly driven by the geometry of the print and its stiffness (elastic modulus) [10]. Moreover, the stresses induced due to the layering of filaments give rise to strains in the material. Although the stress may stay below the yield stress, the cumulative amount of strains in all layers could influence the final geometry of the print. When a print has not collapsed, but instead shows large deformations it must still be considered a failed print as it does not comply with the intended geometry.

Considering the above, characterization of parameters influencing the early-age mechanical behaviour of printed concrete is crucial to correctly modelling the printing process and avoid premature failure. The robustness of the 3DCP process depends on the consistency of these properties. Materials used for 3DCP typically have a high yield stress and viscosity, therefore traditional methods, as rotational or oscillatory rheometry, for measuring properties as plastic viscosity, yield stress and thixotropy can be problematic [17].

To measure the development of mechanical properties of fresh concrete, such as yield stress and elastic modulus, several methods exist. Various empirical tests to measure the hardening and setting behaviour of cementitious material such as the Vicat test [18] or the shear vane test [19] . However, these methods do not directly measure the mechanical properties of the material. They can only give a measure of the rate of structuration, which can be used in comparisons of different materials.

Experiments on determining mechanical properties of fresh concrete by means of uniaxial compression have been conducted in [16] and [20]. However, both adopted a purely strength-based failure criterion. A sample was loaded by load increments (equal to the weight of a layer) at arbitrary time steps until failure was observed by either the formation of cracks, or an increment in the displacement rate. From such experiments can only be determined what the critical vertical building rate is for a particular printing material, but not whether it buckles or deforms.

Wolfs et al. [11] noticed that during their printing experiments print failure was often initiated by a loss of stability, and not by failure of the bottom layer due too high stresses from gravity loading. The same has been observed by Bruil during many printing sessions. Besides that, the critical layer may not even have to be the one with the highest loading (the bottom layer) as sometimes stresses may occur not

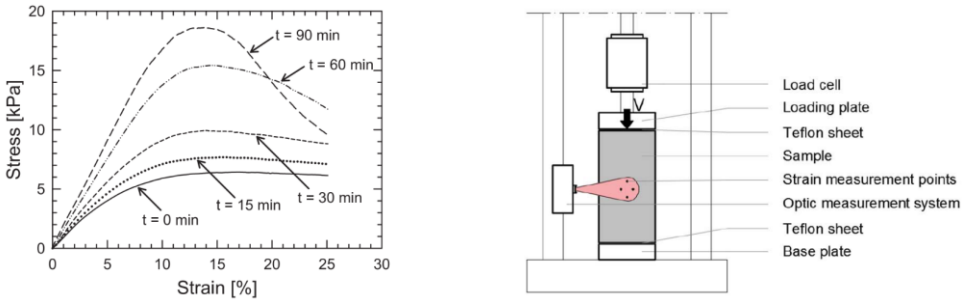

Figure 6: Left: stress-strain relationships determined by uniaxial compression tests at different moments in time after extracting samples from the printsetup. Right: test setup used for the uniaxial compression test by Wolfs et al. Figures reproduced from [11].

exclusively in the vertical direction; some manufacturers fill the printed structure with a secondary material, leading to horizontal loads. Moreover, printed layers may be not be stacked exactly on top of each other due to imperfections or vibrations in the printing process or on purpose when printing cantilevering objects. Considering the aforementioned, an analytical strength-based approach is not sufficient to determine failure during printing. Summarizing, both the mechanical and three-dimensional geometry of the print over time should be taken into account in order to assess the printability of an object.

3.1.2.1 Uniaxial compression test and direct shear test

To measure the time dependent mechanical properties of printed concrete Wolfs et al. [11] conducted uniaxial compression tests. A cylindrical sample is placed inside a test rig which axially loads the sample either based on displacement or on force. With a displacement controlled uniaxial compression test the compressive failure-deformation behaviour can be recorded at different moments in time (see Figure 6). From these stress-strain relationships the Young's modulus and the compressive strength can be determined, as well as the post-peak behaviour of the print material.

In the same study a Mohr-Coulomb yield criterion was adopted as the mechanical behaviour of fresh concrete was deemed similar to that of soils. To determine the cohesion and the angle of internal friction, direct shear tests were performed on cylindrical samples. In a direct shear test a sample is placed between two plates, of which the bottom plate is fixed and the top plate is moveable. A load is placed on top of the samples and the top plate is moved so that a shear force is applied to the sample. This test is repeated with different loads applied to the top so that the Mohr-Coulomb failure plane can be reconstructed, and the cohesion and friction angle can be determined. This procedure can be repeated at different ages of the concrete to determine the relationship of internal friction angle and cohesion with respect to time. Figure 7 shows typical test results of a direct shear test on fresh concrete of different ages and the test setup used in the experiment. By plotting the peak shear stresses against the applied normal force, the Mohr-Coulomb failure plane can be reconstructed.

3.1.2.2 Triaxial compression test

With a triaxial compression test the cohesion, angle of internal friction and the stress-strain behaviour of a material can be determined in a single test. Triaxial compression tests are common practice in evaluating the behaviour of soils and rock-like material, such as clay and concrete. A cylindrical sample

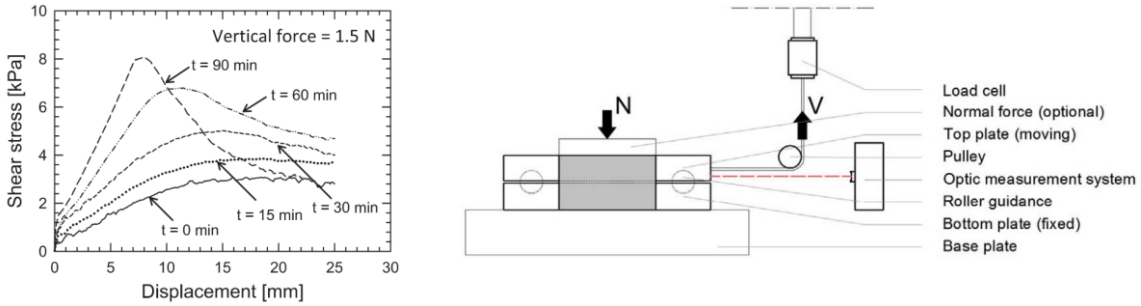

Figure 7: Left: test results form a direct shear test on concrete of different ages with a vertical load of 1.5 N. Right: schematic overview of a test setup of the direct shear test used by Wolfs et al. Figures reproduced from [11].

is placed in a test rig with a pressurized chamber (with water or air) and a vertical force is exerted on it until failure. By applying different lateral pressures, the Mohr-Coulomb failure plane can be reconstructed and with that the cohesion and angle of internal friction can be determined. According to literature triaxial compression tests have not yet been performed on early age concrete.[1]

3.1.2.3 Oscillatory measurements

Wolfs et al. [21] investigated the correlation between destructive compression tests and non-destructive ultrasonic measurements on early age 3D printed concrete. A major advantage of such a non-destructive test is that it allows for the in-print monitoring of the development of material properties to ensure that expected properties are achieved. However, material parameters cannot directly be measured with this technique, therefore destructive tests still have to be performed and correlations have to be established. In the study the results of the ultrasonic tests were compared with uniaxial compression tests performed in an earlier study [11] and a linear relationship was found between pulse velocity, strength and stiffness.

3.1.2.4 Influence of temperature

Golaszewski and Szwabowski [22] and Huang et al. [23] have investigated the temperature dependence of structural build-up of cement pastes. Both found that an increase in mixing temperature can lead to an increase in yield stress. Cement hydration kinetics and the change of colloidal flocculation degree caused by increased temperatures were appointed as the main source of change in rheological properties. Huang et al. [23] found that the initial static yield stress and the increase of static yield stress over time of samples at 40°C can be 3 to 5 time as high as samples mixed at 20°C, depending on the type of cement paste.

Hermens [24] has performed uniaxial compression tests on heated concrete that is used for 3D printing at the Eindhoven University of Technology. An increase in both elastic modulus and compressive strength was observed for heated samples. Samples were cured under warm conditions and tested at ages of 30 and 75 minutes. Samples tested at an age of 30 min. had a temperature of 32°C and samples at an age of 75 min. had a temperature of 45°C. An increase of 30% in the average compressive strength of heated samples was observed at an age of 30 min. compared to unheated samples (22°C). However, due to significant scatter in the obtained results it could not be concluded that the elevated temperatures indeed increase the compressive strength at this age. The average compressive strength of heated samples at an age of 75 min. was found to be 3 times larger compared to unheated samples. Although again a significant scatter in results was obtained, it could be concluded that the compressive strength was increased due to a higher curing temperature.

3.1.3 Printing process parameters

Mortars used for 3DCP must be able to sustain their own weight and the weight of the added layers with little to no deformation after extrusion. Next to that, properties as pumpability, extrudability and buildability are used to describe the material properties of 3DCP mix designs.

The ease with which the concrete mix is transported from the pump to the nozzle is defined as the pumpability of the material. A problem that can occur is segregation of the particles in the hose which can lead to jamming of the hose.

The term open time is often used in 3DCP and is related to the operation window in which a specified volume of material must be extruded. It is associated with the preservation of viscosity and yield stress of the mix. Outside the operation window pumpability and extrudability of a specific batch will be poor and the printing process must be stopped. Printing of an object must therefore occur within the operation window. To overcome this issue some manufacturers, use a continuous ‘micro-batching’ process or even mixing at the nozzle of the printer.

The shape of the extrusion nozzle varies for each printer. However, the majority are either round or rectangular. Extrudability is defined as the ability to extrude the mix through a nozzle without

[1] At the moment this thesis had been finished a research paper by Wolfs et al. [42] was published showing the potential of triaxial compression tests on determining the mechanical properties of early-aged concrete for 3D printing.

considerable cross-sectional deformations and with an acceptable degree of tearing/splitting of the filament (see Figure 8). Both structurally and aesthetically, tearing and splitting of layers in a print is unacceptable as these defects are detrimental to the value of a print.

As the height of a print increases, so does the weight, causing compression of the deposited layers. As it is common practice to maintain a constant layer height throughout the print, the distance between the nozzle and the printing surface increases. This effect becomes more pronounced as the print gets higher eventually causing the filament to 'snake' as it is extruded, leading to incorrect deposition of the material and eventually causing collapse. To overcome this issue two approaches exist: dynamic control of the nozzle height during printing [25] or speeding up the hardening of layers by addition of accelerators, such they are capable of maintaining the increasing load with the minimum amount of strain. [16].

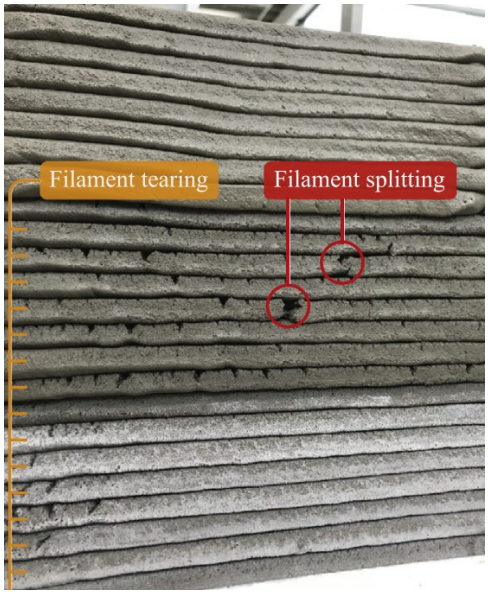

Figure 8: Concrete filament splitting and tearing in a printed wall (from [17]*).*

The length of a layer and the speed at which the material can be deposited by the robot are important factors that have an effect on both the time to lay a single layer and the production time of an object. The time it takes to deposit a single layer is referred to as the layer cycle time. The layer cycle time influences structural build-up time, and thereby the rate of loading of the layers. As it also determines the total printing time it determines the material properties (strength and stiffness) each layer has during printing of an object. Furthermore, the layer cycle time may influence the interlayer adhesion [26].

3.2 Hardened state concrete

The specifically adjusted material compositions as well as the characteristics of the various fabrication processes have a considerable impact on the hardened state properties of 3DCP structures. Accordingly, the performance of printed objects is not to be compared to ordinary concrete structures. Regarding the materials used in 3DCP common deviations to ordinary concrete are: low water-to-cement ratios (or alternative binders), viscosity modifiers, the use of small aggregates (<2 mm) and the use of chemical admixtures as accelerators and retarders [27]. Research into the hardened properties of printed concrete can be divided into the following topics: anisotropy and interlayer adhesion, tensile reinforcement, shrinkage and durability

3.2.1 Anisotropy and interlayer adhesion

Printed concrete can be as strong as cast concrete. Compressive strengths of 75 - 102 MPa are reported by [28]. However, the stacking of layers of extruded concrete filament exposes printed objects to anisotropy which influences performance of the end product. Both the tensile and compressive strength were found to be directionally dependent.

Currently there is no consistent format describing the printing process parameters to conduct a test programme to asses structural performance. Printing variables such as layer height, filament dimensions, nozzle size and print speed, size of the component from which a sample is taken, and layer cycle times are not consistent throughout experimental research and therefore difficult to compare. Discrepancies in reporting process parameters and variability in testing geometry emphasize the need for standardized test methods [17], [26], [27].

Interfaces are not uncommon for concrete structures and are influenced by many factors. However, in ordinary structures these interfaces usually occur between a layer that has already hardened and a fresh layer. In concrete printing the interface exists between two fresh layers of concrete [27]. Existing design codes are therefore not applicable to the interfaces in 3DCP.

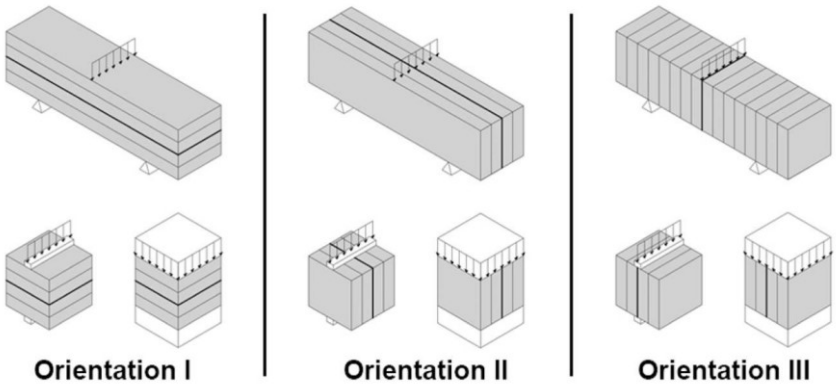

Figure 9: Directionally dependent mechanical testing on 3D printed concrete [26].

Le et al. [28] investigated the tensile strength of the interlayers and found a decreasing strength with increasing interval times. It was also found that an interval time of up to 15 min. did not influence the interlayer adhesion and the bonding strength was greater than the tensile capacity of the material. Wolfs et al. [26] also studied the effect of several process parameters on the bond strength of 3D printed concrete. Here it was also found that as the layer interval time increased, the bond strength decreased. It was found that for layer intervals of 1h and 4h there was only a minor drop in strength of the bond when test specimen were covered by a plastic sheet for the duration of the time gap between the layers to prevent surface dehydration. A reduction of 21% was observed for covered specimen with an interval time of 24 h. Uncovered specimen showed a reduction of up to 51% after 4 hours. It can be concluded that dehydration has a prominent effect on the tensile strength of the interface between filaments with longer interlayer interval times.

In [29] it is suggested that the pressing of layers may have a positive effect on the interlayer adhesion. The pressure generated in the layers improves compaction.

3.2.2 Reinforcement

The material concrete in itself shows brittle behaviour. Its structural performance is defined by a low tensile strength compared to its compressive strength and a low tensile strain compared to its fracture strain. Therefore, reinforcement is added to concrete to obtain save and ductile structural behaviour. Uncertainties in predicting the quality of the interlayer adhesion make the application of reinforcement even more important in 3DCP [27].

In many applications printed components will have to be able to withstand tensile stresses induced by different load situations. Moreover, during lifting and installation even higher stresses may occur and govern the design of certain components. If 3DCP is to become a competitive alternative for standard construction methods, printed objects will have to be able to resist significant tensile stresses beyond the capacity of the mortar itself. Hence, the incorporation of reinforcement is necessary.

The most basic approach is to use the printed concrete as formwork, in which reinforcement bars can be placed and can then be filled with concrete [30]. Figure 10 shows two images in which this technique is applied by the company WinSun. XtreeE has adopted a similar approach to construct a complex shaped column filled with ultra-high performance fibre reinforced concrete [8].

Figure 10: Left and middle: Concrete moulds by WinSun [30], [17]. *Right: External reinforcement* [31].

Asprone et al. [31] suggested an approach that consists of the partition of a member into different printed segments. These segments were then assembled into one component with an external steel reinforcement system (see the right picture of Figure 10).

Prestressing or post-tensioning can also be applied to avoid tensile stresses. Several projects have already shown the successful application of this strategy. A bicycle bridge was successfully constructed in Gemert, The Netherlands showing its potential at full scale [5]. Bruil, Movares and RAP [6] have demonstrated the possibility of topology optimization of a print by adopting post tensioning in the design of a water taxi stop. Both of these projects have in common that the structures were created from different segments, which were then assembled and held together by posttensioning.

Research at the TU Eindhoven [32] introduced a technology to directly entrain reinforcement into the filaments. The steel cables introduced into the printed layers significantly improved post-cracking deformations and strength. Detailed aspects of the bonding of the cable need further study. Reinforcement may however be needed perpendicular to the direction of the printed layers, which is not possible using this method.

Another strategy is to avoid the need for tensile reinforcement at all by designing structures that are under compression in every load situation. This however limits the applicability of printed structures considerably.

3.2.2.1 Fibres

Embedding continuous, discrete reinforcement into printed object proves to be complicated. Therefore, to enhance the tensile strength and ductility of the printed concrete, glass, steel, PP or PVA fibres are often added to concrete printing mix designs. Cementitious composites have been developed that exhibit strain hardening behaviour. Matrix composition, fibre performance, and matrix-to-fibre bond determine the performance of these materials and are also known as Engineered Cementitious Composites (ECCs) or Strain Hardening Cementitious Composites (SHCCs). Structural performance is increased as high tensile strength, strain, significant plastic deformations and smeared crack development can be achieved [33]. In addition to enhanced structural properties, the properties of the material exposed to fire conditions is also increased as the fibres reduce the effect of spalling of the concrete [34].

Development of mix-designs for 3DCP is different from that of castable concretes. The design of a SHCC in 3DCP is not only restricted to the hardened state, but also has to meet requirements for extrudability and buildability. Fibres must be able to pass through various parts of the system such as the pump, hose and nozzle without excessive pressure, while also having adequate strength and stiffness after extrusion to avoid geometrical deformations or premature failure during printing. On the other side, a material that is too stiff may lead to clogging and blocking of the apparatus. When the requirements for printability and buildability have been met the material may be considered printable.

A strong fibre orientation in the direction of extrusion has been observed by several researchers. A significant increase in tensile strength and strain hardening behaviour is found this direction [12], [35]. Perpendicular to the printed layers this effect has been found to be much less.

3.2.3 Shrinkage and durability

Savings in time, costs and materials are advantages associated with building without formworks. However, it also implies significant materials engineering challenges as all the requirements are now directly imposed on the concrete that are normally fulfilled by the formwork [15]. Objects produced with 3DCP often have a greater exposed surface area than cast objects. Combined with the low water-to-cement ratios of the mortars (typically used in 3DCP processes), cracking resulting from shrinkage is likely to occur [17]. Greater care must therefore be taken while curing to minimise dimensional changes due to drying and shrinkage of the concrete. In conventional construction the problem treated by shrinkage reducing admixtures, moist curing and internal curing methods.

Long term effects of printed concrete have not received as much attention as process parameters, printability and structural performance have. Several authors have however pointed out that the use of aggressive chemicals, such as retarders and accelerators, can have negative effects on the concrete and in particular the durability of reinforcement. Studies into the effect of the processes on the printed

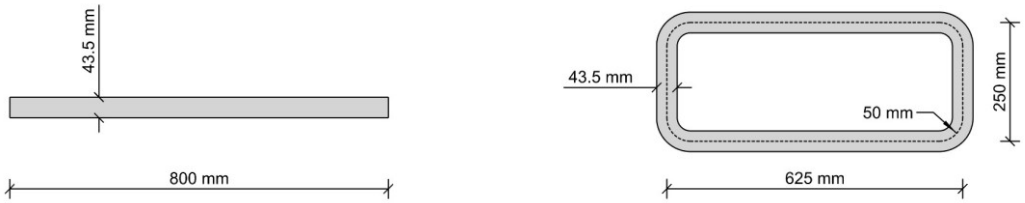

Figure 11: Dimensions of a free wall and a rectangular wall structure printed at the printing facility of TU Eindhoven at a speed of 9.6 s and 21.0 s per layer, respectively. The layer height is 9.2 mm. Reproduced from [10].

mortar itself have shown that the interlayer interval time is an important factor. Not only does it influence the bond strength, it also leads to an increased porosity, increased capillary water ingress and higher chloride penetration levels [27].

3.3 Prediction of print failures

Attempts have been made to predict the failure of structures during printing. Two failure modes are distinguished: plastic collapse and elastic buckling. Plastic collapse is characterised by a layer (generally the bottom) reaching the yield stress of the material and elastic buckling by a loss of stability, while the material still behaves linear elastic. Models that consider both phenomena are discussed in this paragraph.

3.3.1 Analytical model

A mechanical model for predicting the structural performance of straight wall structures in a 3D printing process was presented by Suiker [10]. The developed model provides analytical expressions to calculate the critical length of a 3D printed free wall, simply-supported wall or a fully clamped wall, by considering elastic buckling and plastic collapse. It contains the most relevant process parameters such as printing velocity, curing characteristics (either linear or exponentially decaying), geometrical features, imperfections and non-uniform deadweight loading.

In order to verify the developed model a free wall and a rectangular tube have been printed and compared to predictions of the analytical model. These prints and their dimensions are given in Figure 11. Both prints have a layer height of 9.2 mm and are printed at a speed of 9.6 s and 21.0 s per layer, respectively. Wolfs et al. [11] have determined the development of the Young's modulus and the compressive strength over time of the printing material used at TU Eindhoven by uniaxial compression tests. These properties have been used to predict the critical height of the two prints. The development of the mechanical properties is given by Eqs. (1) and (2). The density of the concrete is 2020 kg/m^3.

$$E(t) = 0.0781 + 0.0012\,t \quad with\ E\ in\ MPa\ and\ t\ in\ min. \tag{1}$$

$$\sigma_p(t) = 5.984 + 0.147\,t \quad with\ \sigma_p\ in\ kPa\ and\ t\ in\ min. \tag{2}$$

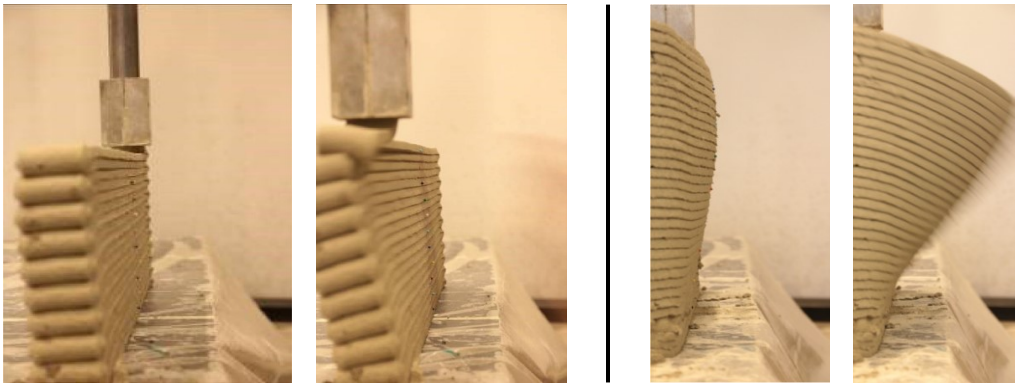

a) 20 layers *b) 22 layers* *c) 33 layers* *d) 33 layers*

Figure 12: Results of the printing experiment performed in [10]. Showing both prints just before buckling and during buckling. Images reproduced from [10].

Suiker predicted that failure of the structures is initiated by elastic buckling, rather than plastic collapse. Failure of the free wall was predicted to occur at 20 layers and failure of the rectangular tube was predicted to happen at 30 layers. In the experiment the walls failed at a height of 22 layers and 33 layers, respectively.

By comparing printing experiments with the results from the developed mechanical model it was shown that the model is accurate and may be used for predictions of elastic buckling or plastic collapse of straight wall structures. Also, the model may be used as a validation tool for FEM simulations of the printing process. Furthermore, it may be used to efficiently explore the influence of the process parameters on the failure resistance of wall structures.

3.3.2 Finite Element Modelling

Wolfs et al. [11] have built a Finite Element Model (FEM) of the printing process of a cylinder using the results of the uniaxial compression and shear box tests. A cylinder with a heart line radius of 250 mm, a thickness of 40 mm and a layer height of 10 mm was modelled in Abaqus. A printing speed of 5000 mm/min was applied leading to a layer interval time of 0.31 minutes. Layers were added stepwise on top of each other during the analysis in which both the evolution of strength and stiffness of each layer are accounted for in the model. Axisymmetric linear 4-noded elements were applied. All layers consisted of 40 by 10 elements in width and height, respectively. A geometrical and material non-linear analysis was performed to take the influence of large deformations and plasticity into account. No initial imperfections have been applied as it is assumed the failure-deformation mode is initiated by the restrained lateral expansion at the support. Results of the model are shown in Figure 13.

By means of a printing experiment the FEM simulations were validated. The same cylinder as used in the numerical model was printed using the same dimensions and printing speed. Images of the experiment are shown in Figure 14. Comparisons between the numerical model and the printing experiment qualitatively show good correspondence as the failure-deformation was similar. However, the printed cylinders collapsed in an earlier stage than predicted and deform more than predicted by the model. An average deviation of 27.5% on the predicted buckling height was obtained between the FEM simulations and printing experiment. Simulations predicted failure at 40 layers using a lower bound solution (meaning the average properties were multiplied by a factor 0.825), whereas the average number of layers that could be printed in the experiment was 29.

Two main reasons were addressed for the difference between the numerical model and the printing experiments. One of them being geometrical imperfections (which were not taken into account in the model) as the critical buckling load of a shell with imperfections can be several times lower than according to classical theory. Secondly, the difference is attributed to the material properties derived from the uniaxial compression test and the shear box test. Samples were compacted before testing, but the actual printed concrete is not. Compacting may lead to significantly improved material properties and may have therefore resulted in an overestimation of the performance of the print.

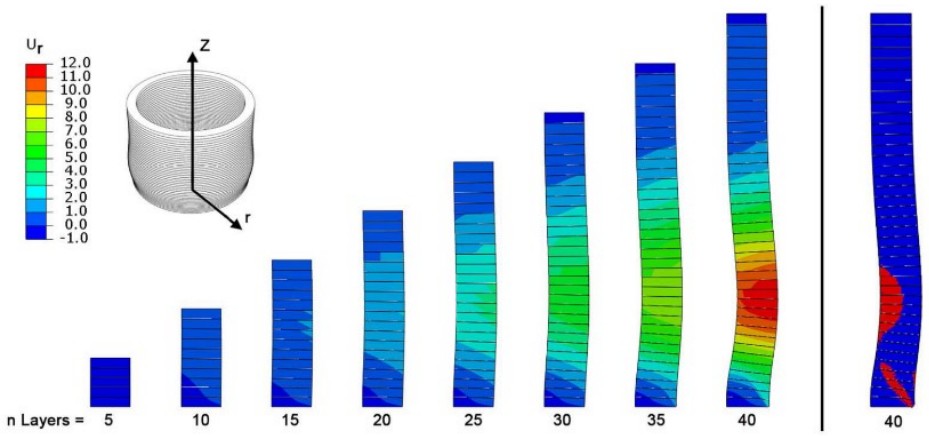

Figure 13: Numerical results of the axisymmetric modelled cylinder with average material properties multiplied by a factor 0.825. The plotted colours represent the radial deformations. On the right the red colour indicates where the yield stress is reached, and plastic deformation occurs. Reproduced from [11].

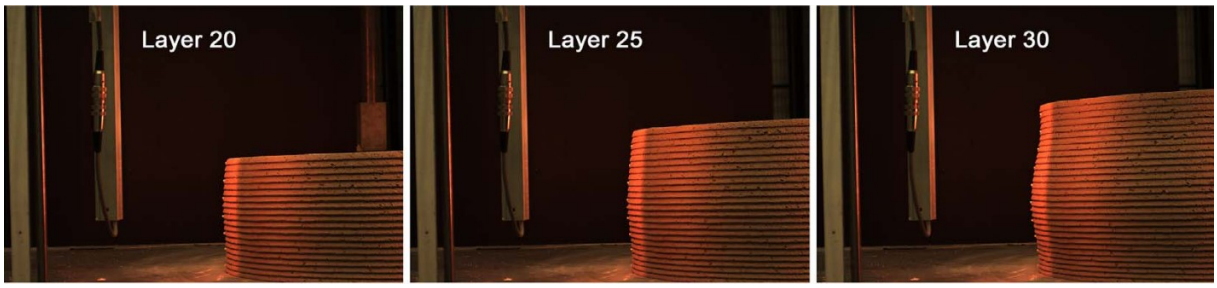

Figure 14: Deformed shape of a cylinder during printing. Reproduced from [11].

3.4 Experience Bruil

A visit to the printing laboratory of Bruil offered a huge insight into the capabilities of their printing setup. Several successful and unsuccessful prints were shown (see Figure 15). This clearly showed the capabilities of the printing process Bruil is using. However, the 'U-shaped' wall depicted in the middle of Figure 15 also shows the issues some of the prints are dealing with, such as local buckling or distortion. The curved cylinder and the balustrade both show the capabilities of Bruil to create rather large curvatures in the vertical plane of the object, demonstrating their ability to create complex freeform structures.

By talking with the operatives of the printer many practicalities in 3D printing were observed and noted. Preparation of the concrete mix used for printing by applying the right amount of water and duration of mixing is essential for a successful printing session. When asked about failure mechanisms, the operatives responded that plastic failure of prints almost never happened, and that failure of prints were predominantly caused by instability of the object.

Moreover, as I joined a printing session the influence of temperature on the stability of a print was experienced first-hand. The printing lab is a semi-controlled environment where the weather can have a major influence on the success of printing. As it had been freezing overnight and the system hadn't been running for some days, the temperature of the dry mix, water, environment and the system had dropped. A cylinder that was successfully printed before was printed again, however it lost its stability already after reaching a height of approximately 0.5 m, whereas it would normally reach a height of over a meter.

A day later I again joined in on a printing session. The water and dry mix were stored in a warm environment overnight and the same cylinder was printed again using the same speed. This time there was no problem and the print remained stable throughout the whole session. Upon measuring the temperature of several other prints during printing (which can have a duration of 3 hours) temperatures of 35°C and higher were measured, while the temperature of concrete entering the hose was about 25°C.

Although this is an extreme case with a large temperature difference, it demonstrates the effect of the temperature. Moreover, by talking to the operatives of the printer, it was noted that the phenomenon of collapsing on one day and successfully printing similar prints on the other has happened more often. Even when there were no large differences in the printing environment such as temperature and

Figure 15: Several prints produced by Bruil. Left: full size mock-up-up of a balustrade of a balcony for the renovation of an apartment building in Den Helder. Middle: unsuccessful print of a U-shaped wall which has locally buckled at the bottom. Right: a curvy cylindrical column, demonstrating the capabilities of printing structures with strong curvatures in the vertical plane.

humidity. This feeds the presumption that there is some natural variability in the printing process and that there is a delicate balance between successful and unsuccessful prints.

3.4.1 Research Joost Mink

Joost Mink [36] has conducted uniaxial compressive tests on two concrete mixes of Bruil at the Microlab of the TU Delft. One mix containing fibres and the other one without fibres. As the fibre-reinforced mix is currently used at Bruil, these results are focused upon in the remainder of this paragraph. Vicat tests were carried out from which followed an initial setting time of 120 minutes, after which the acceleration stage of hydration starts.

Five cylindrical samples with a height of 68.5 mm and a diameter of 33.5 mm were tested at an age of 0, 15, 30, 60, 90, 120 and 180 minutes. Freshly mixed concrete was pressed into cylindrical moulds as casting was not possible, after which the samples were manually compacted. To avoid transportation of test samples, they were directly demoulded in the test rig. Two sheets of Teflon were placed between the testing rig and the sample to avoid friction. A displacement-controlled compression test was then run at a speed of 0.2 mm/s to avoid thixotropic build-up within a single test.

The experiments showed that the fibre-reinforced mix was on average 7 times as strong as the mix without fibres. An exponential development of strength and elastic modulus was observed for both the fibre-reinforced mix and the unreinforced mix. The relationship between strength and time and the relationship between elastic modulus and time of the fibre-reinforced mix are given below:

$$\sigma_c(t) = 61.21e^{0.0111t} \tag{3}$$

$$E(t) = 921.9e^{0.0160t} \tag{4}$$

With t in minutes and σ_c and E in kPa. The Poisson's ratio was found to be decreasing from 0.32 to 0.29, from an age of 0 minutes to 60 minutes. An average density of 2300 kg/m^3 was measured.

A linear function yields a better fit for the first 30 min. as the exponential fit overestimates this stage. The following relationship was therefore found over the first 30 min:

$$\sigma_c(t) = 44.52 + 0.860\,t \tag{5}$$

$$E(t) = 753.9 + 16.13\,t \tag{6}$$

With the determined mechanical properties and density, printing simulations were performed with the simulation software ANSYS. Three square tubes (500 x 500 mm) with a corner radius of 50 mm and varying layer widths (35, 40 and 45 mm) and varying layer heights (15, 11 and 7 mm) were printed at the printing facility of Bruil. The tubes were also printed at three different speeds resulting in vertical growth rates of 2.4, 1.67 and 1 mm/s respectively. The prints were compared to simulations of the exact same prints. Linear buckling analysis showed good correspondence with the theoretical buckling strength. It does however not come close to the buckling heights found in the experiments. It was concluded that the way of preparing specimens, influences the thixotropic built-up of the material. Therefore, the testing method is not representative of real prints and mechanical properties are expected to be higher than measured.

3.5 Conclusion

From literature and practice it has become clear that all parameters involved in successfully printing objects are closely related. Decisions made during printing, material properties and process parameters all influence both the fresh state as well as the hardened state of a print.

It was found that traditional tests, such as a uniaxial compression test, are suitable to determine the mechanical properties of concrete in the fresh state. Suiker [10] and Wolfs et al. [11] showed that both analytical and numerical models can be used to predict premature failure of objects in 3DCP based on mechanical tests. The analytical methods are suitable for the analysis of straight walled structures only, whereas the numerical models are capable of analysing any geometry. Therefore, to analyse structures during printing numerical FE modelling will be adopted in this thesis.

The encountered models regarding stability of printed objects are developed to be used for any given printing duration. However, the models have only been verified with printing experiments of a fairly short duration. The free wall studied by Suiker [10] was printed within 5 minutes and the rectangle within 12 minutes. Both printing experiments have not been repeated. The cylinders that were studied by Wolfs et al. [11] were printed within 10-15 min and the print was repeated five times. These short prints are however not representative for prints in practice which can take up to several hours. Because of this short duration the effects of accumulation of spread in material properties over time cannot be observed.

Moreover, based on the experience of Bruil and research it can be proven that increased temperatures of the printing material can considerably enhance the mechanical properties of fresh concrete during printing. The influence of temperature on the stability of prints can't be observed in short printing experiments. On the one hand the exothermic reaction of the hardening of the concrete that's causing the print to increase in temperature needs a certain amount of time. On the other hand, there is the effect of heating up of the system due to continuously printing. As the effect of heating is not incorporated in the developed models, their accuracy might be much lower than what would be expected from prints the short prints. For now, the models can therefore only be considered valid for prints with a short time duration.

If a model is to be developed in this thesis based on mechanical properties from literature, the model must also be verified with printing experiments found in literature. Only three different, relatively simple geometries that have been printed within a short duration are available. The implications of the short duration have been discussed above and only in one out of three experiments repeatability of the experiment is considered. Moreover, the statistical reliability of the results obtained from the research into the mechanical properties might be questioned as only 6 samples have been tested at each age and a relative standard deviation of ~20% is obtained at each age. On top of that, the mechanical properties are determined specifically for the print setup of the TU Eindhoven. From the results obtained by Joost Mink, it can be concluded that the material used at Bruil behaves differently than the material used in Eindhoven. From the printing experience of Bruil it was noted that printing quality may vary from time to time. This daily variation may be very specific from printer to printer and results from literature can therefore not be used for the printer at Bruil.

It is concluded that it is not possible to create a model that accurately resembles the printing process of Bruil, without knowing the mechanical properties of the concrete used by Bruil. The results of the material research by Joost Mink are considered unrepresentative of the mechanical properties of printed concrete. Nonetheless, it is possible to create a FE model based on the material properties derived by Wolfs et al. However, literature to which the model can be verified is limited. Hence, the accuracy of the model cannot be determined. More importantly, a theoretical model, that cannot be verified and may lack important information as material characteristics are unknown, has no value to neither Bruil nor Movares.

As the objective is to create a model that can be used in practice and not only serve theoretical purposes, it is decided to conduct material research on the concrete mix of Bruil. In this research all relevant process parameters are to be taken into account, such that the tested material resembles the real situation as closely as possible. The temperature can play an important role in the development of mechanical properties. Therefore, the influence of temperature on the mechanical properties of the concrete will be investigated too. To establish a relationship between the material research and real prints, prints will be printed at the same time the material research is conducted. These prints can then be used to determine the reliability of the FE model. When material properties are known and a close resemblance of the printing process is obtained with the FE model, Bruil and Movares have a tool to increase the robustness of the printing process and avoid premature failure of prints.

The experimental programme will contribute to the better understanding of the influence of temperature on the development of mechanical properties of concrete during printing. At the moment it is only known that it can positively enhance the properties of concrete, but it's importance is not clear. In this research the influence on printed concrete will for the first time be quantified and used to model 3D printed structures. Moreover, a direct relation between measured material properties and printed objects has not yet been presented in literature. The research will contribute to the knowledge of testing material properties in-line and the relation between mechanical properties and behaviour of printed objects.

As it is decided to conduct material research, the sub-goal of this thesis will not be able to be accomplished. Optimizing an object for 3D printing and providing optimal parameters as input for the printing process will be considered a bridge too far within the timeframe of the thesis.

4

Numerical modelling

In this section, a numerical model will be created that accurately resembles a true printing process. The model will be compared to published research, discussed in section 3. After the experimental programme, presented in section 5, this model will be used to simulate the printing process of Bruil and determine its accuracy, compared to reality.

In literature it was found that the commercial simulation software Abaqus is capable of modelling the printing process of a cylinder [11]. A student licence of Abaqus, and other packages such as DIANA FEM are available through the TU Delft. At Movares, ANSYS is used for complex finite element simulations. Although having different capabilities, in a broad sense these finite element analysis (FEA) packages are comparable and should all be capable of simulating the printing process. It is therefore decided to use ANSYS as modelling software.

4.1 Stress-strain behaviour in ANSYS

To examine whether ANSYS is capable of simulating the printing process, results of Suiker [10] and Wolfs [11] are reproduced and compared. The ANSYS Workbench environment was used for all simulations, as it allowed for a structured workflow and simple interaction with 3D modelling software such as Rhinoceros.

To simulate the printing process, ANSYS has to be able to vary the material properties of elements over time. Within the static structural module of ANSYS it is not possible to define material properties based on time. Consequently, it is not possible to directly address material evolution over time during an analysis. It is however possible to define material properties based on temperature and temperature loads can be applied during an analysis with respect to time. Therefore, the variable *temperature* can indirectly be used as a *time* variable during the analysis to assign material properties to a print layer.

To test this method, single element tests have been performed on 3D 8-noded solid elements with all sides measuring 10 mm. Material properties were implemented according to Eq. (1), in which the time

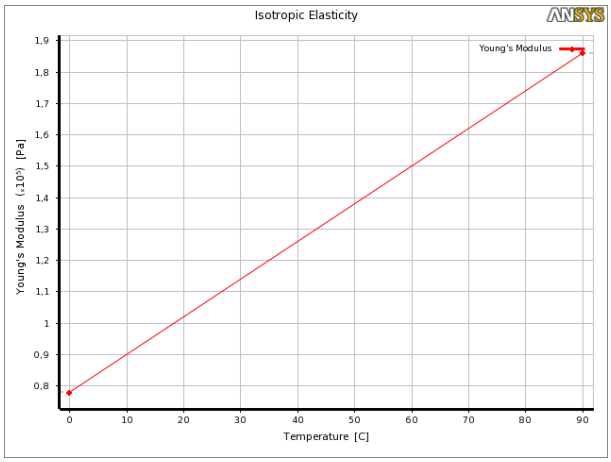

Figure 16: Input of material properties in ANSYS: Young's modulus as function of the temperature.

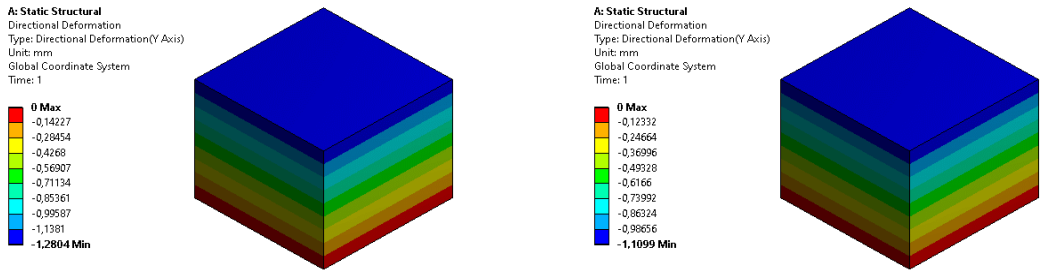

Figure 17: Single element test performed on a solid 8-noded element with a temperature of 0 °C (left) and 10 °C (right) and resulting vertical deformations.

is replaced by temperature. Figure 16 shows the material input in ANSYS. The Poison's ratio was set equal to zero in order to neglect additional strain effects.

Firstly, a linear calculation was performed at temperatures of 0 °C and 10 °C. A total load of 1.0 N was applied on the top of the element. The resulting displacements according to mechanics are given in Eqs. (7) and (8).

$$T = 0\,℃ \quad \rightarrow \quad E = 0.0781\,MPa \quad \rightarrow \quad \Delta l = \frac{\sigma}{E}\,l = \frac{0.01}{0.0781} \cdot 10 = 1.2804\,mm \tag{7}$$

$$T = 10\,℃ \quad \rightarrow \quad E = 0.0901\,MPa \quad \rightarrow \quad \Delta l = \frac{\sigma}{E}\,l = \frac{0.01}{0.0901} \cdot 10 = 1.1099\,mm \tag{8}$$

Figure 17 shows the results of the single element tests in ANSYS. It can be clearly seen that ANSYS correctly adopts the right material properties when assigned a certain temperature. As the material does not have any thermal properties assigned, only the material properties will change, and thermal strains will not occur.

To examine whether ANSYS also correctly adopts the right material properties in a multistep analysis, a varying temperature load is assigned to the element. The temperature is applied over 20 load steps and increases from 0 °C to 10 °C and back to 0 °C with increments/decrements of 1 °C. The load is kept constant throughout the load steps at a magnitude of 1.0 N. The applied thermal load and the resulting vertical deformations over time are depicted in Figure 18**.** From this figure can be concluded that ANSYS correctly adopts the right material properties when the temperature is varied over time. The vertical deformation at 0 °C and 10 °C is equal to the outcome of the single-step analysis (Figure 17).

Displacements and strains are calculated according to the updated stiffness of the element. This in an important property of the model as it assumes that during printing, when the yield strength/plasticity of layers have not been reached, deformations are not permanent and can even be recovered when the concrete matures. This behaviour is observed in the results presented in Figure 18**;** the deformation of the element at step 0 is equal to the deformation at the end of the analysis, while it changes in between.

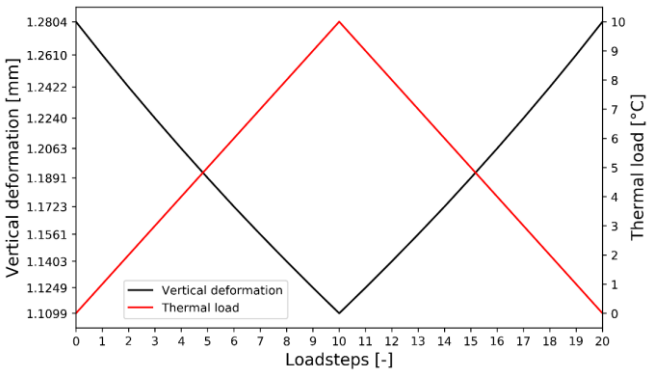

Figure 18: Applied thermal load and resulting vertical deformations in a multistep analysis.

The element behaviour is also tested when plasticity is involved in the model. From research conducted by Wolfs [11] it is known that a Mohr-Coulomb failure criterion fits freshly printed concrete well. Here, for simplicity, a bi-linear stress-strain relationship is assumed. The Young's moduli and compressive strengths found in [11] are adopted. The yield strength of the fresh concrete at an age of 0 min. is equal to 6.37 kPa and the yield strength of concrete at an age of 90 min. is equal to 18.93 kPa. The Young's moduli are defined according to Eq. (1). An isotropic hardening model with a tangent modulus of 30 kPa was used in order to make convergence of the solution simpler. The bi-linear temperature ('time') dependent relationships as inputted in ANSYS are shown in Figure 19.

Firstly, an analysis consisting of two steps is conducted on an element on which the thermal load is kept constant at a magnitude of 90 °C throughout the analysis. In the first step the vertical load is ramped to a magnitude of 2.0 N, causing a stress that is just above the yield stress. In the second step the load is removed. This analysis will be referred to as analysis 1.

Secondly, an analysis consisting of five steps was conducted on the element. During the first step a thermal load of 0 °C is applied to the element and the vertical load is ramped to a value of 0.65 N, causing a stress which is just above the yield strength of concrete at this age and therefore causes plastic strains. The load is then removed at the second step, while the thermal load is kept constant at 0 °C. Only plastic strains will be present in the element. In the third step, while there is no load on the element, a thermal load of 90 °C is applied to alter the material properties and is kept constant at this level until the end of the analysis. In step 4 a load with a magnitude of 2.0 N is applied, causing a stress which is just above the yield strength of the material at an age of 90 min. to invoke plastic strains. In load step 5 the load is removed again. This analysis is referred to as analysis 2.

The results of analysis 1 and 2 are shown in Figure 19. It can be concluded that upon updating the stiffness of the element by assigning a higher temperature, the plastic strains developed at a younger age remain present. Due to hardening effects, the yield stress of the concrete at an age of 90 min. is increased. Therefore, when the load is removed at the end of analysis 2 the same plastic strains have developed as were developed in analysis 1.

4.1.1 Discussion

Whether the observed behaviour is equal to what would happen in a real 3D printed structure can be questioned. Suppose a structure would remain in the elastic range throughout a printing session. According to the model adopted in ANSYS, elastic strains are recovered upon load removal. Which is common behaviour for linear-elastic materials. It was also observed that when the load is constant and the Young's modulus changes, the deformations and the strains change according to the updated Young's modulus. Simply put: ANSYS jumps from one stress-strain relation to the other when the material properties are changed. Therefore, deformed elements are able to recover some of the deformation when the material matures.

When the printing speed is fast enough, the recovery won't be noticed as the effect of the development of the mechanical properties of the concrete is counterbalanced by the weight of the layers that are continuously added. However, when the Young's modulus of the concrete develops fast enough, the structure is able to regain some of its deformations during printing.

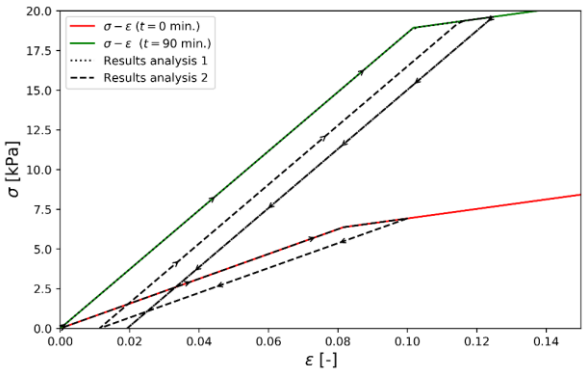

Figure 19: Results of analysis 1 and 2 and the bi-linear stress-strain relationships of the material at an age of 0 and 90 min.

When plastic strains have developed in a print at a particular age, they are permanent and cannot be recovered when the stiffness is updated, as shown by analysis 2. Due to the hardening behaviour adopted in the model, analysis 1 and 2 result in the same amount of plastic strains. Due to hardening occurring at an age of 0 minutes, the elastic region of the concrete at an age 90 minutes is increased. This is presumed to be incorrect, and a model that forgets hardening has occurred at a younger age should be adopted according to the reasoning below:

Imagine a fresh concrete cube which is vertically compressed at t = 0 min. until it develops plastic strains. The load is then removed, leaving only permanent deformations. When the cube would be left to harden for 90 min. and is then loaded again until it reaches plasticity and unloaded after which permanent deformations are left, it could be considered as just loading a new cube with a different stiffness. The total permanent deformation would then be equal to:

$$\Delta l = \varepsilon_{p,0}\, h_1 + \varepsilon_{p,90}\, h_2 \tag{9}$$

In which $\varepsilon_{p,0}$ and $\varepsilon_{p,90}$ are the plastic strains at ages of 0 and 90 min. respectively, h_1 is equal to the original height of the cube and h_2 is equal to the deformed cube after the load is removed in the first cycle. h_2 can also be written as:

$$h_2 = h_1 - \varepsilon_{p,0}\, h_1 \tag{10}$$

Therefore, the total permanent deformation can be written as:

$$\Delta l = h_1 \left(\varepsilon_{p,0} + \varepsilon_{p,90} - \varepsilon_{p,0}\, \varepsilon_{p,90}\right) \tag{11}$$

While at the end of analysis 2 the current model assumes a total permanent deformation of:

$$\Delta l = h_1\, \varepsilon_{p,90} \tag{12}$$

Plastic strains are unwanted in a 3D concrete printing process as they are associated with large deformations. Successful prints must therefore remain well within the elastic region. Therefore, as soon as plastic strains have developed, a print can be considered failed and its post-yielding behaviour is only of interest for theoretical applications, but not of any use in practical applications. It is however important to know the point of yielding, to mark the end of the elastic regime.

Furthermore, in the explanations above an extreme situation is sketched. When small increments of age are considered and slow development of the compressive strength, the hardening effect may not be that large and the way ANSYS treats plasticity with evolving material properties is a sufficient approximation of reality. This thesis will not go deeper into the plastic behaviour of the concrete, as they are not of interest for practical applications.

Moreover, it may well be possible that although the fresh concrete behaves linearly, the strains may not always be elastic, meaning that they can't be recovered upon load removal or maturing of concrete. In this thesis it is assumed that that as long as the strains are within the linear region the deformations are not considered permanent and the strains are elastic and can be fully recovered. When the fresh concrete ages, strains are calculated according to an updated Young's modulus without adding previously induced strains (in accordance with the results plotted in Figure 18**)**. Whether this is true behaviour should be investigated by material tests.

4.2 Print simulations in ANSYS

Results obtained by Suiker [10] are reproduced and compared to test the accuracy of a FEA conducted with ANSYS under the assumptions defined in the previous section. The prints analysed in this study can be found in Figure 11. Suiker predicted failure of the free wall to be at 20 layers and failure of the rectangular tube at 30 layers. The reader is referred back to section 3.3.1 for more information about those prints.

To compare ANSYS to the theoretical model, two types of analysis are conducted: a Linear Buckling Analysis (LBA), which is also referred to as a bifurcation analysis or Eigenvalue buckling analysis, and a Geometrically Non-Linear Analysis (GNLA). To limit the calculation time, both prints were modelled using symmetry. Analysis were performed with solid element as well as with surface/shell elements. The

results of the solid model predicted better results and are therefore presented here. Also, solid elements allow for the creation of more complex geometries than surface elements and are therefore likely to be used for future simulations. Hexagonal 8-noded solid elements (SOLID186) were used in the analyses.

4.2.1 Linear buckling analysis

The only load applied to the prints is gravity loading. The load multiplier (λ) found in an LBA is therefore a scalar of the gravity load. The critical buckling length was found in an iterative fashion: the geometry was imported into ANSYS with slightly more layers than predicted by Suiker. An LBA was performed on the geometry and the load multiplier was noted. When $\lambda < 1$ a layer was removed and an LBA was again performed. This process is repeated until the load multiplier was equal to 1.0 ± 5%. When this value is reached it means that the structure cannot sustain any more layers and will buckle under its own weight with the given number of layers. After each iteration, material properties (Young's modulus) of the layers are recalculated. E.g.: when printing of a layer takes 0.35 minutes and we consider an LBA of a wall with 30 layers, the first layer is 10.5 min. old and the last layer is 0.35 min. old at the moment the LBA is performed. Across a layer the Young's modulus is considered homogeneous and its properties are calculated according to Eq. (1)**.**

The ANSYS Workbench environment allows for a parametric setup of the analysis. This made it possible to supress layers in consecutive analyses and run all linear buckling analyses in one go. An APDL script ensured the correct material properties were assigned every time a layer was removed from the analysis. The APDL script can be found in Appendix A: APDL script LBA.

4.2.2 Geometrically Non-Linear Analysis

To trigger buckling behaviour in the GNLA, imperfections are introduced corresponding to the first buckling mode of the LBA analysis. The shape of the first buckling mode is scaled by 1/1000 times the wall thickness and applied as an initial imperfection to the geometry. To simulate the printing of layers during the GNLA, the Element Birth/Death function of ANSYS is used. With this function a part of a model can become existent or non-existent. To achieve this behaviour, ANSYS does not remove the 'killed' elements. Instead, it deactivates the elements by multiplying their properties, such as stiffness and mass, with a reduction factor (1.0e-6) and element loads that are associated with the elements are cancelled out of the load vector. Likewise, when elements are 'brought back to live' they are reactivated and not actually added to the model. Therefore, the total geometry has to be created before an analysis, after which the desired layers can be 'killed' in the first load step and can be reactivated at the proper load step.

The evolution of material properties over time is controlled by assigning a temperature load to a layer at the appropriate load steps with the appropriate magnitude. The analysis is controlled by two APDL scripts of which one is applied at the first load step and the other one is assigned to run at all load steps. In the first script, executed at the first load step, all layers except the first layer are 'killed' and temperature loads belonging to each layer at each step are defined to assign the right material properties at the right moment in time. The second script makes sure the appropriate layer is reactivated at the corresponding load step, which is run before the ANSYS solves for a particular load step.

Both scripts can be found in Appendix B: APDL scripts GNLA and are again defined parametrically. It is therefore possible to define the total number of layers, printing speed and the number of layers to be analysed every consecutive load step. The real value of the parametric script comes with the ability to analyse prints at different print speeds, which is the main variable that can be altered to improve the stability of a print. The ability to analyse multiple layers at a time can drastically improve the calculation time of the analysis as theoretically the calculation time of for instance analysing a print layer by layer is double that of analysing two layers at a time. It can however affect the accuracy of the analysis.

4.2.3 Results

The results of the LBA can be found in Table 1, showing the load multipliers obtained when performing a buckling analysis at different heights. The results of the GNLA can be found in Figure 20, in which the normalised maximum horizontal displacement is plotted against the number of layers. For comparison the results obtained by Suiker's model and the number of layers at which the LBA analysis reached unity is plotted. The step just before buckling and the buckled shape found in the GNLA of both prints

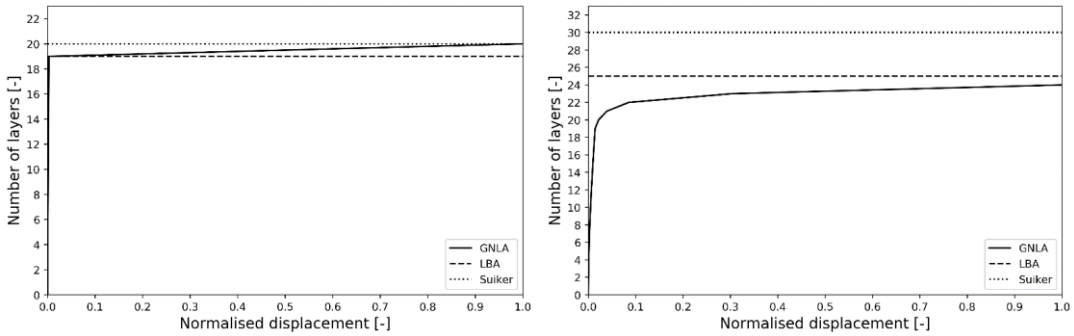

Figure 20: Results of an LBA and a GNLA performed on a free wall (left) and a rectangular tube (right) in ANSYS plotted against the results obtained by Suiker

are shown in Figure 21**,** illustrating the sudden collapse of both prints. Moreover, it demonstrates the qualitative agreement between the buckled shape found in the printing experiments and the FEM results.

Regarding the free wall, there is good correspondence between the LBA, GNLA and the theoretical model of Suiker. The difference between the LBA analysis and the model of Suiker is 5%. The GNLA converges towards the critical length found by Suiker.

The results of the analysis of the rectangular tube show less accurate results when being compared with the theoretical model of Suiker. A difference of 16.7% is found between the LBA and Suiker's solution. Also, a discrepancy between the results of the GNLA analysis and Suiker's prediction is observed. The GNLA does however converge towards the critical buckling length found in the LBA, indicating a consistency between the LBA and the GNLA.

Clearly, there is a discrepancy between results generated by ANSYS and results obtained from the theoretical model of Suiker. As the model of Suiker was compared with real printing experiments and showed great correspondence with these, this model is deemed accurate and FEM should yield similar results. Moreover, in the paper describing the model [10] it is stated that FEM yielded similar results and that those results will be communicated in a later stage.[2] Why there is a discrepancy between ANSYS and Suiker's model is unclear. Furthermore, it can be concluded that an LBA can give a good indication of the buckling behaviour of prints that are insensitive to imperfections as the GNLA converges towards the LBA.

Table 1: Results of the LBA analysis on the free wall and the rectangular tube.

Free wall		**Rectangular tube**	
Number of layers	Load multiplier (λ)	Number of layers	Load multiplier (λ)
25	0.451	31	0.758
24	0.508	30	0.783
23	0.576	29	0.811
22	0.656	28	0.844
21	0.752	27	0.883
20	0.868	26	0.928
19	1.008	25	0.980
18	1.181	24	1.042

4.2.4 Mesh refinement study

As the use of solid elements requires a lot of computational power, it is valuable knowledge to know the requirements of the mesh to reach accurate results. In this study the load multiplication factor found in the LBA is tracked upon refinement of the mesh. Three meshes of three different sizes were created, starting with elements with an edge length of 9.2 mm (one element over the height of a layer and five over the width) until elements with an edge length of 2.3 mm (four elements over the height of a layer and 19 over the width). This study was repeated for both the LBA of the rectangular wall with 24 layers

[2] Extensive comparisons between Suikers model and FEM models developed by Wolfs are published in [43] and showed excellent correspondence. This paper was published after the results presented in this chapter had been obtained.

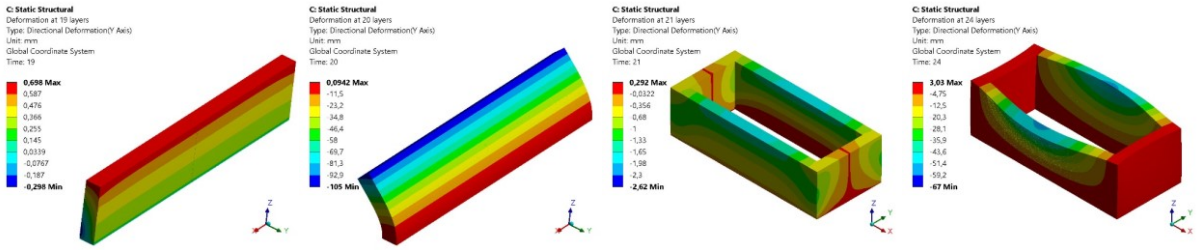

Figure 21: Results of the geometrical non-linear analysis of the free wall (left) and the rectangular tube (right) just before buckling and the buckled shape.

as with 25 layers as the resulting buckling factors were both close to 1.0. The results of the analyses are shown in Table 2**.**

From the results can be concluded that refining the mesh does not lead to significant changes in the resulting load multiplier. The difference between the load multiplier calculated with the coarsest mesh and the one calculated with the finest mesh is only 0.7%, while the calculation time is improved by a factor 144. Moreover, the load multipliers of an LBA performed with 24 layers are almost equal to the ones performed with 25 layers and are both very close to one.

Table 2: Results of the mesh refinement study on the rectangular tube using 8-noded solid hexagonal elements

Number of layers	Element size [mm]	Number of elements	Number of nodes	Calculation time (mm:ss)	Load multiplier (λ)
25	2.3	351,500	465,000	43:10	0.974
25	4.6	46,500	77,550	01:55	0.975
25	9.2	5,875	14,400	00:18	0.980
24	2.3	337,440	446,400	41:51	1.035
24	4.6	44,640	74,448	01:51	1.037
24	9.2	5,640	13,824	00:17	1.042

4.3 Model including plasticity

Research of Wolfs et al. [11] have shown the possibility of adopting a Mohr-Coulomb yield criterion to model the non-linear behaviour of the fresh concrete. The accuracy of the model presented in this paper was determined by comparing the numerical results of a cylindrical print to a real print of the cylinder. Significant plastic deformations developed in this print, leading to collapse. For details of the model and the results of this experiment the reader is referred to section 3.3.2. The ability of ANSYS to model plastic behaviour during printing has already been discussed in section 4.1. To determine the effect of the assumptions made in the model, the same cylinder will be modelled in this section, using the stress-strain relations given in [11].

In ANSYS it is not possible to define a Mohr-Coulomb model with hardening, which was adopted in the research of Wolf et al. Therefore, the Menetrey-Willam constitutive model is adopted in ANSYS. According to the ANSYS user manual [37] the yield surface of this model is similar to the Mohr-Coulomb yield surface, but without the sharp edges that can cause convergence issues. Besides that, it shares some characteristics with the Drucker-Prager model and can model similar materials. Unlike the Mohr-Coulomb model, the Menetrey-Willam model is not defined by cohesion and inner friction angle

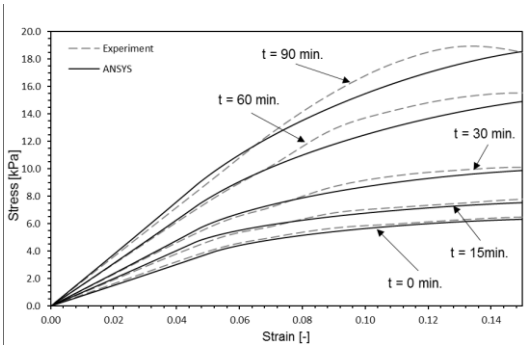

Figure 22: Results of the uniaxial compression test performed by ANSYS compared to the experimental results of Wolfs et al. [11].

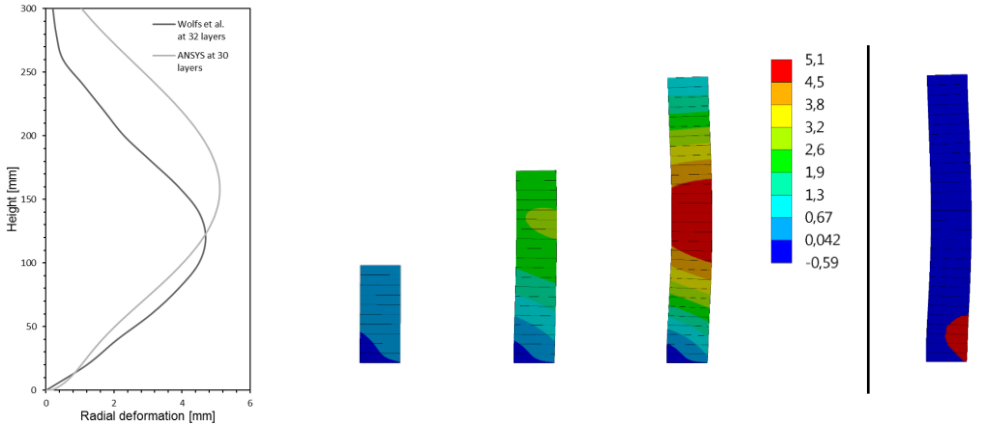

Figure 23: Left: radial deformation of the cylinder compared to Wolfs et al. Middle: radial deformations after printing 10, 20 and 30 layers. Right: Plastic strains at 30 layers (regions in red have developed plastic strains).

parameters. Instead, it is defined by the uniaxial compressive strength, uniaxial tensile strength and the biaxial compressive strength. As the biaxial strength cannot be determined from the results obtained by Wolfs et al. is assumed to be equal to 1.2 times the uniaxial compressive strength, which is a common value for concrete. For the hardening and softening parameters reference is made to the ANSYS user manual.

The uniaxial compression test performed by Wolf et al. has been modelled in ANSYS to evaluate the correct adoption of the stress-strain relationships when the Menetrey-Willam material model is used. The results of the simulation of the uniaxial compression test in ANSYS are shown in Figure 22, in which they are compared to the results of the uniaxial compression test of Wolfs et al. The results are cut-off at a strain of 15% as generally softening starts at this level of strain, which is not of interest. The results of the simulation until an age of 30 min are deemed very accurate. The results at the ages of 60 and 90 min. are accurate in the linear stage of the material but are considered less accurate in the non-linear part of the stress-strain relationship. It is concluded that ANSYS can accurately simulate the uniaxial behaviour of fresh concrete with a Menetrey-Willam material model.

The results of the cylindrical print modelled in ANSYS are shown in Figure 23. Unfortunately, the model was not able to converge after 30 layers due to extreme element distortion in the bottom right corner of the model. Even after multiple mesh refinements and trying different integration schemes, it was not possible to advance the simulation of the print beyond this point. Next to that the deformation of the print at the end of the analysis is plotted against the deformation found by Wolfs et al. at 32 layers.

Although there is a difference of two layers between the results plotted in the graph of Figure 23, the results can be considered to be similar. The radial deformations are approximately equal, but the height at which the maximum deformation occurs is different. When two layers are additionally added to the model in ANSYS, the height at which the maximum deformation is expected to drop. The radial deformation is however expected to increase.

The development of plastic strains is at the bottom right corner is similar to what was found in the model of Wolf et al. (see Figure 13). The plastic strains encountered in ANSYS are however more severe than found by Wolfs et al. The plastic region that has developed on the inside of the cylinder of Wolfs et al. is not found in the ANSYS model. It is expected that this region will also develop in the ANSYS model when it is able to pass beyond the point of unconvergence.

The difference in results may be attributed to the use of the Menetrey-Willam material model, which differs from the Mohr-Coulomb model in Abaqus. Secondly, there was no raw data available to fit the material model on. Instead, the model was fitted to results directly extracted from the paper which is less accurate. Thirdly, the adding of layers in the simulation may have been defined differently to what is defined in this thesis. Overall, the findings are in line with the results obtained by Wolfs et al.

4.4 Conclusions

It can be concluded that ANSYS is capable of modelling the printing process of arbitrary geometries. A swift workflow can be adopted where first a linear buckling analysis is performed on the final structure. The buckling mode can be then be scaled and used as an initial imperfection on the structure in a geometrically non-linear analysis. The mechanical properties of the layers can be updated during the non-linear analysis as the print grows by assigning temperature loads. With a parametrically defined APDL script the print can be analysed at different speeds to find the optimal result. Furthermore, the computational time needed to complete an analysis can be decreased by analysing multiple layers at a time.

In the model it is assumed that when the strains in freshly printed concrete are still in the linear part of the stress-strain curve, they are elastic and hence recoverable when concrete matures. Both the LBA and the GNLA show good correspondence with literature, although not exactly similar.

A mesh with one element over the height of a layer proved to be sufficient enough to correctly predict the load factor of a linear buckling analysis. It is assumed that a similar mesh is sufficient enough to be used in a geometrically non-linear analysis.

Furthermore, it has been proven that the Menetrey-Willam material model in ANSYS can accurately model fresh concrete under uniaxial compression. Computational times are however increased as plastic strains are introduced, due to the added complexity of the model and the finer mesh needed to capture the behaviour accurately.

As was concluded before, in literature there is a limited amount of geometries available to which the ANSYS model can be verified. In fact, al the literature that have published both material properties and printing experiments have been exploited in this section of the thesis. The model shows a good correspondence with these results. How accurate the model is in predicting the stability of structures that are printed over longer timespans than encountered in the presented literature is unknown. This is however of major interest as generally prints take much longer than 15 minutes. Furthermore, all these tests are performed with the printing equipment of the TU Eindhoven, using material of which the mechanical properties are known from experiments. Material behaviour of the concrete mix used at Bruil may be significantly different than this. Joost Mink has already proven that the material used at Bruil is several times stronger than that found in literature. His research did however not incorporate the printing process itself.

To make the model suitable for use at Bruil, material tests have to be performed to determine the mechanical properties of the concrete mix used at Bruil. When mechanical properties are known, printing experiments can be conducted to verify the accuracy of the model for print with a longer duration. When the accuracy of the model is characterized it can be used for predicting the printability of arbitrary geometries.

5

Experimental research

An experimental programme was designed to define the printing process at Bruil. This includes characterisation of the mechanical properties of freshly printed concrete at ambient and elevated temperatures and determining the reliability of the printing process itself.

As proven in section 4, results of uniaxial compression tests are suitable to serve as input for FE analyses of printed objects. From the compression tests on freshly printed concrete the Young's modulus, Poisson's ratio and uniaxial compressive strength can be derived at different ages of the concrete. These properties will be used as input parameters for the FE analysis in ANSYS and to characterise the accuracy of FE predictions.

As discussed, experiments on the concrete used at Bruil have been conducted by Mink [36] by performing uniaxial compression tests. These experiments have however not been conducted on material directly extracted from the printer. It is expected that the printing process will influence the material's performance as it is known that mixing speed, pump pressure, compaction and accumulation of heat in the system can greatly influence the curing rate of fresh concrete. Therefore, in this research a method is developed to directly extract cylindrical samples from printed concrete to incorporate all of these effects. Furthermore, during printing sessions at Bruil an increase of temperature of printed objects was observed. Within the first 2 hours of printing objects can reach a temperature of around 35 °C, while material exiting the nozzle has a temperature between 24 °C and 27 °C. To incorporate the effect of temperature on the mechanical properties of printed concrete, uniaxial compression tests are conducted at room temperature and at an elevated temperature.

From printing experience of Bruil it is known that the ability to print a certain object can vary daily. To be able to characterize the reliability of the printing process and directly couple measured properties of printed objects, a printing experiment was conducted during the execution of the uniaxial compression tests. During these tests multiple process parameters were monitored and the objects were recorded during printing to capture their failure-deformation behaviour.

It is known that for freshly printed concrete a Mohr-Coulomb yield criterion can be adopted to determine the yield strength [11]. The parameters that determine the Mohr-Coulomb yield criterion, the friction angle and cohesion, cannot be measured with a uniaxial compression test. The uniaxial compressive strength can therefore only be used as an estimation of the stress at which plastic failure will occur. As stated in section 4, plastic failure of a print is actually not of primary concern, as it will be associated with high levels of strain and therefore large deformations. These large deformations are unwanted and are therefore considered a failure criterion too. Besides that, post buckling behaviour in which plastic strains are highly likely to form is not of interest. Hence, experiments to determine the yield surface of the concrete at different ages are not considered.

It may however be possible that the elastic region of concrete at higher ages is relatively short, meaning that the concrete at those ages will show little deformation before failure. This suggests that the assumption that yielding occurs at large deformations, and can therefore be neglected, will no longer be valid. Based on Mink's experiments this is not expected as the concrete fails at strains > 2% after 180 min. and even fails at strains > 6% for concrete of ages up to 60 min. Compared to conventional

concrete, where compressive yield stress is reached at strains of 0.175%, these are relatively large strains.

5.1 Method

5.1.1 Uniaxial compression test

Uniaxial compression tests are performed on cylindrical samples that are directly extracted from a printed wall. The samples are then either stored at room temperature or in an oven at a temperature of 35 °C until testing. A photograph of the oven in which the samples are stored is given in Figure 24. As the experiments are conducted in a semi-controlled environment the room temperature fluctuated between 18 and 20 °C. The samples are kept inside their mould until they are tested.

The tests on samples stored at room temperature are performed at concrete ages of 0, 15, 30, 60, 90, 120 and 180 minutes. In which an age of 0 min. represents the earliest testing time possible taking into account extracting, demoulding and running the test. These ages have been chosen to obtain results at the same ages as were obtained in the experiments by Mink [36] and Wolfs et al. [11], allowing for direct comparison. As the time needed to complete a full print is generally not longer than three hours it is decided to not test beyond this age.

The samples stored at 35 °C are tested at ages of 15, 30, 45, 60, 75 and 90 min. Due to strength limitations of the testing rig it was not possible to test beyond an age of 90 min. Hence, it was not possible to test the samples at the same ages as the samples stored at room temperature. Moreover, as it takes time for the samples to heat up, not all samples will have a temperature 35 °C at the moment of testing. The development of the temperature of the samples over time is part of the results. For practical reasons testing at an age of 0 minutes was omitted for samples stored in the oven.

The dimensions of the test samples are designed according to ISO 17892-7 [38]. According to the standard, the diameter of the cylindrical samples must be greater than six times the maximum particle size to eliminate size effects. The largest particles in the mix are the fibres which have a length of 6 mm. Therefore, the diameter of a mould must be at least 36 mm. The ratio of the height to the diameter of the samples has to be between 1.8 and 2.5 to allow a diagonal failure plane to form.

Based on the experiments conducted by Joost Mink it could be determined what magnitude of loads was to be expected in the compression tests, depending on the cross-sectional area of a sample. Knowing this beforehand meant the costs of the experiment could be greatly reduced, since renting heavier equipment would be more expensive (a testing rig with a capacity of 5.0 kN would be twice as expensive as a testing rig with a capacity of 2.5 kN). Based on this criterion and partly based on ease of handling, extraction and demoulding (see section 5.1.1.1) it is decided to create cylindrical samples with a diameter of 43 mm and a height of 90 mm having a height-to-diameter ratio of 2.1.

In the thesis of Mink, a maximum stress of 0.580 MPa was measured at an age of 180 min. in a single test on fibre reinforced concrete. Based on this value it is calculated that a force of 0.84 kN would be needed to load a sample with a diameter of 43 mm until failure. A test rig with a capacity of 2.5 kN is therefore deemed sufficient as is will allow to record stresses that are three times higher than measured by Mink. A Mecmesin single leg testing rig with a 2.5 kN loadcell was rented for two weeks at Hartech B.V., which was one of the few companies renting testing rigs to conduct compression tests on location.

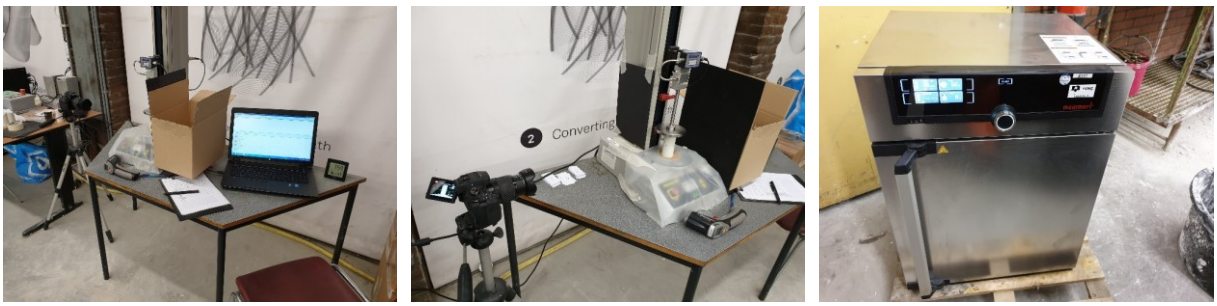

Figure 24: Left and middle: setup of the uniaxial compression test. Right: the oven in which the samples are stored.

Figure 25: Left: three different mould configurations. Middle: distorted sample. Right: final mould configuration.

In order to realize a nearly frictionless interface between the samples and the testing rig, a double sheet of Teflon is provided on the top and bottom side of the samples. To neglect the effects of thixotropic build-up during a single test the samples are loaded at a rate of 30 mm/min up to a displacement of 30 mm, corresponding to a strain of 33%. The time for a single test will therefore be equal to one minute and thixotropic build-up is deemed negligible within this timeframe.

Before testing, each sample is weighted on a scale and its surface temperature is measured using an infrared thermometer. Furthermore, the room temperature and relative humidity of the printing lab are noted each time a sample is tested. As samples are created by extracting concrete from a printed wall (see section 5.1.1.1) the parameters defining the print process during printing are noted. These are: the pressure in the hose, the pressure in the nozzle, temperature of the water, temperature of the mixer and temperature of the print itself. The moment the printer starts printing the wall is denoted as the starting time of the experiment. This time equal to an age of 0 min.

At the start of each testing day the water content and the air content of fresh concrete exiting the nozzle was measured. Only when the measurements showed proper values a testing day was started. This meant that the water content had to be around 15±1% and the air content around 6.2%.

The forms used for noting the parameters mentioned above can be found in Appendix C: Forms used during experiments.

5.1.1.1 Pilot test: extracting samples and demoulding

It is essential that samples are tested at the correct age. Any delay in demoulding affects the results and may cause problems in the strict planning of the experiment (see section 5.1.3). In order to swiftly conduct the tests, it is crucial that the preparation and test procedure is simple. As conventional mould release techniques, such as using compressed air, may severely affect the unhardened concrete a mould is designed that can easily be deconstructed. A simple and fast workflow had to be obtained that allowed demoulding and testing within a timeframe of approximately 2 min. Therefore, a pilot test was organised to test three different types of moulds and two different methods of extracting the concrete from the printing setup.

The basis of the moulds was constructed using PVC-pipes with an outer diameter of 50 mm and an inner diameter of 43 mm. These pipes were then sawn into parts to create moulds with a height of 90 mm. The advantage of using PVC pipes is that they are cheap and attributes such as caps and clamps that directly fit the pipe are readily available. A downside is that the tolerances on the dimensions of the pipe are not that tight and small differences between the real diameter, wall thickness and manufacturing specifications exist. The three variants of the mould are shown in the left picture of Figure 25 and listed below:

1. The base mould is cut in halve. The two halves are then put inside a cap and pressed together using a clamp. The clamping force provided by a bolt was enough to ensure a tight fit between the two halves. To release a sample from the mould the clamp can be removed after which the two halves can easily be separated from the sample. The configuration of the mould including caps is shown in the right picture of Figure 25.
2. The base mould. With this mould is expected that the a concrete sample can slide out of the mould under its own weight, without additional force.

Figure 26: Left: extracting samples by pushing a mould into the print. Right: demoulded samples ordered in age from left to right (0, 15, 30, 60, 90, 120 and 180 minutes) during testing of the proof of concept.

3. One side of the base mould is cut. After it was cut the backside was slightly heated to give the mould a permanent opening. Again, this mould was put inside a cap and a clamp was used to firmly close the mould (see the right picture of Figure 25). To release a sample the clamp can be removed, after which the mould automatically opens. The mould can then be lifted to release the sample.

The three different moulds that are shown in the left picture of Figure 25 are moulds with an outer diameter of 75 mm and height of 150 mm. This size was used in the first proof of concept, as large sample were considered a geometrically more stable and easier to handle. However, a testing rig with a relatively high capacity had to rented to load samples of this size until failure. Therefore, the diameter of the moulds was changed to 50 mm.

Before filling the mould with concrete the moulds are lubricated with special formwork oil. The moulds were filled with concrete in two ways:

1. The concrete is directly extracted from the printer head. The printer is fixed in one position and while the concrete exits the nozzle a mould is held under it to fill the mould. After extraction the top of the mould is closed with a cap.
2. The concrete is extracted from a wall that was printed within 2 minutes by pushing the mould into the print. The wall consists of 8 layers with a layer height of 14 mm was. As soon as the print was finished moulds were pushed into the fresh concrete (see left picture of Figure 26). After that, the moulds were directly removed from the print, closed with a cap and stored.

Extraction of samples by method 1 gave mixed results. Some samples were perfectly straight (left picture of Figure 25), whereas other were highly distorted (middle picture of Figure 25). Such distorted samples were obtained when not enough counterpressure was applied by the person filling the mould. As the amount of pressure applied to the samples cannot be controlled, and samples can only be visually inspected after demoulding it was decided that this method does not fulfil the requirements. Moreover, due to the impossibility of controlling the pressure applied during filling, samples would have a different degree of compaction causing inconsistencies in the results.

Extracting the samples by method 2 yielded better results. Visually, no layering of the structure was found after demoulding (see right picture of Figure 26). Also, compaction of the samples is not an issue anymore. By directly extracting the samples from the printer the compaction that is found in the print will also be present in the test sample. A slight additional compaction may however occur due to the pushing of the mould into the print. As this degree of additional compaction will be similar for all samples it does not influence the results from sample to sample. Hence, method 2 is chosen as the most convenient method of preparing samples.

Within the first 30 min. for all three mould configurations the samples could easily be released from their mould by turning the mould upside down and lifting it: the sample slides out under its own weight. After this timeframe it became increasingly difficult to extract the samples in this way without exerting, sometimes very large, pressures on the samples to push them out. Mould configuration 2 was therefore not good enough to be used during the experiment. Mould configuration 3 proved to work best, as upon releasing the clamp the mould would pop open. This reduced the friction between the sample and the mould by a sufficient amount to easily lift the mould and release the sample. Mould configuration 1 did

not work that well at all times. When one half of the mould was released, the other half would sometimes stick to the sample. It was often difficult to get the other half off without affecting the sample. Mould configuration 3 was chosen to be used during the experiment.

Upon opening the moulds for the first time it was noticed that the samples were actually smaller than the mould. The problem was attributed to air pockets inside the mould. The problem was solved by making holes in the caps through which the air could escape when they are pushed into the printed wall, but small enough to not let any concrete through. Only samples of the earliest age, that were demoulded immediately after extraction, showed deformation. This problem was attributed to the fact that due to the geometry of the sample, the fresh concrete was not able to sustain its own weight when directly demoulded and therefore settles a bit. This settling is shown in the first sample on the right picture of Figure 26.

5.1.1.2 Camera measurements

From the uniaxial compression tests force-displacement diagrams will be obtained. In order to derive the mechanical properties, these force-displacement diagrams have to be converted to stress-strain relationships. The stress is calculated by dividing the applied force by the cross-sectional area of the sample. In the calculation of stresses, the self-weight of a sample is not taken into account as the stress at the bottom of the sample is relatively low (1.9 kPa). Moreover, failure does not occur at the bottom of a sample, but rather trough the formation of a shear plane across the sample.

Due to the softness of the fresh concrete and the occurring large lateral deformations it is not possible to apply a physical measurement instrument, such as a strain gauge, without severely affecting the sample. Hence, to calculate the applied stress and to determine the Poisson's ratio, the lateral deformations are tracked by a high-resolution camera. The vertical strains are derived from the displacements recorded by the testing rig.

Figure 27 gives a schematic overview of a camera recording a sample. In order to measure the correct diameter of the sample, the camera may not be placed too close to the samples. The camera must also not be too far away as this will mean that the number of pixels per unit of length will decrease. The true diameter of the test sample is given by d_s and the camera measurement of the sample diameter is given by d_c. The difference between the real diameter and the diameter measured by the camera is governed by the distance l_c which is the distance of the camera to the centre of the sample. As the distance increases x will become smaller and d_c will approach d_s. This can be proven with the following equations:

$$\sin\alpha = \frac{d_s}{2\,l_c} = \frac{2\,x}{d_c} \quad \rightarrow \quad x = \frac{d_s\,d_c}{4\,l_c} \tag{13}$$

$$x = \sqrt{\left(\frac{d_s}{2}\right)^2 - \left(\frac{d_c}{2}\right)^2} \tag{14}$$

Combing Eqs. (13) and (14):

$$d_c = \frac{2\,l_c\,d_s}{\sqrt{d_s^2 + 4\,l_c^2}} \tag{15}$$

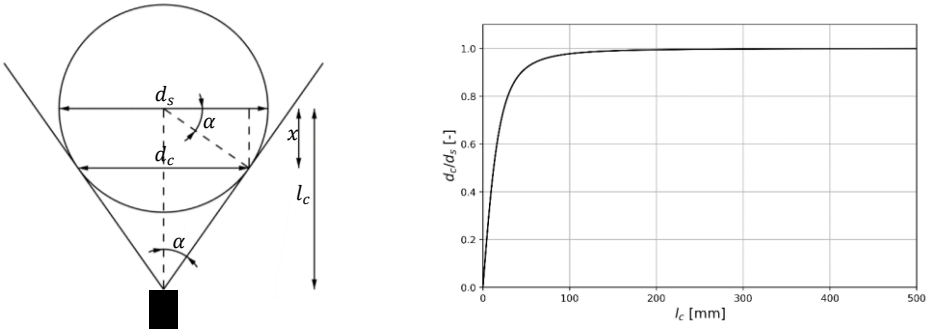

Figure 27: Schematic overview of a camera recording a sample and a plot of the camera distance l_c against the normalised measured sample diameter d_c/d_s .

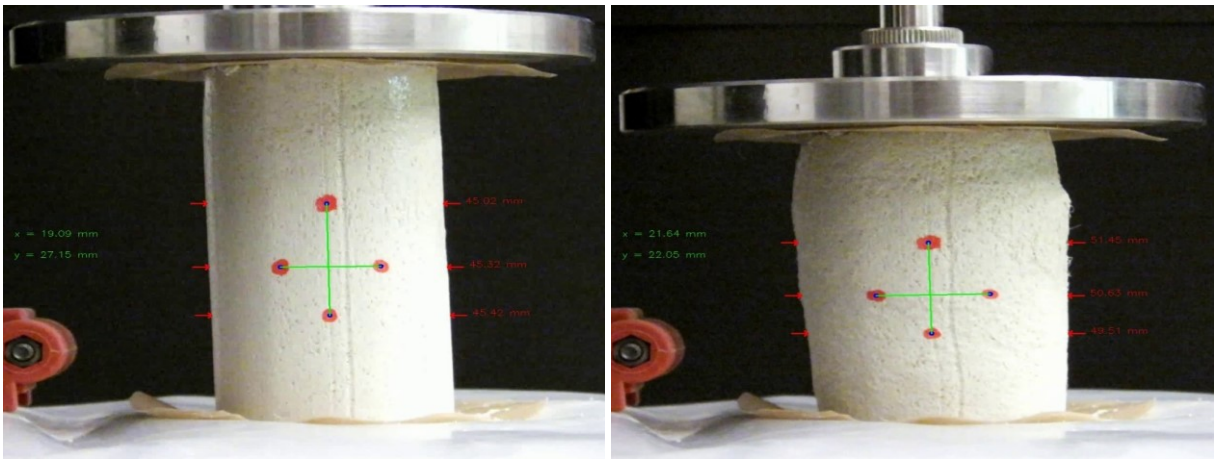

Figure 28: Automatic detection of sample width and height at the start of a test and halfway through a test of a sample at an age of 15 min.

From the plot in Figure 27 it can be concluded that from a distance of ~200 mm there is no significant difference between the real sample diameter and the measured diameter by the camera. Therefore, during the experiments, the camera was placed at a distance of more than 200 mm away from the sample.

As a large number of samples was going to be tested, a script was written to automatically track the deformations of the samples. This was done by making use of the OpenCV module in Python. To be able to locally detect deformations of the samples, red dots were painted on the samples (measured by the green lines in Figure 28). The red dots also function as a marker to track the deformation of the edges of the samples at specific heights (shown by the red arrows in Figure 28). Furthermore, to create a large contrast, the white samples were tested in front of a black background. The large contrast allowed for an accurate edge detection of the samples by the script. Camera measurements on the samples were taken every second until large cracking of the samples occurred. As large cracks propagate through the sample it was not possible anymore to take accurate measurements.

Before starting the experiment, a picture of a marker was taken to be used for calculating the number of pixels per mm (see Figure 29). This procedure was repeated for each testing day as the camera position may have changed. The marker has black circles with a diameter of 30 mm drawn on a white background, which allowed for automatic detection in the written script. The accuracy of the measurements proved to be ~0.1 mm per pixel.

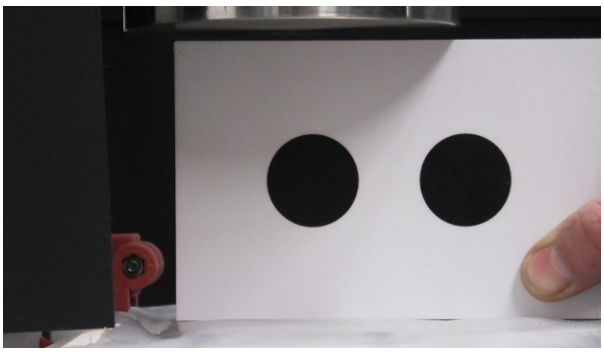

Figure 29: Picture of a marker, which was taken before each experiment.

5.1.1.3 Confidence interval and required number of samples

It is assumed that in the experiment similar variances are to be expected as obtained in experiments conducted by Wolfs et al. [11] at the TU Eindhoven. Therefore, the number of samples to reach a desired confidence level can be calculated according to the following:

If $X_1, \dots, X_n$ is a random sample from an $N(\mu, \sigma^2)$ distribution, then $\bar{X}_n$ has an $N(\mu, \sigma^2/n)$ distribution, and from the properties of the normal distribution we know that $\frac{\bar{X}_n - \mu}{\sigma/\sqrt{(n)}}$ has a $N(0,1)$ distribution. If c_l and c_u are chosen such that $P(c_l < Z < c_u) = \gamma$ for an $N(0,1)$ distributed random variable Z, then:

$$\gamma = P\left(c_l < \frac{\bar{X}_n - \mu}{\sigma/\sqrt{n}} < c_u\right) = P\left(\bar{X}_n - c_u \frac{\sigma}{\sqrt{n}} < \mu < \bar{X}_n - c_l \frac{\sigma}{\sqrt{n}}\right) \tag{16}$$

We have found the upper and lower bound for the true mean μ:

$$L_n = \bar{X}_n - c_u \frac{\sigma}{\sqrt{n}} \quad and \quad U_n = \bar{X}_n - c_l \frac{\sigma}{\sqrt{n}} \tag{17}$$

The interval (L_n, U_n) covers μ with probability γ. Therefore, the interval $\left(\bar{x}_n - c_u \frac{\sigma}{\sqrt{n}}\ ,\ \bar{x}_n + c_l \frac{\sigma}{\sqrt{n}}\right)$ is a $100\,\gamma\%$ confidence interval for μ of a dataset. A common choice is to divide $\alpha = 1 - \gamma$ between the tails, that is, to solve c_l and c_u from:

$$P(z \geq c_u) = \alpha/2 \quad and \quad P(z \leq c_l) = \alpha/2 \tag{18}$$

So that $c_u = z_{\alpha/2}$ and $c_l = z_{1-\alpha/2} = -z_{\alpha/2}$. Summarizing, the $100(1-\alpha)\%$ confidence interval for μ is:

$$\left(\bar{x}_n - z_{\alpha/2} \frac{\sigma}{\sqrt{n}}\ , \bar{x}_n + z_{\alpha/2} \frac{\sigma}{\sqrt{n}}\right) \tag{19}$$

Using this, the sample size can be determined. When the desired confidence level is γ, the width of the confidence interval will be equal to $2 \cdot z_{\alpha/2} \frac{\sigma}{\sqrt{n}}$. Requiring that this is at most w means finding the smallest n that satisfies:

$$2 \cdot z_{\alpha/2} \frac{\sigma}{\sqrt{n}} \leq w \tag{20}$$

Leading to:

$$n \geq \left(\frac{2 \cdot z_{\alpha/2}\, \sigma}{w}\right)^2 \tag{21}$$

For this study a 95% confidence interval is aimed for with an upper and lower bound of the true mean μ equal to:

$$L_n = \bar{x}_n - 0.1\,\bar{x}_n \quad and \quad U_n = \bar{x}_n + 0.1\,\bar{x}_n \tag{22}$$

Meaning a maximum deviation of $\pm$10% around the mean will be accepted as accurate enough in this study. Hence, it follows that the allowable interval width w is at most:

$$w = 2 \cdot 0.1\,\bar{x}_n \tag{23}$$

The relative deviation of the interval limits from the mean, defined by $1 - \mathrm{w}/(2\,\overline{\mathrm{x}}_\mathrm{n})$, will be referred to as RDOM in the results section. When RDOM is larger than 10% the desired accuracy is not reached. Table 3 displays the Young's moduli at different ages as obtained by Wolfs et al. and the number of samples that have to be tested according to this data given a confidence interval $\gamma = 95\%$ and the defined interval width w. As $\alpha = 0.05$, the right tail probability of the standard normal distribution is equal to $z_{0.025} = 1.96$. Based on the number of samples stated in Table 3 it was decided to conduct at least 19 compression tests at each age. The exact number of samples that will be tested is given in 5.1.3.

Table 3: Young's modulus with average values μ, standard deviation σ and relative standard deviation RSD, obtained from the uniaxial compression test performed by Wolfs et al. [11]. The number of samples are determined with a confidence interval of 95% and an interval width w defined in Eq. (23).

Age [min]	μ [MPa]	σ [MPa]	RSD	Interval width [MPa]	Number of samples
0	0.074	0.015	20%	0.015	16
15	0.099	0.022	22%	0.020	19
30	0.117	0.016	14%	0.023	7
60	0.154	0.021	14%	0.031	7
90	0.186	0.036	19%	0.037	14

5.1.2 Printing experiment

The second part of the experimental programme consists of printing two relatively simple objects: a cylinder and a square tube. The goal of the printing experiment is to capture the way the prints deform during printing and how they collapse. The results will be used to validate the FE models with material properties derived from the uniaxial compression tests. In this experiment it is desirable that the objects collapse at a later stage than currently available in literature, to also verify the behaviour of the models for prints that are printed over a longer duration of time. Moreover, the printing experiment is used to characterize the printing process itself in terms of reliability, predictability and consistency.

5.1.2.1 Pilot test: stability of prints

Also for this part of the experiment a pilot test was performed to make sure the objects collapse during the experiment. The cylinder and the square tube that were tested in this pilot are shown in Figure 30. The cylinder had a diameter (d) of 500 mm, a layer width (w) of 50 mm, a layer height (l) of 10 mm and was printed at a speed of 11.7 seconds per layer. The print already collapsed after printing 36 layers (~7 min.). The square tube had sides (h) measuring 500 mm, a layer width (w) of 50 mm, a corner radius (R) of 50 mm, a layer height (l) of 10 mm and was printed at a speed of 14.1 seconds per layer. This print collapsed after printing 106 layers (~25 min.).

Because the cylinder collapsed too fast it was decided to alter the diameter of the cylindrical print to increase the length of the printing path. This improves the stability as the vertical building rate is decreased. To increase its stability even more the width of the path is increased slightly by 5 mm. The dimensions of the cylinder that was used at the start of the experiment is shown in the table in Figure 30 and referred to as print C1. The collapse of the square tube happened after a satisfactory amount of time. To slightly increase the moment of collapse the width of this print was also increased by 5 mm. The dimensions of the square tube that was used at the start of the experiment is shown in the table in Figure 30 and referred to as print S1.

5.1.2.2 Procedure

During a single test day print C1 was printed three times at different speeds, after which print S1 was printed three times at different speeds. As the printing system of Bruil is not controlled by printing speed but rather by output volume, the output volume was changed between prints. This indirectly controls the printing speed of the robot. The printing speed of consecutive cylindrical prints is increased by approximately 10%. The printing speed of consecutive square tubes is increased by approximately 20%.

Throughout the testing days, the three speeds at which C1 and S1 are printed are kept the same. However, sometimes failure of the prints did not occur, even when printed at a relatively high speed. The printing speed was then sometimes increased even further to initiate failure. Therefore, on some testing days the objects are printed at speeds that do not occur on any other day.

The maximum height of both prints is equal to 1500 mm. Therefore, print C1 is finished after printing 150 layers and a maximum of 214 layers can be printed of print S1. For each print it is registered whether

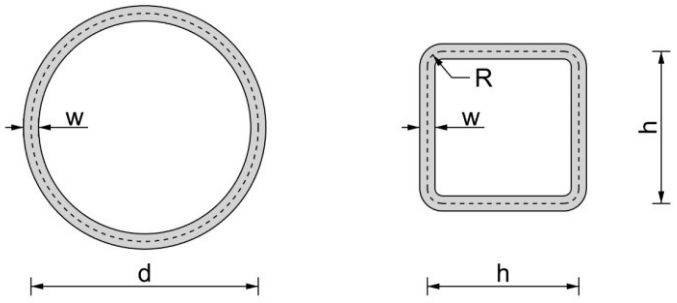

Cylinder				Square tube				
Print	**d [mm]**	**w [mm]**	**l [mm]**	**Print**	**h [mm]**	**w [mm]**	**R [mm]**	**l [mm]**
C1	750	55	10	S1	500	55	50	7
C2	750	50	10	S2	500	50	50	7
				S3	700	50	50	7

Figure 30: Printed objects during experiment and corresponding dimensions. The layer height is represented by the letter l.

Figure 31: Camera setup for monitoring the prints.

it collapses and/or if it showed large deformations. When a print did collapse, the number of layers at which it collapsed is denoted. To save material during the experiment, some prints were stopped prematurely. These prints reached a height at which still no noteworthy deformations occurred, and collapse was very unlikely. Based on experience of the operators with other prints and the experience gained with this particular print it was then decided to stop a print. Furthermore, prints either collapsed or were prematurely stopped within 45 minutes.

All prints are recorded with a camera. By filming the printing process, the behaviour of the objects during printing could be tracked. These recordings can then be used for comparisons with numerical analyses of the objects. Figure 31 shows a picture of the camera setup during printing session. Furthermore, during the printing of the objects the following parameters were logged every 5 minutes: Temperature of the print, temperature of the water, temperature of concrete in the mixer, pressure in the hose and pressure at the printer head. All temperatures are measured with an infrared thermometer. The form that was used to monitor the prints can be found in Appendix C: Forms used during experiments.

Although a pilot tests had been conducted before commencing the experiment, the prints proved to be much more stable than expected and did not always collapse. Sometimes the objects were perfectly straight, sometimes they were deformed and other times they collapsed. While the intent was to purposely collapse the prints, this behaviour demonstrated the unreliability of the printing process and proved to be valuable information on the deformational behaviour during long printing sessions.

To increase the probability of failure it was decided to alter the geometry of the print C1 after four days of testing. Hence, there are two different cylinders: C1 and C2. The geometry of square tube S1 was also changed after four days of testing. This change didn't work out as planned and the print was therefore altered for a second time after two days. So, three different square tubes were printed: S1, S2 and S3. The dimensions of the prints are shown in Figure 30. Besides changing the geometry of the prints, the printing speed and increments in speed between consecutive prints was also increased.

5.1.3 Planning of the experiment and grouping of results

To make optimal use of the two-week renting period of the testing rig, a tight schedule has been used to conduct the printing experiment and test the required number of samples at the same time. To fit as many test as possible in a single day it was decided to split a testing day into two batches. Hence, the wall from which the samples are extracted is printed twice a day. After the samples have been extracted from the wall, three cylinders are printed. After that, a second wall is printed from which samples are extracted. Then, three square tubes are printed.

Samples originating from the wall that is printed first are referred to as samples from batch 1 (B1). Samples originating from the second wall are referred to as samples from batch 2 (B2). The printing experiment is deliberately performed on the same days as the uniaxial compression tests. The mechanical properties that are derived from the uniaxial compression tests of samples from B1 and B2 can than possibly be related directly to the behaviour of the cylindrical and tubular print, respectively. Moreover, the behaviour of prints on a single testing day can be related to the results of the samples from both B1 and B2.

At each age, two samples are tested. Hence, each batch consists of 14 samples at room temperature and 12 samples at elevated temperature. It is not possible to test two samples at the same time. Therefore, ages discussed previously (e.g.: 0, 15, 30, 60, 90, 120 and 180 min. for samples stored at room temperature) are not the exact ages at which the samples will be tested, but rather act as guidelines and samples will be tested around these ages. Samples that differ in age by 4 min. are deemed comparable in terms of mechanical properties. Therefore they are grouped together.

The samples that were stored at room temperature were tested for the first five days. These days are denoted with an 'R' in the results. After that, one day was reserved to test working with the oven and to determine the effect of different temperatures. This day will be referred to as 'extra day'. On this day samples were stored at a temperature of 35 °C and at 45 °C. As there was no significant difference between the results of the two, it was decided to conduct experiments at a temperature of 35 °C for the remaining 4 days. Besides that, a temperature of 35 °C seemed like a value that can easily be maintained in practice if it was decided to use a heated system in the future. The days at which samples were stored in the oven are denoted with an 'H' in the results section.

140 samples stored at room temperature are tested during the first five days. Another 10 samples have been tested on the extra day at ages of 15, 30, 60, 90 and 120 min. Therefore, a total of 22 samples have been tested at these ages and 20 samples at the other ages. For all ages considered, the samples had an average age that was slightly different than their intended test time: 9, 16, 32, 61, 91, 121 and 181 min. As the tested samples have an age somewhere around these ages, the results are reported within ranges. Ranges have been defined in time segments of four minutes (a maximum of two minutes around the average is allowed). The defined ranges and the number of samples contained in each range are stated in Table 4.

Table 4: Ranges of ages and the number of samples in each range for samples stored at room temperature.

Range [min.]	[7-11]	[14-18]	[30-34]	[59-63]	[89-93]	[119-123]	[179-183]
Number of samples	19	22	21	22	18	19	19

Some of the ranges stated in Table 4 contain less than 20 or 22 samples. This does not mean that less samples have been tested at these ages. For instance, some samples were tested at an age of 12 min. and therefore fall outside the range. These samples will be discarded when a direct comparison of samples inside a particular range is made. These samples are however included in the results when the development of mechanical properties over the full testing period is considered.

A total of 96 samples sored at 35 °C were tested divided over four days. This means that 16 samples have been tested at each age. Also, for these samples the real age of each sample is somewhere around the age that was aimed for. The average ages encountered during the experiment are 16, 31, 46, 61, 76 and 91 min. Again, the results will be reported in time ranges of 4 minutes. The defined ranges and the number of samples contained in each range are stated in Table 5. Also here, the ranges contain less than 16 samples. The samples that fall outside a range are treated the same way as stated in previous paragraph.

Table 5: Ranges of ages and the number of samples in each range for samples stored at 35 °C.

Range [min.]	[14-18]	[29-33]	[44-48]	[59-63]	[74-78]	[89-93]
Number of samples	16	16	15	16	15	14

To conduct the experiments three persons were needed. One person operates the printer and takes the measurements of the printing experiment. The other two persons conduct the compression tests, where one operates the testing rig and the other one demoulds the samples, weighs them and prepares the moulds for reuse in the next batch.

A Gantt-chart was made that could be adapted each testing day based on the exact starting time of the experiment. With this tool it was possible to monitor the exact time at which demoulding of a sample should take place to test it at the correct time. Furthermore, as during the uniaxial compression test the

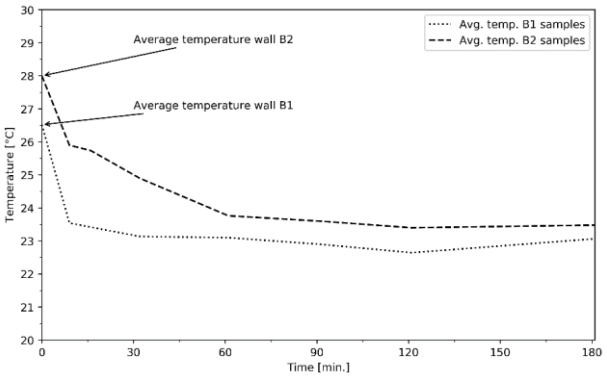

Figure 32: Average temperature of samples stored at room temperature at the moment of testing.

printing experiment was also taking place, careful planning was needed to print the second batch on time. To finish a testing day on time, part of batch 1 and batch 2 were run in parallel. The testing days of the heated samples didn't have to run parallel as testing only lasted up to 90 min. This left enough time to conduct the experiments in series. The Gannt-charts used for the experiments can be found in Appendix D: Gantt-charts.

5.2 Results uniaxial compressive test

The results are divided into two parts: The uniaxial compression tests and the printing experiments. The uniaxial compression test results are further subdivided into three parts: samples tested at room temperature, samples tested at elevated temperatures and comparisons between both groups.

5.2.1 Samples tested at room temperature

During the course of the five testing days and the extra day the average measured water content was 15.18%, with a relative standard deviation of 2.1%. The average measured air content was 6.1% with a relative standard deviation of 1.8%. These values indicate that throughout all testing days, the fresh concrete mix was very constant. The average density of the samples is 2203 kg/m^3 , measured with a relative standard deviation of 1.3%. The Poisson's ratio was approximately constant at 0.36 over all ages.

Figure 32 shows the average temperatures of the samples over time. A distinction has been made between samples of batch 1 and batch 2. The average temperatures of the walls from which samples are extracted are included too. The fact that wall B2 has a higher average temperature than wall B1 suggests that over the course of the printing experiment, heat accumulates in the printing system causing a temperature difference between wall B1 and B2. For both batches the samples cool down to approximately the same temperature. In range *[29-33]* the average temperature of a sample from wall

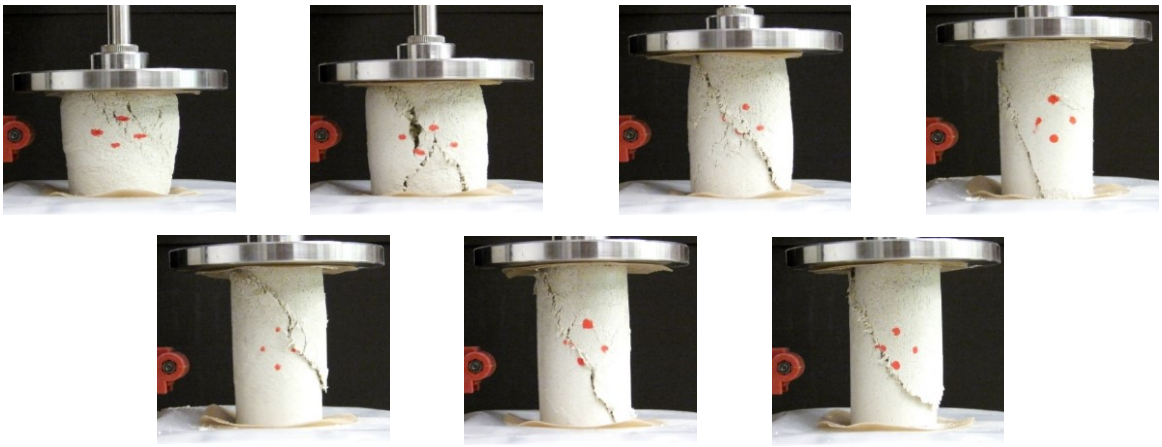

Figure 33: Typical failure behaviour of concrete samples at different ages. Top row from left to right: [7-11], [14-18], [30-34] and [59-63]. Bottom row from left to right: [89-93], [119-123] and [179-183].

B2 is 7.6% higher than a sample from wall B1. After this, the difference between B1 and B2 reduces to 1.8%.

Typical failure patterns of samples at each range are shown in Figure 33. The youngest samples fail by bulging while in older samples a clear failure plane develops. It was also observed that before failure lateral deformations are considerable for samples up to an age of 60 minutes, while lateral deformations are small for older samples. Furthermore, it was noticed that the failure plane gradually developed at younger samples whereas a sudden failure occurred in older samples.

5.2.1.1 Load-displacement data

The load-displacement data of the uniaxial compression tests are shown in Figure 34 and 35. It appears to be that the results can be divided into two groups, as the behaviour of a group of samples is less stiff and the compressive strength lower than the majority of the samples. From samples with an age of 30 min. and older the difference is clearly visible. The black lines in Figure 34 indicate the samples that clearly lag behind all other samples at the same age. These samples originate from B1 and B2 of the first test day and from B1 of the second test day. Samples from B2 of the second test day do not show different behaviour and their stress-strain behaviour is comparable to the rest of the population.

That there can be a relatively large between the weakest and strongest samples was anticipated based on the expected variability of the mechanical properties. However, a more continuous-like spread in results would be expected from this type of experiment and not a clear distinction between two groups of samples. As will be shown later, the samples that were stored in the oven do show such a continuous spread in results.

A possible explanation of the split in results is the fact that after test day two a part of the printer head had been revised during a regular maintenance check. It may well be that this revision has a significant impact on the mechanical properties of the fresh concrete. Either due to enhanced compaction or increased friction leading to more heat accumulation inside the printer head. Also, significantly less collapses and smaller deformations were observed in the printing experiment after day two. Why the samples of B2 of day two do have a load-displacement curve that fits in with the majority of samples is not clear. As all the samples of day 1 and the samples of B2 of day 2 highly influence the results, these samples are excluded from further analysis.

For some of the samples in range *[179-183]* the capacity of the testing rig (2500 N) was reached. Therefore the peak load of these samples could not be measured. It also explains the spikes in the average curve of this range as suddenly some samples are not taken into account anymore.

As samples are older, peak forces increase and the applied displacement before reaching failure gets shorter. It is also observed that concrete of older age has a more distinct peak than at a younger age and softening behaviour is getting shorter. Also, as samples increase in age a kink starts to develop in the load displacement diagrams. This kink starts developing at samples in range *[30-34]* until range *[119-123]*. For samples of the oldest age, the kink has partly disappeared and is not visible anymore on the average curve.

From range *[59-63]* and onwards the load-displacement diagrams show a partly horizontal plateau at the start of the test. This indicates that a displacement is applied to the samples without any or little resistance.

5.2.1.2 Stress-strain data

The stress-strain diagrams per range are depicted in Figure 36, with the average stress strain curves indicated with a solid black line. As after the peak loads have been reached significant cracks occur in a sample, area corrections performed with camera measurements are highly inaccurate and post-peak behaviour is included only for illustration purposes. Graphs should therefore not be used to model the softening behaviour. As the softening behaviour of the concrete is not of interest the post-peak behaviour will not be further discussed.

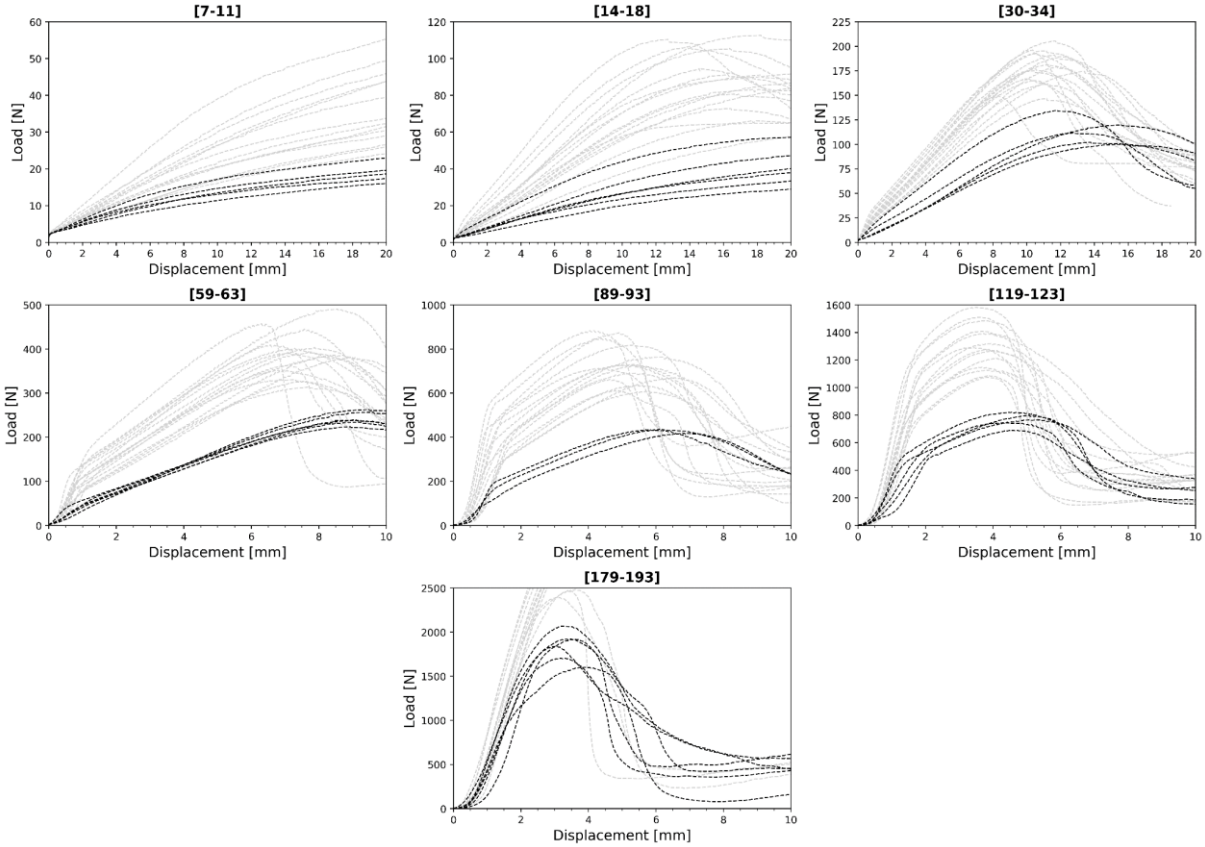

Figure 34: Load-displacement curves of samples tested at room temperature. The black lines indicate samples that are clearly weaker than the rest of the population at the same age. Please mind the different scales of the axes.

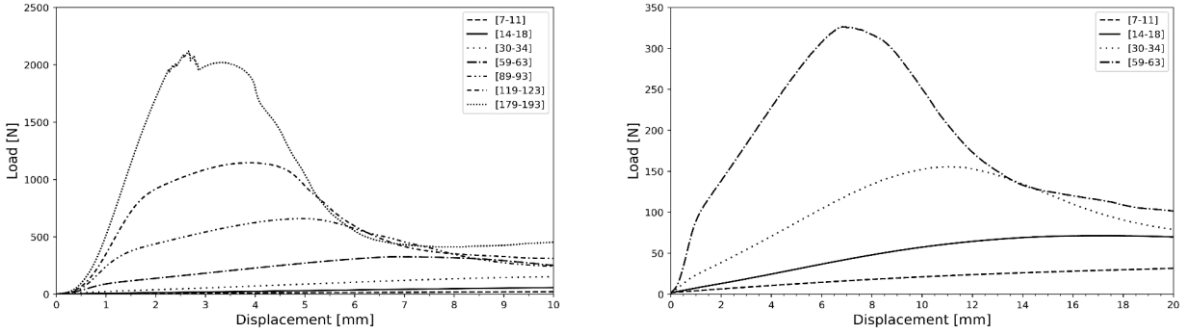

Figure 35: Average load-displacement curves of samples stored at room temperature. Left: all ranges. Right: until range [59-63]. Please mind the different scales between the graphs.

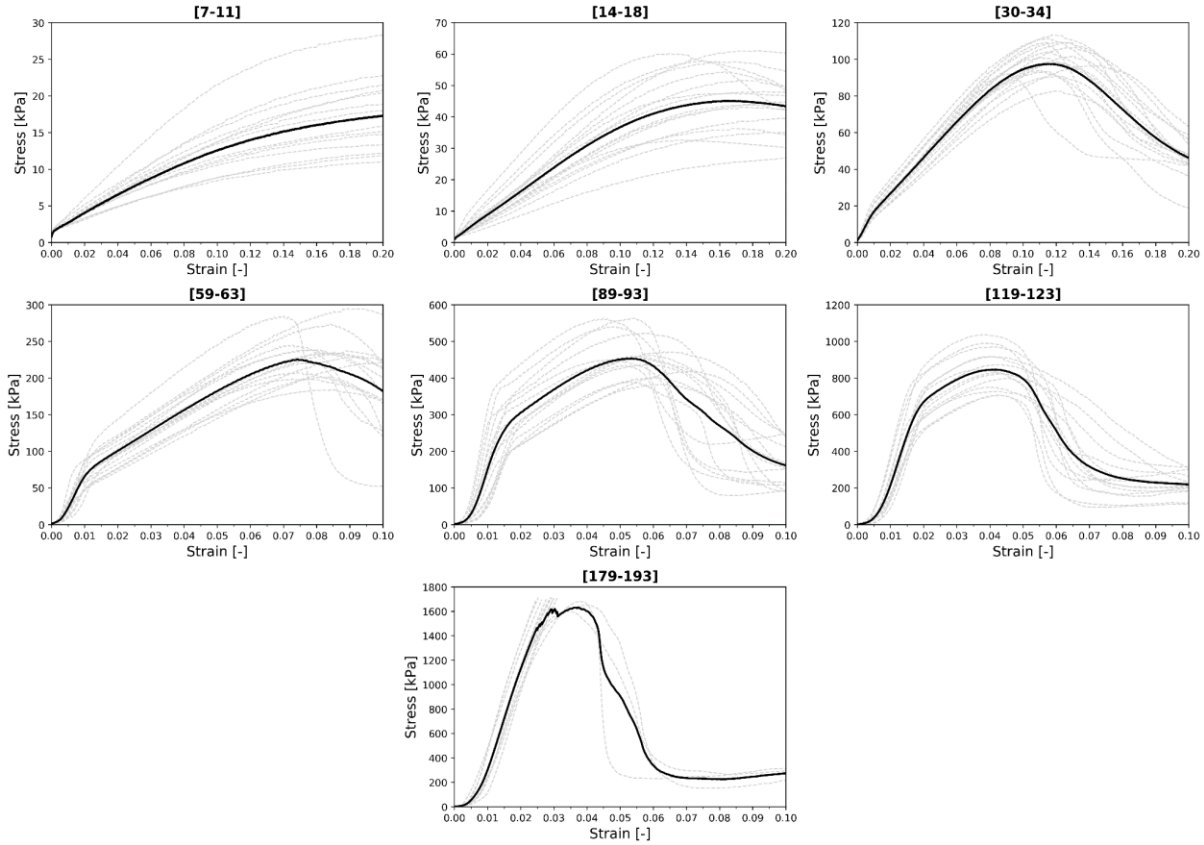

Figure 36: Stress-strain relationships of samples tested at room temperature. The black line indicates the average results. Please mind the different scales of the axes.

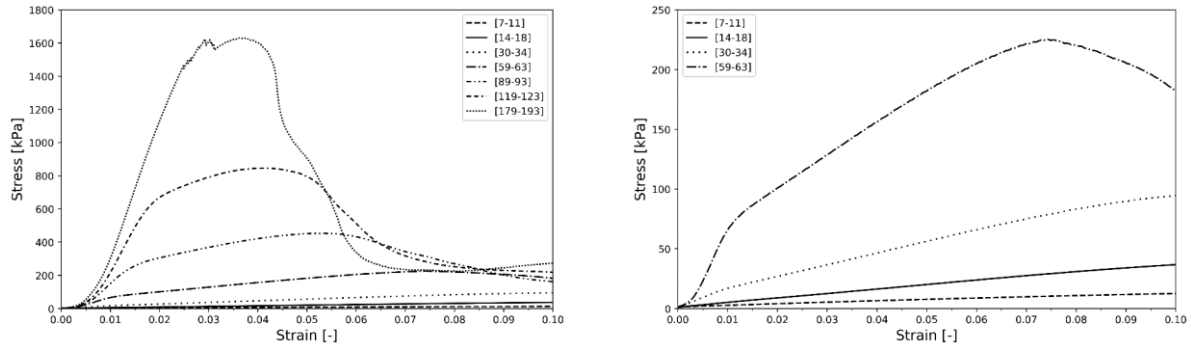

Figure 37: Left: Average stress-strain curves of samples tested at room temperature of all ranges. Right: Average stress strain curves of samples tested at room temperature until range [59-63]. Please mind the different scales between the graphs.

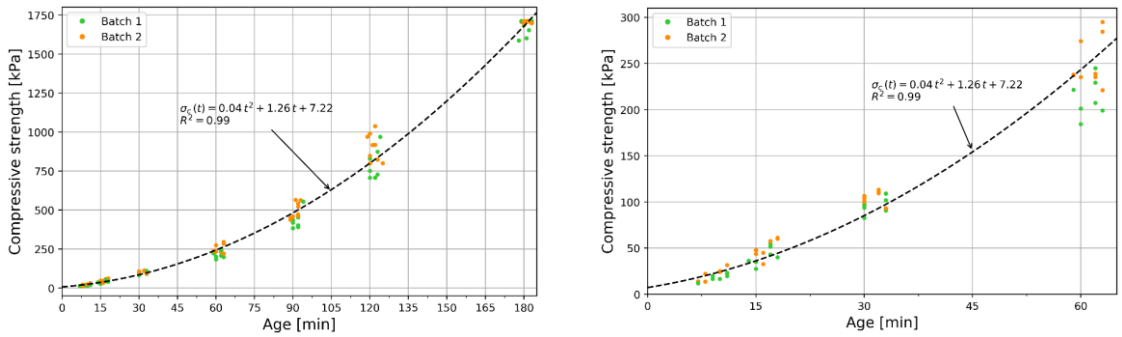

Figure 38: Development of compressive strength over time of samples tested at room temperature with a second order polynomial fit. A distinction is made between samples tested in batch 1 and samples tested in batch 2. Left: full test range. Right: close up of the left graph until an age of 65 min.

The average curves have been plotted together in Figure 37 to indicate the development of the material properties over time relative to each other. The results are shown for all time ranges up to a strain of 10%. As material properties significantly increase over time, close-ups of the first 60 minutes are stated as well. Moreover, prints printed during the printing experiment were finished within 60 minutes.

Similar observations that were made for the load-displacement data can be made for the stress-strain relationships. The peak stress, as well as the initial stiffness, increases as samples are older. As samples reach an age of 30 minutes, a kink starts to develop that divides the curve into two separate linear parts before the ultimate stress is reached. This indicates that from this moment a strain hardening effect starts to develop in the samples that becomes even more pronounced in older samples and fades away again when samples reach an age of 180 min. At the moment of onset of the hardening behaviour no visible cracks observed in the test samples. Furthermore, it is noticed that from range *[59-63]* and onwards the stress-strain diagrams show a partly horizontal plateau at the start of the test. Reasons for the development of such behaviour will be discussed in section 5.4**.**

The compressive strength is measured as the maximum stress in each sample. The development of the compressive strength is shown in Figure 38. The development over time can be approximated very well with a quadratic polynomial:

$$\sigma_{c,rt}(t) = 0.04\,t^2 + 1.26\,t + 7.22 \tag{24}$$

with t in minutes and σ_c in kPa. The polynomial fit yields an excellent fit to the full testing range of three hours. By extrapolating the fitted curve to 0 minutes, the initial strength of the concrete is determined as 7.2 kPa. A distinction has been made between samples tested in batch 1 and samples tested in batch 2. It can be observed that at all ages, the strongest sample was a sample from batch 2 and the weakest sample was a sample from batch 1. Not all samples tested in batch 2 are stronger than samples tested in batch 1. It is however observed that on an overall basis test results of samples tested in batch 2 are stronger than samples tested in batch 1.

The Young's modulus was measured at a strain of 5% for samples up to and including range *[30-34]*. At this moment the strains are still well within the elastic limit. The Young's moduli of samples of older age have been measured as the tangent of the first straight part of the stress-strain curve, as stresses are not expected to rise beyond this first linear part of the curve (i.e.: when a print is printed at a speed of 15 s/per layer (which is considered very fast) with a layer height of 10 mm, the stress in the bottom layer will be approximately equal to 53 kPa after 61 min. of printing ($\sigma = \rho g h_p$)).

The development of the Young's modulus over time is different than the development of the compressive strength over time and cannot be approximated by a second order polynomial (as seen in Figure 39). A different development is observed in the first 30 minutes than in the range of 60 to 180 minutes. Therefore, the evolution of the Young´s modulus over time can be described with the following equations:

$$E_{rt}(t) = \begin{cases} 119.8\,e^{0.0727\,t}, & t < 51.13 \\ 622.8\,t - 26910.4, & t \geq 51.13 \end{cases} \tag{25}$$

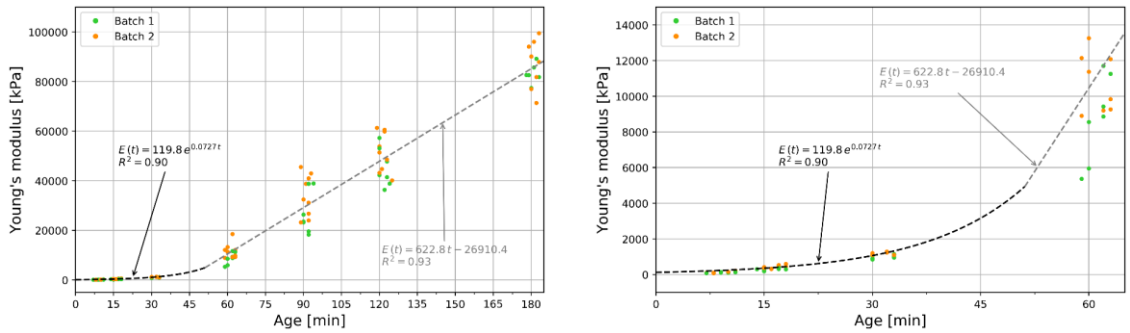

Figure 39: Development of the Young's modulus over time of samples tested at room temperature. A distinction is made between samples tested in batch 1 and samples tested in batch 2. Left: full test range. Right: close-up of the left graph until an age of 65 minutes.

with t in minutes and E in kPa. The intersection of these two curves is found to be at an age of 50.81 minutes. Meaning that somewhere around this age the development of the Young's modulus changes from an exponential growth rate into a linear growth rate. The exponential fit overestimates the data measured in range of 7 to 11 minutes but fits the other ages very well. When the curve is extrapolated to an age of 0 minutes the initial stiffness of the concrete is found to be 119.8 kPa.

Statistical properties of the compressive strengths and Young's moduli at each time range are given in Table 6 and 7, respectively. An extra range *[8-10]* is provided as it was noticed that a smaller interval at the youngest age reduced the relative standard deviation by 4.5% and 5.9%, respectively. This can be explained by the fact that the range of four minutes is too large for samples with an average age of 9 minutes, as it is nearly equal to 50% of its age. Although the relative standard deviation is decreased by decreasing the time range, the RDOM is increased. This is due to the reduced number of samples contained in the smaller range *[8-10]*. Would there have been more samples, the RDOM would also have been improved. For the other ranges there was no significant effect when the time range was reduced.

When considering the compressive strength of samples with an age higher than in range *[7-14]*, RDOM is near or below the 10% that was aimed for. When considering the RDOM of the Young's moduli at different ages, mixed results have been obtained and the desired accuracy has only been reached for samples in range *[30-34], [119-123]* and *[179-183]*. the RDOM at ages where the desired accuracy has not been reached are still acceptable. Especially when considering the large RSD at some ages and the fact that at all ages 6 samples are discarded due to rejecting samples of day one and two.

Table 6 shows a very low relative standard deviation of samples contained in range *[179 -183]*. This is due to the fact that samples that reach the limit of the testing rig (2500 N) are all reported to fail at the same stress. As a large number of samples reached this limit, it influences the RSD a lot and is therefore not a representative value. The mean is probably also higher than reported but could not be measured due to the limits of the testing rig. The fact that the limit of the testing rig is reached does not influence the Young's moduli measured for this specific range.

Table 6: Compressive strengths derived from the stress-strain relationships of samples stored at room temperature with average values $\bar{x}_n$, standard deviation s_n and relative standard deviation RSD. The interval width of the 95% confidence interval of the mean are given. The relative deviation of the interval limits from the mean is defined by $1 - w/(2\bar{x}_n)$ and denoted as RDOM. Values are based on the Student's t-distribution.

Time range	number of samples	$\bar{x}_n$ [kPa]	s_n [kPa]	RSD	Interval width limits [kPa]		RDOM
					-	+	
[7-11]	14	20	6	28.4%	16	23	16.4%
[14-18]	16	46	10	22.2%	41	52	11.8%
[30-34]	16	101	9	8.7%	96	105	4.7%
[59-63]	16	234	30	13.0%	218	250	6.9%
[89-93]	15	464	59	12.8%	431	497	7.1%
[119-123]	14	850	107	12.6%	788	911	7.2%
[179-183]	13	1693	32	1.9%	1673	1712	1.2%
[8-10]	8	19	5	23.9%	15	23	20.0%

Table 7: Young's moduli derived from the stress-strain relationships of samples stored at room temperature with average values $\bar{x}_n$, standard deviation s_n and relative standard deviation RSD. The interval width of the 95% confidence interval of the mean are given. The relative deviation of the interval limits from the mean is defined by $1 - w/(2\bar{x}_n)$ and denoted as RDOM. Values are based on the Student's t-distribution.

Time range	number of samples	$\bar{x}_n$ [kPa]	s_n [kPa]	RSD	Interval width limits [kPa] -	+	RDOM
[7-11]	14	125	37	29.4%	104	146	17.0%
[14-18]	16	374	108	28.8%	316	431	15.4%
[30-34]	16	1089	123	11.3%	1024	1155	6.0%
[59-63]	16	10358	3065	29.6%	8725	11991	15.8%
[89-93]	15	30384	8977	29.5%	25412	35355	16.4%
[119-123]	14	50131	7922	15.8%	45557	54705	9.1%
[179-183]	13	85744	8127	9.5%	80833	90655	5.7%
[8-10]	8	115	27	23.5%	92	137	19.6%

To be able to compare the results of the printing experiment of the first to days to the results found in the uniaxial compression tests, the results of the compression tests are presented again in Figure 40. However, now the results of day 1 and 2 are included. As relationships between the age and the strength and stiffness are clear now, the results are plotted on a logarithmic scale. From these graphs it can clearly be seen that both the strength and the stiffness of samples in the first two days are lower than the rest of the testing days. The samples of B2 of day 2 do fit in with the rest of the test results. In both graphs these samples are represented by the red dots that clearly fit in with the rest of the results. Possible explanations of this observation will be discussed in section 5.4.

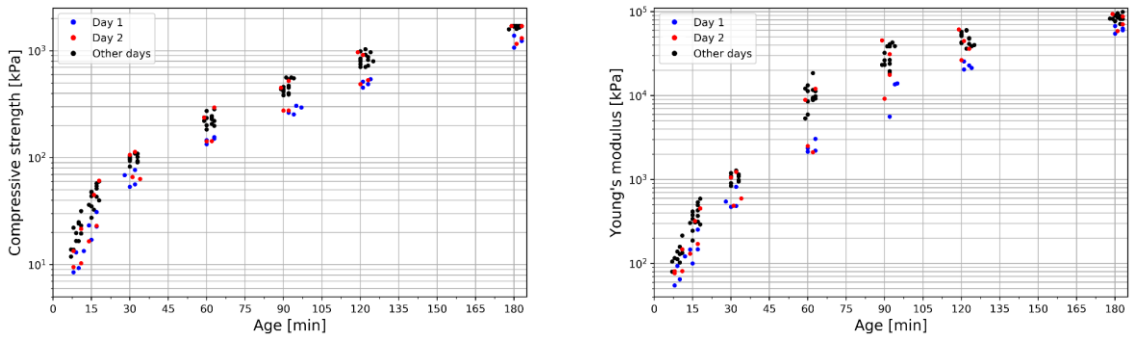

Figure 40: Development of compressive strength (left) and Young's modulus (right) over time in which day 1 and 2 are highlighted to indicate the relatively weak samples on these testing days.

5.2.2 Samples tested at elevated temperature

The average measured water content was 15.34%, with a relative standard deviation of 2.1%. The average measured air content was 6.1% with a relative standard deviation of 1.8%. These values indicate that throughout all testing days, the fresh concrete mix was very constant. Measured densities (2198 kg/m^3) and Poisson's ratio (0.35) are similar to that encountered in the normal test samples.

Figure 41 shows the average temperatures of the test samples over time. A distinction has again been made between samples of batch 1 and batch 2. The walls of B1 had an average temperature of 28.2 °C. The walls of B2 had an average temperature of 29.9 °C. Similar to what was found for the normal

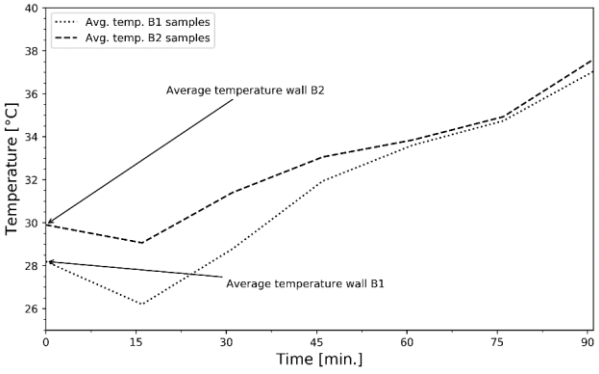

Figure 41: Average temperature of samples stored at 35 °C temperature at the moment of testing.

samples, the average temperature of wall B2 is higher than that of wall B1. During the first 15 minutes the samples cool down. This is attributed to the fact that between extracting and placing samples in the oven, the samples cool down over the course of several minutes. After that, the samples rise in temperature to a level above the storage temperature of 35 °C. This can be explained by the hardening process that is exothermic. The internal heat that is generated during this process leads to an increase in temperature.

5.2.2.1 Load-displacement data

The load displacement data of the heated samples and the average load-displacement diagrams are shown in Figure 42 and 43. A behaviour similar to the samples stored at room temperature is found in the samples stored at 35 °C. The peak load increases considerably over time and the displacement at which this peak is reached becomes less. Again, a kink is found in the load displacement curves as the samples get older. Also, for samples in with an age range *[44-48]* and older the curve develops nearly horizontal until ~0.5 mm.

5.2.2.2 Stress-strain data

The stress-strain diagrams per range are depicted in Figure 44. The average stress strain curves are shown in Figure 45. The results of the first 30 minutes are shown up to a strain of 20% whereas the results of older ages are shown up to 10% stain. The stress-strain behaviour is comparable to that of samples at room temperature. The biggest difference is that peak stresses that could only be reached at an age of 3 hours are now reached within 90 min. Similar to samples tested at room temperature, a kink starts to develop when samples reach an age in the range of 30 minutes, after which a hardening effect is observed.

An exponentially increasing compressive strength over time was observed (see Figure 46). The compressive strength can be described by the following exponential function:

$$\sigma_{c,et}(t) = 25.3\, e^{0.0443\, t} - 11.2 \tag{26}$$

With t in minutes and σ_c in kPa. By extrapolating the fitted curve to an age of 0 minutes, the initial strength of the concrete is determined as 14.1 kPa. A distinction is also made between samples tested in batch 1 and samples tested in batch 2. It is observed that at each age, the strongest sample is a sample coming from batch 2 and the weakest sample comes from batch 1, except for samples with an age of ~90 min. where a sample from batch 1 is strongest. On an overall basis, it is observed that test results of samples tested in batch 2 are stronger than samples tested in batch 1. After 60 minutes this difference becomes less.

The development of the Young's modulus over time is different than the development of the compressive strength over time and cannot be approximated by a single exponential function (see Figure 47). The development of the Young's modulus can be described by an exponential function in the first 60 minutes, but after that the Young's modulus develops linearly. The evolution of the Young´s modulus over time can be described with the following equations:

$$E_{et}(t) = \begin{cases} 51.1\, e^{0.0917\, t}, & t < 62.14 \\ 1769.9\, t - 94735.1, & t \geq 62.14 \end{cases} \tag{27}$$

With t in minutes and E in kPa. The intersection of these two curves is found to be at an age of 62.14 minutes. Meaning that at this age the development of the Young's modulus changes from an exponential function into a linear function. When the curve is extrapolated to an age of 0 minutes the initial stiffness of the concrete is found to be 51.1 kPa.

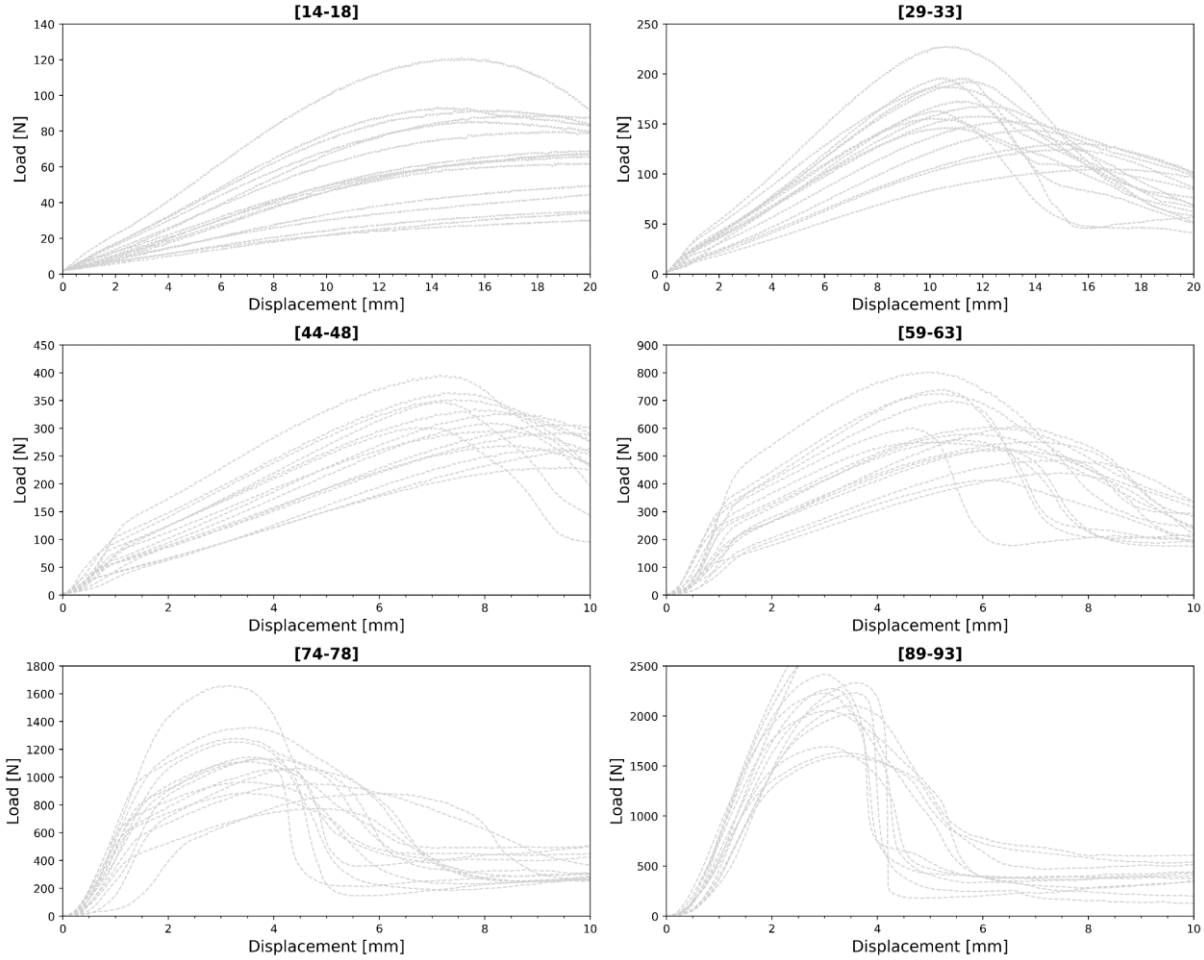

Figure 42: Load-displacement curves of samples tested at elevated temperatures. Please mind the different scales of the axes.

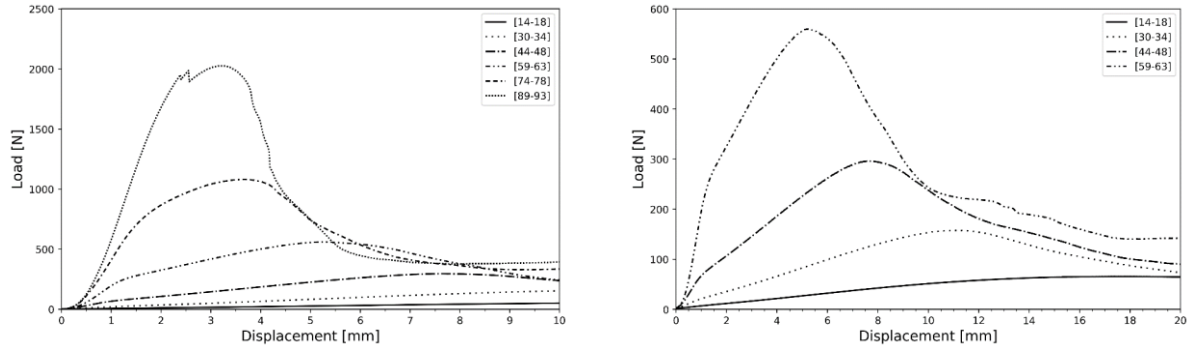

Figure 43: Average load-displacement curves of heated samples. Left: all time ranges considered. Right: samples until an age of one hour.

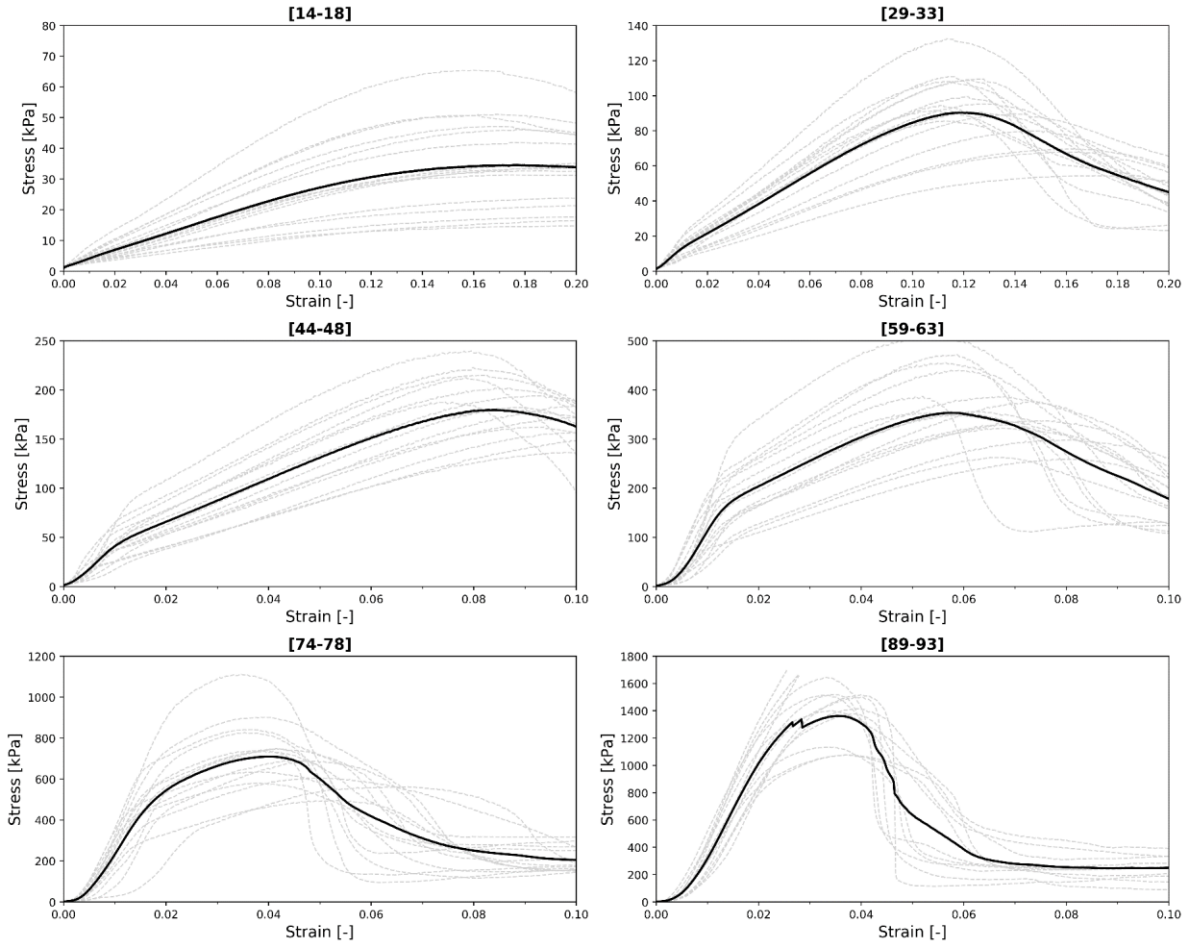

Figure 44: Stress-strain relationships of samples tested at elevated temperatures. The black line indicates the average results. Please mind the different scales of the axes.

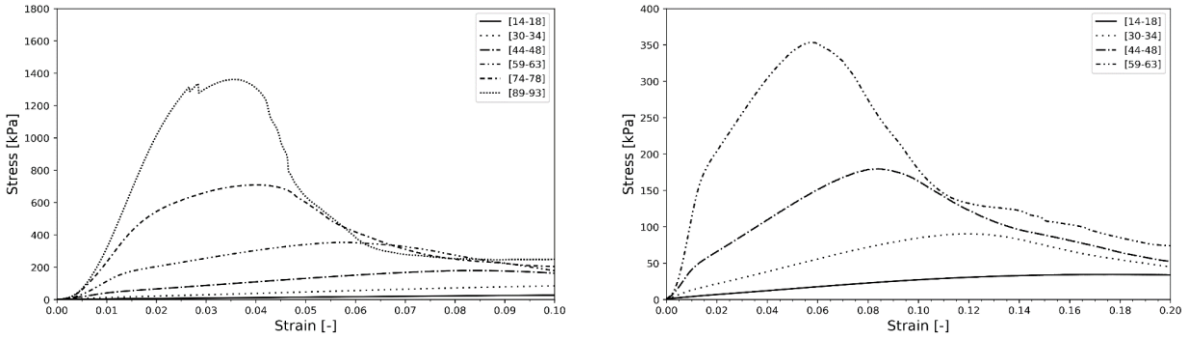

Figure 45: Left: Average stress-strain curves of samples tested at elevated temperatures of all ranges. Right: Average stress strain curves of samples tested at elevated temperatures until range [59-63]. Please mind the different scales between the graphs.

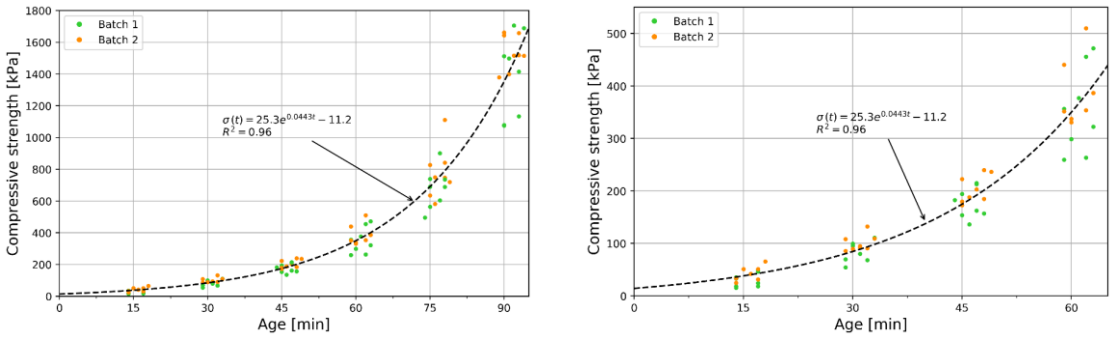

Figure 46: Development of compressive strength over time of samples tested at elevated temperatures. A distinction is made between samples tested in batch 1 and samples tested in batch 2. Left: full test range. Right: close up of the left graph until an age of 65 min.

It is again noticed that the stiffest sample of each age belongs to batch 2 and the least stiff sample belongs to batch 1. The stiffness of samples from batch 2 is generally higher than that of samples from batch 1 when considering an age until 60 min. After this, there is no clear difference between the samples tested in batch 1 or batch 2.

Statistical properties of the strength and stiffness of each time range are shown in Table 8 and 9, respectively. An extra range *[15-17]* is provided as it was noticed that a smaller interval at the youngest age reduced the relative standard deviation by 6.8% and 8.9%, respectively. For the other ranges there was no significant effect when the time range was reduced. The spread in results measured for the compressive strength is much lower than the spread measured for the Young's modulus. The average RSD of the compressive strength is equal to 21.8% whereas the average STD of the Young's modulus is 28.7%. Moreover, the spread of results at range *[14-18]* is much higher than the spread found at any other time range. As mentioned, this is partly caused by the fact that the range of 4 minutes is relatively high for samples of this particular age and is reduced when a smaller range is considered.

When considering the compressive strength, the upper and lower limits of the 95% confidence interval of the mean are near the 10% of the average value that was aimed for. Only at range *[14-18]* min. the limits are higher (21.0%). When considering the RDOM of the Young's moduli, the aimed accuracy has not been reached. Strictly speaking, the accuracy has only been reached for samples in range *[89-93]*.

Similar to the samples in range *[179-183]* min. of samples stored at room temperature, some samples in the range of *[89-93]* min. of the heated samples reached the load capacity of the testing rig. This value was then noted as the compressive strength while the true strength is higher. The results of range *[89-93]* in Table 8 are therefore less accurate than the others and the spread in results is lower. The fact that the limit of the testing rig is reached does not influence the Young's as this is measured way before failure.

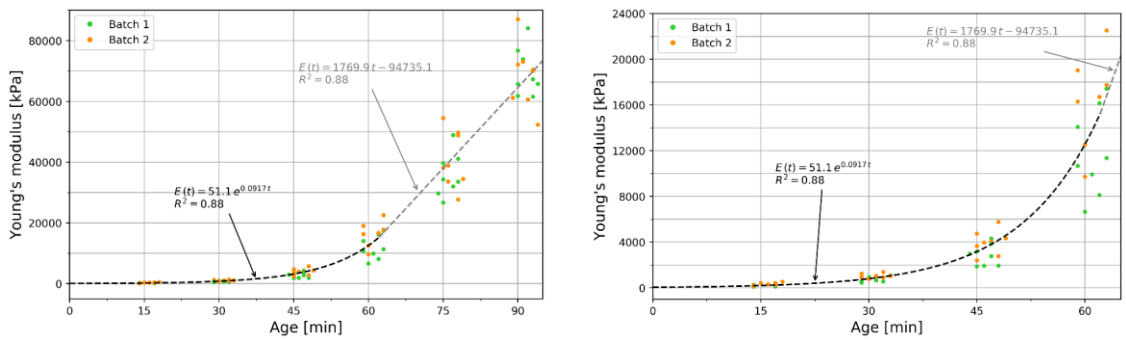

Figure 47: Development of the Young's modulus over time of samples tested at elevated temperatures. A distinction is made between samples tested in batch 1 and samples tested in batch 2. Left: full test range. Right: close-up of the left graph until an age of 65 minutes.

Table 8: Compressive strengths derived from the stress-strain relationships of samples stored at 35 °C with average values $\bar{x}_n$, standard deviation s_n and relative standard deviation RSD. The interval width of the 95% confidence interval of the mean are given. The relative deviation of the interval limits from the mean is defined by $1 - w/(2\bar{x}_n)$ and denoted as RDOM. Values are based on the Student's t-distribution.

Time range	number of samples	$\bar{x}_n$ [kPa]	s_n [kPa]	RSD	Interval width limits [kPa] -	+	RDOM
[14-18]	16	36	14	39.5%	28	43	21.0%
[29-33]	16	93	19	20.7%	83	103	11.0%
[44-48]	15	187	28	15.2%	171	203	8.4%
[59-63]	16	369	72	19.4%	331	407	10.4%
[74-78]	15	727	154	21.1%	642	812	11.7%
[89-93]	14	1442	214	14.8%	1319	1566	8.5%
[15-17]	8	39	13	32.7%	28	49	27.4%

Table 9: Young's moduli derived from the stress-strain relationships of samples stored at 35 °C with average values $\bar{x}_n$, standard deviation s_n and relative standard deviation RSD. The interval width of the 95% confidence interval of the mean are given. The relative deviation of the interval limits from the mean is defined by $1 - w/(2\bar{x}_n)$ and denoted as RDOM. Values are based on the Student's t-distribution.

Time range	number of samples	$\bar{x}_n$ [kPa]	s_n [kPa]	RSD	Interval width limits [kPa] -	+	RDOM
[14-18]	14	274	124	45.3%	202	346	26.2%
[29-33]	16	915	252	27.6%	780	1049	14.7%
[44-48]	16	3350	1129	33.7%	2749	3952	18.0%
[59-63]	16	14104	4409	31.3%	11754	16453	16.7%
[74-78]	15	38491	8646	22.5%	33703	43279	12.4%
[89-93]	14	70403	8278	11.8%	65623	75182	6.8%
[15-17]	8	308	112	36.4%	214	401	30.4%

The development of the compressive and the Young's modulus over time are again presented in Figure 48 on a logarithmic scale. This time a distinction is made between the two weakest days of this test series and the other days. Even though there is not a clear distinction between testing days as was found in the results of the samples tested at room temperature, samples from day 2 and 4 are relatively weak. Interestingly, samples tested on day 2 produce both the weakest samples as well as the strongest samples on day 2. Investigating this day further, it was found that the stronger samples are all from batch 2 and the weaker samples are all from batch 1. Possible explanations of this phenomenon will be discussed in 5.4.

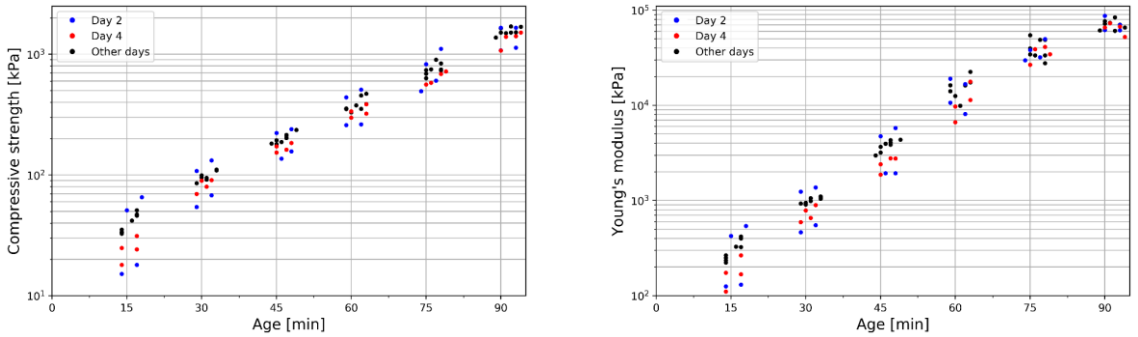

Figure 48: Development of compressive strength (left) and Young's modulus (right) over time of samples tested at elevated temperatures, in which day 2 and 4 are highlighted to indicate the relatively weak samples of these testing days.

5.2.3 Comparisons

The development of the compressive strength over time of both the samples tested at room temperature and samples tested at elevated temperatures are shown in Figure 49. From these graphs can be concluded that heating of the 3D printed concrete has a positive influence on the compressive strength of the concrete. The effect of heating of the concrete becomes apparent at an age of 45 minutes. At this age the strength of the heated concrete starts to develop at a higher rate than the concrete at room temperature.

Table 10 shows a comparison between the statistical values derived for both the heated samples and the samples tested at room temperature, at the time ranges at which both groups were tested. Interestingly, the average compressive strength of samples with an age in range *[14-18]* of samples that

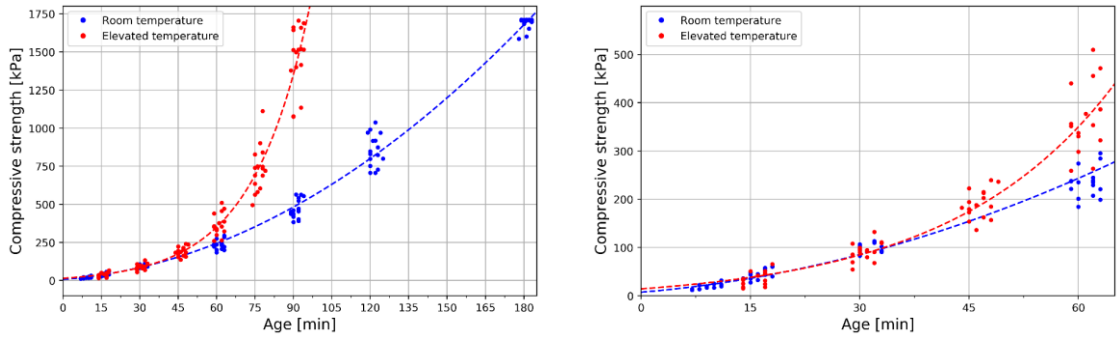

Figure 49: Development of the compressive strength of samples tested at room temperature and samples tested at elevated temperatures. Left: full test range. Right: close-up of the left graph until an age of 65 minutes.

are tested at room temperature is higher than the average strength of samples tested at an elevated temperature. As it was noticed that in this time range the relative standard deviation of the heated samples is highly influenced by the time range, the range was reduced to *[15-17]*. When considering this time range the average values are nearly the same and the 95% confidence intervals for the mean greatly overlap and the strength at this age can be considered the same.

The average strength of samples tested at an age in range *[30-34]* minutes is again slightly higher for samples tested at room temperature than for samples tested at elevated temperatures. However, as the 95% confidence interval largely overlaps, the strength at this age can be considered the same.

When considering ages of over 59 minutes it can also statistically be shown that the heated samples are stronger than non-heated samples. The average strength of heated samples with an age in the range of *[59-63]* minutes is a factor 1.6 stronger than samples stored at room temperature. This difference becomes even larger at an age in the range of *[89-93]* minutes as the heated samples are 3.1 times stronger. If the compressive strength of heated samples was to follow the same development until an age of 180 minutes, the strength of the heated concrete would be 43 (!) times higher than the strength of concrete at room temperature.

Moreover, it is found that the relative standard deviation of samples tested at elevated temperatures is always higher than that of samples tested at room temperature. A major difference is predominantly present in samples tested at ranges *[14-18]* and *[30-34]*.

Table 10: Tabular comparison of the compressive strength at different time ranges with average values $\bar{x}_n$, standard deviation s_n, relative standard deviation RSD and the interval limits of the 95% confidence interval of the mean.

Samples tested at room temperature						**Samples tested at elevated temperature**					
Time range	$\bar{x}_n$ **[kPa]**	s_n **[kPa]**	**RSD**	**Interval width limits [kPa]**		**Time range**	$\bar{x}_n$ **[kPa]**	s_n **[kPa]**	**RSD**	**Interval width limits [kPa]**	
				-	**+**					**-**	**+**
[14-18]	46	10	22.2%	41	52	**[14-18]**	36	14	39.5%	28	43
[30-34]	101	9	8.7%	96	105	**[29-33]**	93	19	20.7%	83	103
[59-63]	234	30	13.0%	218	250	**[59-63]**	369	72	19.4%	331	407
[89-93]	464	59	12.8%	431	497	**[89-93]**	1442	214	14.8%	1319	1566
[15-17]	45	10	21.3%	39	51	**[15-17]**	39	13	32.7%	28	49

The development of the Young's modulus over time of the heated samples and the samples tested at room temperature are shown in Figure 50. From this graph can be concluded that heating of the 3D printed concrete has a positive influence on the Young's modulus of the concrete. The effect of heating of the concrete becomes apparent at an age of 60 minutes. At this age the stiffness of the heated concrete starts to develop at a higher rate than the concrete at room temperature.

Table 11 shows a comparison between the statistical values derived for both the heated samples and the samples tested at room temperature, at the time ranges at which both groups were tested. Similar to what was found for the compressive strength, the average Young's modulus of samples tested in the range *[14-18]* and range *[30-34]* are higher for samples tested at room temperature than at an elevated temperature. Also, here the considered time range has a major influence on the outcome of the results

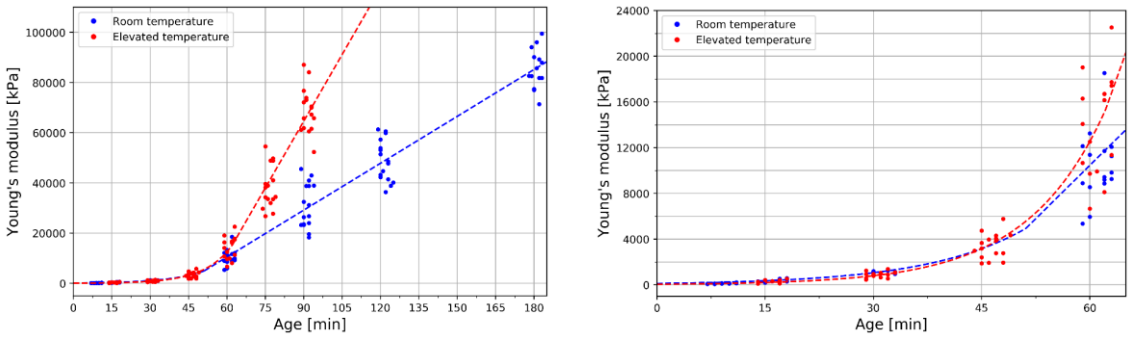

Figure 50: Development the Young's modulus of samples tested at room temperature and samples tested at elevated temperatures. Left: full test range. Right: close-up of the left graph until an age of 65 minutes.

and range *[15-17]* again shows more consistent results between both groups of samples, as the 95% confidence intervals of the mean largely overlap. Therefore, both heated and non-heated concrete is considered to have the same stiffness during the first 30 minutes.

Heated concrete with an age in range *[59-63]* minutes is on average 1.4 times stiffer than concrete at room temperature. The 95% confidence intervals of the mean do however partly overlap each other, albeit very small. From the right graph of Figure 50 it can be noted that there is not a very distinct difference between heated samples and samples tested at room temperature as the results of the heated samples are widely scattered. Resulting in a higher average stiffness of heated samples, but also four heated samples having even a lower stiffness than the average stiffness of samples stored at room temperature. The difference between the compressive strength at the age of *[59-63]* minutes was much more distinct.

When considering the range *[89-93]* minutes it can statistically be shown that the heated samples are stronger than non-heated samples. The average stiffness of heated samples with an age in the range of *[89-93]* minutes is a factor 2.3 higher than samples stored at room temperature, which is not in line with the factor that was found for the compressive strength. If the stiffness of heated samples was to follow the same development until an age of 180 minutes, the stiffness of the heated concrete would be 2.3 times higher than the stiffness of concrete at room temperature. This is much less that the factor 43 that was found for the difference in compressive strength at an age of 180 minutes. This is largely because of the linear relationship that is found for the development of the Young's modulus and the exponential relationship that is found for the compressive strength. It does however still stipulate the difference between the development of the Youngs modulus and the compressive strength.

Moreover, it is found that the relative standard deviation of samples tested at elevated temperatures is always higher than that of samples tested at room temperature, except for samples in the range of *[89-93]* minutes where the measurements prove to be relatively accurate. The difference is predominantly present in samples tested at time ranges *[14-18]* and *[30-34]* minutes.

Table 11: Tabular comparison of the Young's modulus at different time ranges with average values $\bar{x}_n$, standard deviation s_n, relative standard deviation RSD and the interval limits of the 95% confidence interval of the mean.

Samples tested at room temperature						**Samples tested at elevated temperature**					
Time range	$\bar{x}_n$ **[kPa]**	s_n **[kPa]**	**RSD**	**Interval width limits [kPa]** -	+	**Time range**	$\bar{x}_n$ **[kPa]**	s_n **[kPa]**	**RSD**	**Interval width limits [kPa]** -	+
[14-18]	374	108	28.8%	316	431	**[14-18]**	274	124	45.3%	202	346
[30-34]	1089	123	11.3%	1024	1155	**[29-33]**	915	252	27.6%	780	1049
[59-63]	10358	3065	29.6%	8725	11991	**[59-63]**	14104	4409	31.3%	11754	16453
[89-93]	30384	8977	29.5%	25412	35355	**[89-93]**	70403	8278	11.8%	65623	75182
[15-17]	362	98	27.2%	299	424	**[15-17]**	308	112	36.4%	214	401

5.3 Results printing experiment

The results of the printing experiment will be presented per print type (C1, C2, S1, S2 and S3). From each of the print types a table is presented with the results ordered by print speed. For each print it is registered whether it collapses and/or if it showed large deformations.

5.3.1 Cylinders

5.3.1.1 Cylinder C1

The printing information of print C1 is shown in Table 12. From the table can be concluded that during the first four testing days only three prints collapsed. Of which one was printed at an extremely high printing speed, to force the print to collapse. During printing at this speed two extra effects were noticed: 1) The quality of the print was greatly reduced as the layers showed cracks and a grainy structure. 2) The layer width was not the same as the specified width of 55 mm and reduced by nearly 20% to 45 mm. It can be concluded that this print did not only collapse because of the increased printing speed, but also due to reduced layer width and quality.

Table 12: Printing information of print C1 ordered by printing speed.

Time per layer [s]	Speed [mm/s]	Test day	Collapse	Large deformations	Number of layers
20.64	114.2	R1	No	Yes	-
20.64	114.2	R2	No	Yes	-
20.64	114.2	R3	No	No	-
20.64	114.2	R4	No	No	-
18.74	125.7	R1	No	Yes	-
18.74	125.7	R2	Yes	Yes	94
18.74	125.7	R3	No	No	-
16.70	141.1	R1	Yes	Yes	71
16.70	141.1	R2	No	Yes	-
16.70	141.1	R3	No	No	-
16.70	141.1	R4	No	No	-
10.49	224.6	R4	Yes	Yes	75

None of the prints printed at 20.64 seconds per layer collapsed. They did however show large deformations on the first two days of testing (see Figure 51). It can be seen is that at the top of the print, the radius is smaller than lower down the print. This means that even when printing at the lowest speed, deformation occurs. A similar deformation pattern can be seen for completed objects printed at 18.74s per layer.

Typical failure deformation behaviour of a print that did collapse is shown in Figure 52. Before collapse, a print typically shows extreme deformations in a wave-like pattern. The print then starts cracking and finally collapses. Interestingly, only part of a print collapses while the other part remains intact.

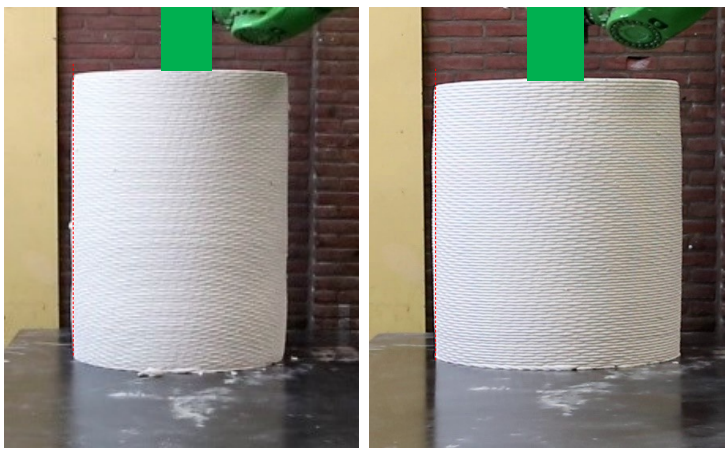

Figure 51: Print C1 printed at 20.64 s. per layer showing large deformations. Left: day R1. Right: day R2. Note that the photographs are taken at different moments in time. The red line indicates the original location of the layers.

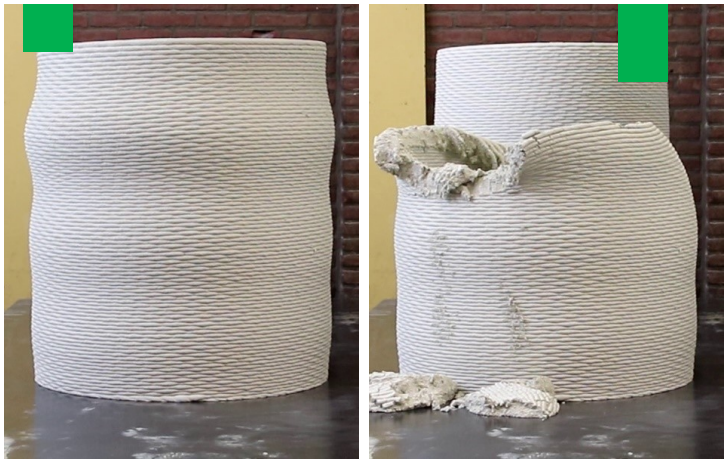

Figure 52: The moment before collapse and the collapsed cylinder C1 printed at 18.74 s. per layer on day R2.

Furthermore, a strange observation is made when considering only the prints of day R2. At the slowest speed the print already turns out to be slightly deformed. It then collapses when the print printing speed is increased by 10%. When the printing speed is increased by another 10%, the print does not collapse and only shows deformations comparable to the ones found in Figure 51. One would expect the print to collapse again at, at least the same number of layers (94), but the print managed to stay upright until 150 layers as this was the maximum print height.

After the first two testing days, prints did not collapse anymore and when they did show deformations, they were minor. Only the print printed at an extremely high speed, that does not represent a print that would be printed in practice, did collapse.

5.3.1.2 Cylinder C2

Table 13 shows the results of print C2. First of all, it is noted that far more prints collapsed and the combination of changing the geometry and the printing speed has had a significant effect on the number of failures. Prints printed at a speed of 15.08 seconds per layer show mixed results, whereas prints printed at higher speeds than 188.9 mm/s all collapsed. The only print that collapsed when printed at a speed of 15.08 seconds per layer is shown in Figure 53 and collapsed at the moment 83% of the print was completed. Prints that did not collapse typically developed large deformations in a wave-like pattern as shown in Figure 54, while some remained as good as straight.

Table 13: Printing information of print C2 ordered by printing speed.

Time per layer [s]	Speed [mm/s]	Test day	Collapse	Large deformations	Number of layers
18.67	126.2	Extra day	No	No	-
18.67	126.2	R5	No	Yes	-
15.08	156.2	R5	No	Yes	-
15.08	156.2	Extra day	No	No	-
15.08	156.2	H1	No	No	-
15.08	156.2	H2	No	Yes	-
15.08	156.2	H3	No	No	-
15.08	156.2	H4	Yes	Yes	125
13.68	172.3	H1	No	Yes	-
12.47	188.9	H1	Yes	Yes	91
12.47	188.9	H2	Yes	Yes	87
12.47	188.9	H3	Yes	Yes	77
12.47	188.9	H4	Yes	Yes	47
10.92	215.8	Extra day	Yes	Yes	58
10.92	215.8	H2	Yes	Yes	42
10.92	215.8	H3	Yes	Yes	52
10.92	215.8	H4	Yes	Yes	44

Prints did collapse when printed at 12.47 seconds per layer and 10.92 seconds per layer. However, it must be noted that speeds of 215.8 mm/s, that are reached at 10.92 seconds per layer, are very high and cracking and poor print quality are observed. Although the prints collapsed at both printing speeds, the number of layers at which it did is inconsistent.

Furthermore, it is observed that on day H4 all prints collapsed. When compared to objects printed with the same speed, the prints print on day H4 all collapsed at the lowest height.

Figure 53: Print C2 before collapse and after collapse printed at 15.08 s. per layer on day H4.

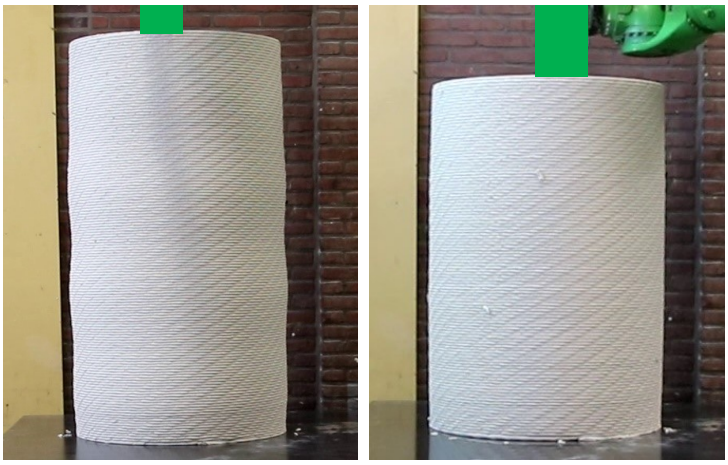

Figure 54: Left: print C2 printed at 15.08 s. per layer on day H2 having large deformations in a wave-like pattern. Right: a nearly straight print of C2 printed at 15.08 s. per layer on day H1.

5.3.2 Square tubes

Three square tubes were printed during the testing days. As again not many of them collapsed, it was decided to change them resulting in tubes S1, S2 and S3. As the printer slows down at the corners and speeds up on the straights, the printing speed was not constant. Therefore, the printing speed is denoted as an average printing speed.

5.3.2.1 Square tube S1

The results of square tube S1 are shown in Table 14. Relatively few prints collapses over the course of the first four testing days. Compared to the cylindrical prints, the squares did not show as much deformation before collapse and are therefore characterised by a more sudden collapse of the print. A typical print, printed at 9.84 seconds per layer, that did not collapse is shown in Figure 55**.** In the same figure a print that was printed at the highest speed is shown. Both do not show the same magnitude of deformations that were observed in the cylinders but do show the bulging behaviour that was also observed in the cylinders.

The prints that did fail, all failed at different printing speeds. Strangely, the print printed at the highest speed collapsed at a greater height than prints that collapsed at a lower printing speed. Moreover, the prints printed at 9.84 seconds per layer only collapsed once at a height of 65 layers, which is equal to 0.45 m. All the other prints printed at this speed managed to reach a height of 1.5 meters, again showing the variability in the printing process. Furthermore, test day R1 is the only day at which all prints showed either large deformations or all collapsed.

Table 14: Printing information of print S1 ordered by printing speed.

Time per layer [s]	Average speed [mm/s]	Test day	Collapse	Large deformations	Number of layers
14.70	130.2	R1	No	Yes	-
14.70	130.2	R2	No	No	-
14.70	130.2	R3	No	No	-
11.91	160.7	R1	Yes	Yes	90
11.91	160.7	R2	No	No	-
11.91	160.7	R4	No	No	-
9.84	194.6	R1	Yes	Yes	65
9.84	194.6	R2	No	Yes	-
9.84	194.6	R3	No	Yes	-
9.84	194.6	R4	No	Yes	-
8.40	227.9	R3	No	Yes	-
8.40	227.9	R4	Yes	Yes	157

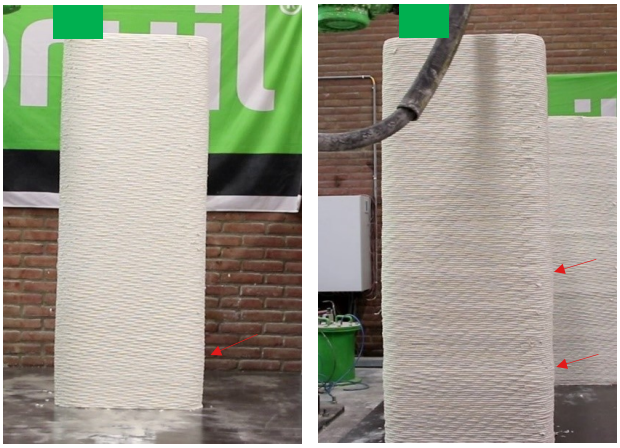

Figure 55: Typical deformation patterns occurring during printing of square S1. Left a print printed at a speed of 9.84 s. per layer and right a print printed at a speed of 8.40 s. per layer

Figure 56: Typical deformation behaviour before failure of print S1. Picture shows the print printed at a speed of 8.40 s. per layer.

5.3.2.2 Square tube S2

The results are shown in Table 15. S2 could not be printed on the fifth day as technical issues were encountered with the printer and the experiment was aborted for that day. Therefore, there is no data of square tubes on day R5.

All the prints, except the print printed at 7.58 seconds per layer, neither collapsed nor showed large deformations. The print that did collapse was printed at such a high speed that it started cracking and the layer width was reduced. Therefore the quality of the print was very poor and not representative of the ordinary printing process.

Table 15: Printing information of print S2 ordered by printing speed.

Time per layer [s]	Average speed [mm/s]	Test day	Collapse	Large deformations	Number of layers
13.29	144.0	Extra day	No	No	-
10.57	181.1	Extra day	No	No	-
10.57	181.1	H1	No	No	-
8.84	216.5	H1	No	No	-
8.12	235.7	H1	No	No	-
7.58	252.5	Extra day	Yes	Yes	121

5.3.2.3 Square tube S3

Based on the limited number of collapses the geometry of the print was changed again. By increasing the length of the sides, it was attempted to increase the probability of local buckling of the walls. The results of print S3 are shown in Table 16.

Table 16: Printing information of print S3 ordered by printing speed.

Time per layer [s]	Average speed [mm/s]	Test day	Collapse	Large deformations	Number of layers
18.01	150.7	H2	No	No	-
14.53	186.8	H2	No	No	-
14.53	186.8	H3	No	No	-
14.53	186.8	H4	Yes	Yes	86
12.01	226.0	H3	No	No	-
12.01	226.0	H4	Yes	Yes	69
10.33	262.7	H2	Yes	No	116
10.33	262.7	H3	Yes	No	96
10.33	262.7	H4	Yes	No	74

The print is characterised by an extremely sudden collapse, meaning that it showed very little deformation before collapse compared to prints S1 and S2. Therefore, no prints are recorded that only show large deformations as they would have collapsed by then. Figure 57 shows pictures of a print three seconds before collapse and during collapse.

Comparable to other prints, it is noticed that when prints do collapse at the same printing speed it doesn't necessarily happen at the same number of layers. Furthermore, it is observed that all prints printed at day H4 collapsed.

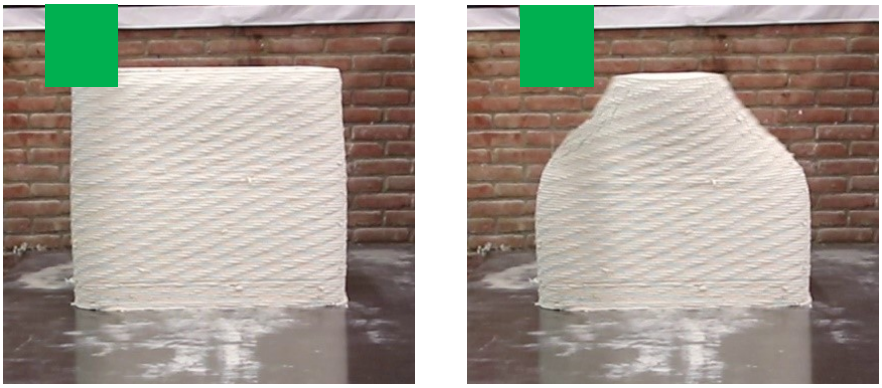

Figure 57: Typical failure behaviour of print S3. Left: Three seconds before collapse. Right: during collapse of the print. The pictures show the print printed at a speed of 14.53 s. per layer on day H4.

5.3.3 Printing temperatures

The temperatures of the prints fluctuated between approximately 24 and 29 C°. The temperature of the printed cylinder and square tubes, along with the average temperatures of the tested samples is depicted in Figure 58.

Generally, the temperature of the cylinders is lower than the temperature of the square tubes. This corresponds to what was found in the temperatures of the test samples, where batch 2 generally had a higher temperature than batch 1. The temperature of the prints is nearly constant during the first 40 minutes of printing.

During the first 15 minutes the average temperature of the heated samples shows good correspondence with the temperature of the prints, and more specifically with the square prints. After that the average temperature of the samples rise and is approximately 2.5 C° higher than the average temperature of the prints at 30 minutes.

The average temperature of samples tested at room temperature is, after 10 minutes, always lower than the temperature found in the during printing. After 30 minutes the average temperature of these samples is approximately 2.5 C° lower than the average temperature of the prints.

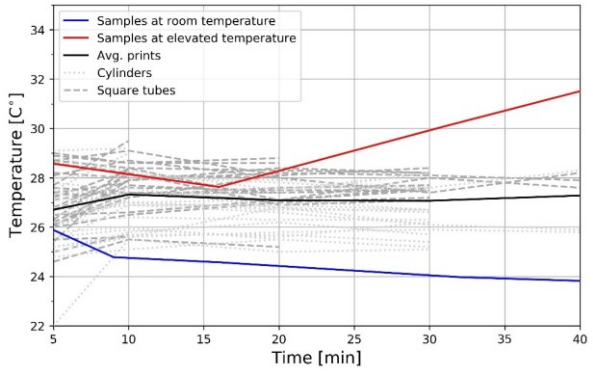

Figure 58: Temperature of prints during the printing experiment, with a distinction between the cylinders and the square tubes. The average temperature of the test samples is plotted for comparison.

5.3.4 Relationship printing experiment and uniaxial compressions test

When the results of the printing experiment are combined with the uniaxial compression test it is observed that on days where relatively low values of the compressive strength and Young's modulus are measured, also many prints collapsed.

Consider for instance the first two testing days of the samples tested at room temperature that were rejected and left out of the results. The results of these days are depicted in Figure 40 along with the rest of the results. Clearly, the samples on these days had a lower compressive strength and a lower stiffness than the rest of the samples (except samples from batch 2 on day 2). Interestingly print C1 either showed large deformation or collapsed during these two days, while on the other days the prints did not collapse and neither did they show large deformations. Similarly, when considering prints S1, all prints either collapsed or showed large deformations on day R1 (a print also collapsed on day R4, but this print was printed at a very high speed). When looking at day R2 of print S1, no collapsed prints are observed, while only large deformation are observed at a speed of 9.84 seconds per layer. However, at this speed large deformations are observed on all days. Taking a look at the results of the compressive tests on day R2 it is not surprising that these prints did not collapse on day R2, as batch 2 samples (which are taken just before printing square S1) are one of the strongest samples measured during the experiment. Reasons for how such a big difference between samples from batch 1 and 2 can exists are discussed in 5.4.

The weakest heated samples can be found on day H2 and H4 (see Figure 48). When the same days are considered in the results of the printing experiment of cylinder C2 it is found that at a speed of 15.08 seconds per layer the prints either collapsed or largely deformed at these days, while at the other heated

days prints did not even show large deformations at this speed. At other printing speeds all prints collapsed. When print S3 is considered, it is observed that all prints collapse on day H4, while at every other day the print did not collapse. Here again samples from batch 2 of day H2 produced strong and stiff samples and print S3 did not collapse on this day and neither did it show large deformations.

5.4 Discussion and conclusions

Results of the experimental programme will be discussed here along with a couple of remarks. First the relationship between the uniaxial compression tests and the printing experiment will be discussed, after which conclusions will be drawn and how to use the results in computational modelling.

In section 5.3.3 the temperatures of the samples and the prints have been compared. The temperature of the heated samples seems to rise faster than what is encountered in a print. On the other hand, the samples tested at room temperature tend to cool down to approximately room temperature, while based on experience it is known that temperatures of prints tend to rise to temperatures of over 30 C° within the first couple of hours. Although the samples are kept at room temperature within a closed mould, the temperature of these samples drop. It was expected that due to the exothermic reaction, which the hardening of concrete is, that the concrete would at least remain at the same temperature as at the moment of extraction. From the exponential development of the compressive strength it is certain that a reaction has taken place. Probably, due to the sample size, the heat of the reaction is released to the environment allowing the samples to cool down. Moreover, the temperature of the samples is not measured in the core of the sample but rather on the outside with an infrared thermometer. It is likely that the core of the sample has a somewhat higher temperature than the outside. From some samples the core temperature was measured after they had been crushed by the testing rig. From these samples the core was approximately 0.5 – 1.0 C° higher that the outside temperature of the sample.

The opposite was observed in the temperature of the heated samples that were placed in an oven at 35 C°. Temperatures of over 38 C° were measured on these samples, meaning that the heat of the exothermic reaction led to a temperature of above 35 C° as the heat could not be released into the environment. Again, a temperature gradient was observed in the experiments, with the core being approximately 0.5 – 1.0 C° higher than the outside temperature of the sample.

As it is known from practice that prints rather heat up than cool down, it is likely that due to the mass of a printed object, it is able retain the heat of the exothermic reaction of the hardening concrete. Likely, a temperature gradient will exist from the core to the surface of a print. From the experiments can be concluded that the development of the temperature of the heated samples is faster than in a printed object and might overestimate the temperature of a real print. The samples tested at room temperature underestimate the temperature of a print as a print is able to retain some of the heat that is generated by the exothermic reaction.

From comparing the heated samples and the samples stored at room temperature it can be concluded that the temperature difference starts to influence the compressive strength only after approximately 45 minutes. The Young's modulus is influenced after approximately 60 minutes. After this age the difference between the heated samples and unheated samples becomes larger very rapidly. While the strength of the concrete is similar at an age of 45 minutes, the heated samples are already three times stronger than the unheated samples at an age of 90 minutes. The average Young's modulus the of heated samples and the unheated samples is similar at an age of 60 minutes, while at an age of 90 minutes the heated samples are more than twice as strong than the unheated ones.

It can be concluded that prints that are printed within 45 minutes are not greatly influenced by the temperature. When objects take more than 45 minutes to print, the temperature of a print will play a major role in both the capacity to resist elastic buckling as well as the ability to resist plastic collapse. All prints that were printed during the printing experiment were finished before 45 minutes. This means that these prints are not greatly influenced by the temperature.

There is a strong indication that the temperature can be considered to also have an important influence at ages under 45 minutes, although not as large as after 45 minutes. This is supported by samples of batch 2, that generally had a higher temperature than samples of batch 1. At each age the strongest samples originated from batch 2, while the weakest samples originated from batch 1. This was observed

in both the samples stored at room temperature and the samples stored at 35 C°. In contradiction, a actively heated sample was not always stronger and stiffer than a sample stored at room temperature. Besides that, for some ages the samples stored at room temperature the average strength and stiffness is even higher than that of the samples stored in the over. Considering the above, it cannot irrefutably be concluded that also at younger ages (< 45 min.) a higher temperature influences the strength and stiffness of the concrete positively. There are however some indications that it does.

It was observed that failure of all prints was initiated by elastic buckling, rather than by plastic collapse. This means that when considering failures of these prints, the Young's modulus is the most important mechanical property. Also, prints would sometimes collapse and sometimes remain standing without showing large deformations, even though they had been printed at the same speed. This can be explained by the high variability found in the Young's modulus. The Young's modulus could sometimes be more than half the average Young's modulus found at a particular age. Apparently, this variation can be the difference between a collapsed print or a successful print.

It can be concluded that there is a clear connection between the values encountered in the uniaxial compression test and the printing experiment. On days that samples proved the be relatively weak, prints showed more severe deformations and collapsed more often. Furthermore, relatively strong and stiff batches meant relatively strong prints.

The variability of the Young's modulus is always larger than the variability of the compressive strength for both the heated and the unheated samples. This can be explained by the fact that at older ages the concrete develops a bi-linear stress-strain diagram with a fairly abrupt transition between the two parts. To illustrate this, a closeup of the stress-strain relationships of the heated samples is given in Figure 59. Here the transition zones are indicated on the average curves. From the figure can be observed that the initial linear part, where the Young's modulus was measured, can be very different among samples of the same age, explaining the high variability in the measured Young's modulus. After the transition, the samples start to behave very similarly. Therefore, at the ages where the variability before the transition is most severe (range *[44-48]* and *[59-63]*), the tangent of the curves after the transition zone was measured. The relative standard deviations of these tangents are 20% and 21%, respectively. This is in line with the compressive strength at these ages and a significant change to the relative standard deviations that were found for Young's modulus (34% and 31%, respectively). Similar observations can made for the samples tested at room temperature.

The bi-linear behaviour observed in the experiments is commonly observed in ultra-high fibre reinforced concrete loaded in tension or bending [39]. Although the samples are loaded in compression in this experiment, the concrete will eventually fail by tensile forces. It may be possible that due to the amount of fibres present in the concrete mix, the fibres will take a part of the tensile stresses allowing the concrete to fail in a ductile manner, even under compression.

The stress-strain relationship of samples at older ages is also characterized by an initial part where the stress does not increase upon increasing strain. These parts are encircled in red in Figure 59. A possible explanation of this phenomenon is given by Weijermars [40]. In his book the stress-strain behaviour of rocks is described. A typical stress-strain relationship of a uniaxial compression test on rock is shown in Figure 60, of which stage A is of particular interest. Stage A is described as the closing of microcracks and pore spaces oriented at suitable angles at the onset of loading, causing an initial non-recoverable strain non-linearity. A similar explanation is found by Corkum [41], who studied the response of claystone. The concrete used for printing by Bruil has a relatively high air content and more importantly: it is not compacted. As the concrete is not compacted, voids may exist, and particles are less densely packed. At early ages, this effect is not noticed as the concrete itself is already relatively weak. In numerical modelling this behaviour will not be accounted for, because it will be assumed that due to the gradual load increase during printing the layers are compressed and the microcracks and voids will therefore be closed at older ages.

A linear development of compressive strength over time was found by Wolfs et al. [11], [42]. Perrot et al. [16] reported an exponential evolution of the yield stress over time. The evolution of the compressive strength of the samples tested at room temperature cannot be described by a linear function nor an exponential function. Instead, it is described by a second order polynomial function. The evolution of

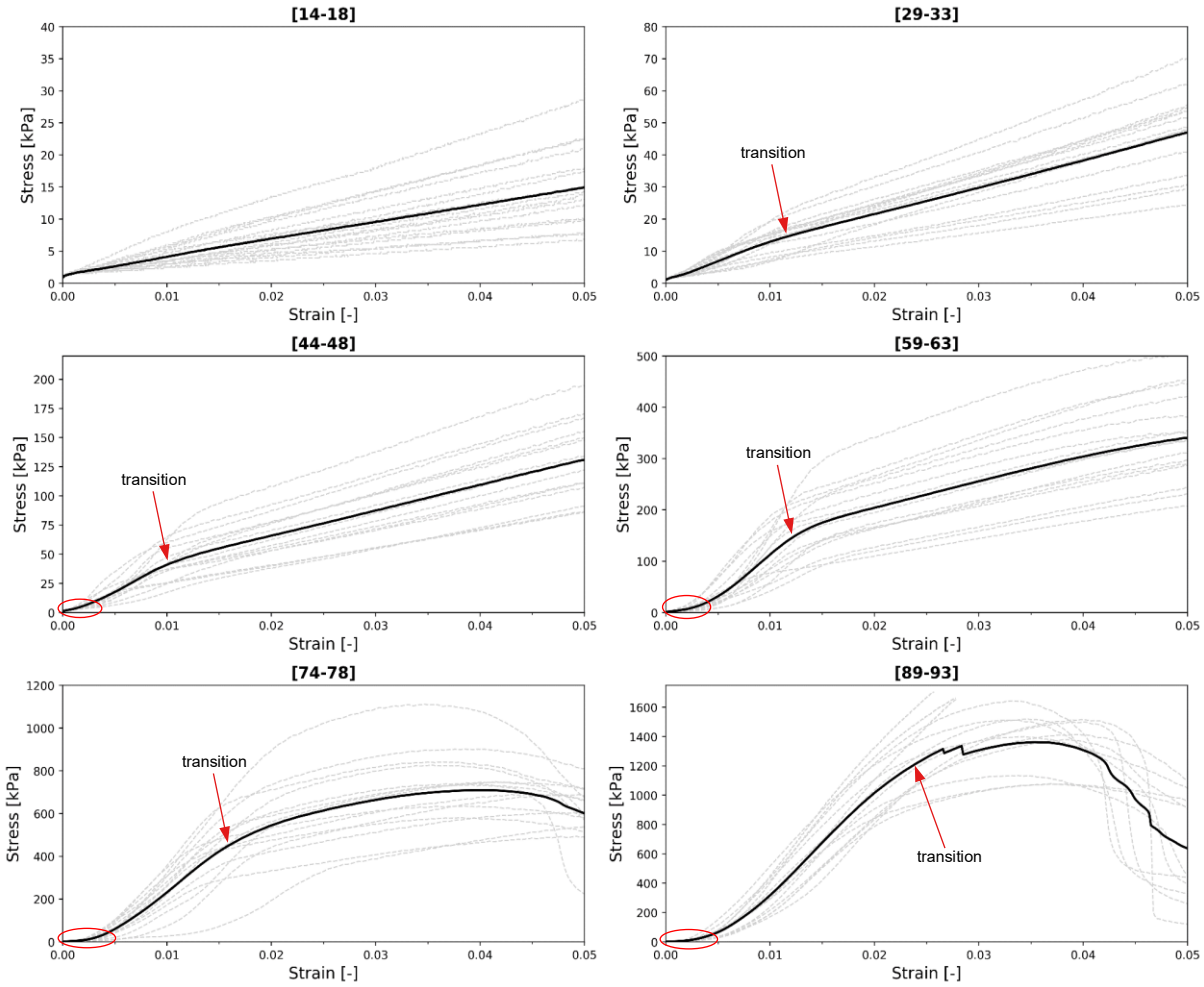

Figure 59: Stress-strain relationships of the heated samples until 5.0% strain. The transition zones are indicated with red arrows and the initial settlement is encircled with red.

compressive strength over time of the heated samples is described by an exponential function, which is in line with Perrot et al. It was expected that both groups of samples would follow the same type of development, albeit at a different rate. It can be concluded that heating the concrete alters the way the compressive strength of the concrete develops.

It was expected that the evolution of the Young's modulus would follow the same relationship as the evolution of the compressive strength: an exponential function for the heated samples and a polynomial function for the room temperature samples. The evolution of the Young's modulus can however be described similarly for both the heated as well as the room temperature samples: First by an exponential function and at older ages by a linear function. It can be concluded that the type of development of the Young's modulus is not influenced by the addition of heat. This division of behaviour between relatively young and old concrete has not been encountered in literature. The rate at which it develops is however influenced by elevated temperatures. Reasons for why the development of the Young's modulus is different to that of the compressive strength are unknown. It is likely that at older ages different failure mechanism prevail than at younger ages, that do not play a role in the stiffness behaviour of the concrete.

The spread in measured mechanical properties are partly explained by the type of moulds that were used. As one can imagine, the geometric tolerances of PVC pipes are not that tight. A steel mould would could have led to much tighter geometric tolerances of the moulds and more equal samples.

Temperature measurements have been executed with infrared thermometers. These measurement devices are not as accurate as for instance a thermocouple. Measuring the temperature of every single print with a thermocouple is however not practical as the printing process has to be stopped to insert

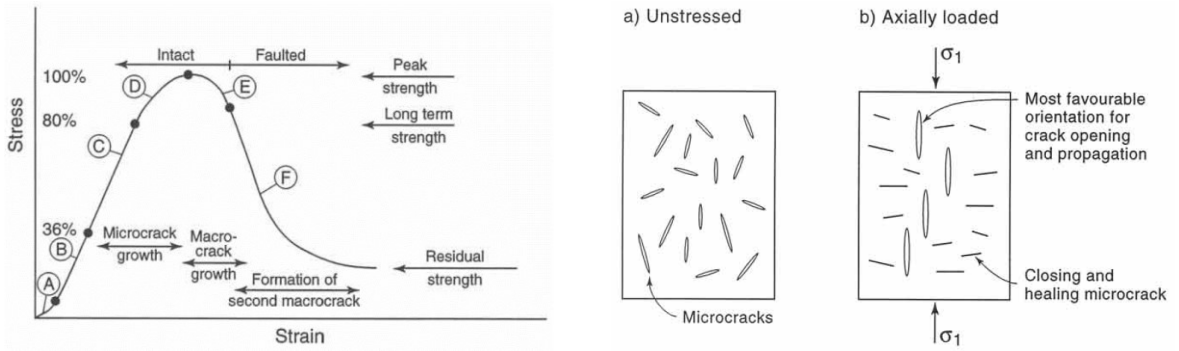

Figure 60: Left: Typical stress-strain diagram for a uniaxial compression test on a rock sample. Right: a) Randomly oriented micro-cracks in the undeformed continuum. b) Upon loading, only those microcracks, which are favourably oriented. May open and propagate. From [40].

the thermocouple. Besides that, it is difficult to remove the thermocouple once the concrete has hardened. Many couples would then be needed to conduct this experiment. They could also have been used to measure core temperature of the samples. One sample of each batch could have been sacrificed to measure the temperature over time and consider this as representative for the whole batch. Again, this would increase the cost of the experiment as it will be difficult to remove the thermocouple from hardened samples.

After the first two days of testing a part of the printed head was revised. This seems to have had a positive influence on the mechanical properties of the concrete. Not only was this noticed by the increased strength and stiffness measured by the uniaxial compressive tests, also the prints collapsed fewer times and deformed less. The results of these test days were considered to differ so much from the rest of the samples that they were deemed unsuitable to represent the mechanical properties of the concrete used in practice. Therefore, the results of day 1 and 2, except for batch 2 of day 2, were left out of the results. The question still remains whether the revision of the printer head was indeed responsible for the increase of strength on all other test days as there are only two testing days before revision of the printer head and 7 after that. Moreover, the samples of batch 2 of test day 2 were among the strongest of all testing days at room temperature, while the revision had not taken place yet. It can be debated whether this batch should have also been rejected as the batch was printed with the unrevised printer head. It was decided not to, as they did not deviate from the rest of the samples.

More interesting is the answer to the question: How can the revision of the printer head have such a major influence on the strength of concrete? A theory is that the due to the revision of the printer head the temperature of the concrete increases as a result of increased friction. This is supported by the fact that the temperature of prints printed with the revised printer head are approx. 2 °C higher than the days before. This is however not supported by the temperature of the test samples. The temperature of the samples of day 1 and 2 was lower than average, but not lower than the temperature of some of the samples tested at other days. Furthermore, it may be possible that the degree of compaction is increased due to the revision, increasing the strength and stiffness. Moreover, it still does not explain the high strength and stiffness encountered in batch 2 of day 2. Differences in the water and the air content on day 1 and 2 cannot be a reason for the enhanced properties. They were similar to the measurement on all other days. To conclude, there is no hard evidence that can explain the enhanced properties after revision of the printer head. The abrupt change in material properties after the revision is however a strong indicator that it does.

During the printing experiment a wavelike pattern of the printing path was noted. This resulted in a variable layer width over the length of a layer. A top view of a typical printing path is shown in Figure 61. The difference between w_1 and w_2 could be as large as 5 mm. From some of the prints that did not fail, the average width of the printing path was measured too. The width of these prints were sometimes up to 5 mm smaller than specified when printed at relatively high speeds. When prints were printed at relatively slow speeds the opposite was true as the printing paths appeared to be approximately 5 mm wider than specified. The deviations of the printing path to the specified path can have a serious influence on the stability of the prints, both positive as negative. In order to improve the reliability of the printing process the tolerances on the layer width must be improved.

The need for predictive models of the printing process is proven by the results of the printing experiment. It shows that, when printing on the boundary of what is possible with a particular geometry the difference between a successful and unsuccessful print is very small and highly dependent on the strength and stiffness properties of the particular day the object is printed. Numerical models can help to increase the reliability of the printing process by using lower bound mechanical properties in their prediction of printability.

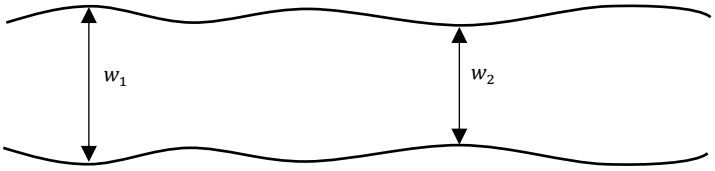

Figure 61: Top view of a typical printing path encountered during the printing experiment.

6

Numerical modelling of experiments

The results obtained from the experiments are used to model the cylinder and square tubes that were printed during the experiments. The prints will be analysed with average mechanical properties.

Initially, only elastic properties are considered in the numerical models. From the types of failures that occurred during the printing experiments it is known that failure of the prints is dominated by elastic buckling phenomenon. This is most apparent during printing of the square tubes, which often collapse very suddenly. It is assumed that the wrinkles/bulges occurring in the cylinders are due to elastic buckling, after which the bulges grow and ultimately fail by plastic collapse and cracking due to excessive deformations.

In section 4.3 it was noticed that plastic material properties require a finer mesh and may lead to convergence issues due to local mesh distortions. When 3-dimensional solid elements are used, mesh refinements may increase the computational time severely. Besides that, a yield criterion has to be adopted. Since only uniaxial compressive test have been performed, the type of yield criterion that fits the material best is not known. In section 6.2.1 plasticity will however be considered by adopting the Menetrey-Willam model and estimating the material parameters. Only cylinder C1 will be analysed with plastic material properties.

6.1 Mechanical properties

The maximum duration of a print is 52 minutes, except for one print of square tube S3 which takes 64 minutes to fully print (18.01 seconds per layer). Within this timespan there is no clear difference between the mechanical properties of the fresh concrete at room temperature or at elevated temperatures. Therefore, the prints that were printed during the printing experiment can't be used to verify whether the results of the heated samples or the results of the room temperature samples represent the true material properties in a print the best way.

It is assumed that the mechanical properties measured on the days that a particular geometry was printed, represents the mechanical properties of the concrete in those prints. Therefore, the average properties of the samples tested at room temperature will be used to analyse prints C1 and S1 and the average mechanical properties of the samples tested at elevated temperatures will be used to analyse the results of print C2 and S3. Print S2 will not be numerically analysed as there is too little information about the samples on the days it was printed and the print has been printed very few times.

Rather than using the fitted functions that were established for Young's moduli, a multilinear approach is used. The fitted results are merely used to extrapolate the mechanical properties to an age of 0 minutes. Also, for the mechanical properties at room temperature the fitted curve is used to estimate the elastic properties at an age of 45 min. When a linear development of material properties between an age of 30 min. and 60 min. is assumed, it would greatly overestimate the stiffness between these two ages.

The weight of the concrete is equal to 2200 kg/m^3 and the Poisson's ratio is 0.36.

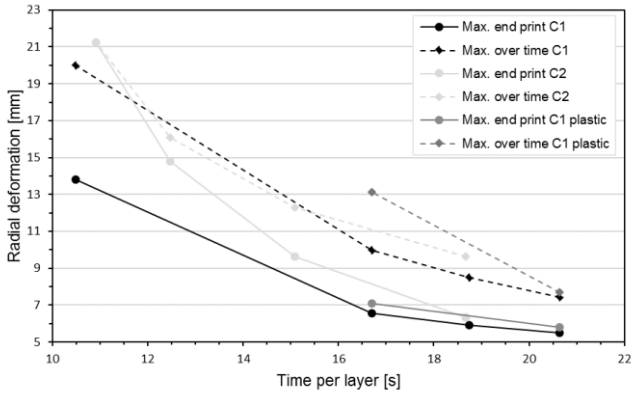

Figure 62: Radial deformation of prints C1 and C2. Results of both the maximum deformation over time as well as the maximum deformation at the end of the print are plotted.

6.2 Cylinders

The cylinders are analysed with an axisymmetric model consisting of quadrilateral 4-noded elements with an edge length of 1 mm. Simulation results of cylinder C1 and C2 at the fastest speeds are shown in Figure 64 and 65. The bulging behaviour of the print as the print progresses, shows great correspondence with the experiments (see Figure 53 and 54). Also, the bulging of prints that occurs after printing 50 to 100 layers is captured very well (see Figure 51).

It can be observed that the maximum deformation in the simulation of print C1 is reached after printing 80 layers. When the print is finished, this deformation is not present anymore. This phenomenon is attributed to the influence of pure elastic properties, and the recovery of elastic strains as the Young´s modulus increases. It is of great influence on the geometry of the print at the end of the simulation.

Cylinder C2 shows similar behaviour. At 120 layers the deformation of the bottom bulge is at its maximum, while at the end of the simulation the deformation has become less. Nevertheless, at the end of the simulation the prints still show good resemblance with the experiments. Furthermore, it is observed that apparently the thickness of the print influences the number of bulges when prints are printed at a comparable speed. This is attributed to the fact that the thinner structures are more vulnerable to buckling behaviour.

Prints printed at slower speeds showed the same behaviour, but with less deformations. The maximum deformations of print C1 and C2 during the simulations, as well as at the end are presented in Figure 62 for different printing speeds. As the printing speed decreases the deformations become considerably less too. Also, the maximum deformation at the end of a print is always lower than during a print.

In reality, the prints printed with a layer cycle time of 10.49 seconds (C1) and 10.92 seconds (C2) collapse. The actual failure of the cylindrical print could not be captured with the model in ANSYS. This is due to the fact that plasticity is not incorporated into the model. In reality, the bulging of the print is initiated by elastic instability, but final failure occurs due to very large strains that cause plastic deformation. When these deformations keep growing, the print will eventually rupture and collapse.

In geometrically and material non-linear model, when large deformations are present at the early stage of a print they are likely to be caused by plastic strains. They will keep growing due to the additional layers until they cause convergence failure of the model. As currently the models only consider elastic material properties, this behaviour cannot be observed.

6.2.1 Plasticity

To approximate the plastic behaviour of the cylinders, they were modelled with plastic material properties too. Similar to section 4.3, the Menetrey-Willam material model is adopted, based on results of a uniaxial compression test only. The biaxial strength is conservatively chosen as 1.1 times the uniaxial compressive strength. No softening was introduced as this may lead to convergence issues. Instead the residual compressive strength is defined to be equal to the compressive strength. Single element tests were performed to compare the adopted material model with the average stress-strain

relationships found in the experiment. The results of the single element test are shown in Figure 63. The results until 16 minutes are very accurate. The results at $t = 32$ min. and $t = 61$ min. are less accurate due to the straight part of the stress-strain curve after yielding at these ages. The results are however deemed accurate enough for exploring the effects of plasticity during printing of the cylinders.

Only cylinder C1 was modelled with plastic properties to investigate the effect of plasticity. Similar to what was encountered in modelling the cylinder in section 4.3, the model did not converge at the highest printing speed (10.49 seconds per layer) due to excessive element distortions at the bottom of the print. When the speed was decreased to 16.70 seconds per layer, the model did converge, and plastic strains had developed. The results are shown in Figure 66. The maximum deformation over time and the final deformation are plotted in Figure 62.

When print C1 is simulated at a speed of 16.70 seconds per later plastic strains develop at a very early age. They already develop after printing 30 layers, which is equal to approximately 8 minutes of printing. The plastic strains that develop throughout the print have a maximum of ~0.5%, apart from locally at the bottom of the structure where much larger plastic strains occur. Although plastic strains have developed, the print still recovers its elastic strains. Therefore, at the end of the print the maximum deformation is similar to what was obtained with purely elastic properties. The larger deformations found during printing with plastic properties than with elastic properties are attributed to the accumulation of plastic strains. Although the plastic strains are very small, they increased the deformations by ~3 mm.

Moreover, it can be concluded that a print does not necessarily have to collapse as soon as it develops plastic strains. They do however increase the deformations compared to purely elastic properties.

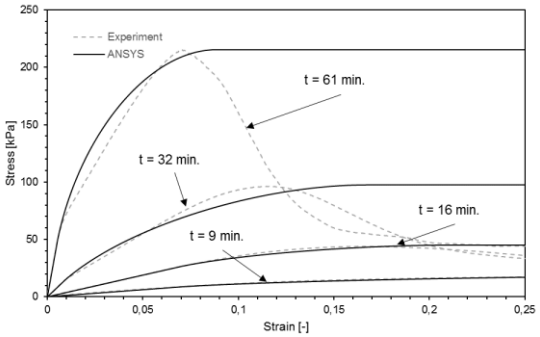

Figure 63: Results of the single element test in ANSYS compared to the results of the average stress-strain curve of the uniaxial compression test of samples tested at room temperature.

6.3 Square tubes

The simulations of the square tubes show good correspondence to the behaviour that was observed in the printing experiments. The results of the simulations of the tubes are given in Figure 67-69. The bulging of the print at the bottom corners observed during the experiment (see Figure 55 and 56) is also captured by the simulations. This is most clearly seen in Figure 68, which shows the results of S1 printed at 8.4 seconds per layer. The failure-deformation behaviour corresponds very well with the observations during the experiments too. Moreover, also during these simulations recovery of elastic strains was present, although less pronounced as in the simulations of the cylinders.

The height at which buckling occurs during the simulations of the tubes are presented in Table 17. ANSYS predicts buckling failure of square tube S1 at all speeds except for the tube printed at 14.7 seconds per layers. On the one hand, this corresponds to what was found in the experimental programme, while on the other hand it does not. The prints that collapsed during the experiment, collapsed on testing days from which the samples were rejected as they were considered to be too weak and unrepresentative for the printing process under normal circumstances. Therefore, the material properties used for modelling correspond to all the other days, where S1 did not collapse (except when printed at 8.40 seconds per layer). Hence, it was expected that the numerical model would also predict the prints to remain stable during printing.

When the speed of printing is increased, the number of layers at which collapse takes place decreases. This is in line with expectations. When the results obtained during the printing experiment are compared to these values, there is a discrepancy. This discrepancy is mainly attributed to the randomness in the collapsing of prints during the printing experiment. Theoretically it cannot be possible that a print printed at a higher speed collapses at a higher number of layers than a print printed at a lower speed. This can only be true when material properties were different during printing.

Table 17: Buckling predictions of the simulations in ANSYS and the number of layers at which buckling occurred during the experiment. Prints that did not buckle are denoted by '-', else the average number of layers at which the print buckles is denoted.

S1			S3		
Time per layer [s]	**Number of layers experiment**	**Number of layers ANSYS**	**Time per layer [s]**	**Number of layers experiment**	**Number of layers ANSYS**
14.70	-	-	18.01	-	133
11.91	- / 90	192	14.53	- / 86	54
9.84	- / 65	158	10.33	95	45
8.40	- / 157	148			

Similar observations are made for tube S3. The numerical models predict failure of all S3 tubes, which is again partly correct. During the printing experiment collapses were noted at all speeds except at 18.01 layers per second. However, prints also remained fully stable during prints at the exact same speeds.

To investigate the effect of the wall thickness on the stability of the print, S3 was also analysed with a wall thickness of 60 mm at a print speed of 18.01 seconds per layer. Still, the model predicted buckling of the tube, but at 178 layers. It shows that a small change in wall thickness can improve the stability a lot. In this case it is however not enough to keep S3 stable, according to the simulation.

6.4 Discussion and conclusions

The numerical model has proven to be capable of accurately describing the behaviour of prints during the printing. Exact prediction of the moment of buckling proved to be difficult when results are compared to the printing experiments. The moment of collapse was not fully in agreement with what is observed during the experimental programme. The randomness of the stability of print plays a major role in this. On top of that, the average results of the measured mechanical properties were used in the model. As the material properties showed considerable spread, it may well be that when upper bound values had been used during the simulations, the numerical model would have predicted stable structures at many of the printing speeds.

The numerical models can be considered conservative as they predict failure at a lower number of layers than encountered during the experiments. A part of the lower predictions of the stability of the printed objects may also be explained by the fact that the width of the layers appeared to be wider than was specified. The analysis of print S3 with an increased width of 60 mm showed than a change of width by 10 mm can already improve the stability of prints by multiple layers. When printing on the boundary of what is possible, as was done during the experiments, this can mean the difference between a failed and a stable print.

From section 4 it was already clear that due to the definition of the model, elastic strains were able to be recovered as the fresh concrete matures. The impact of this assumption becomes clear in modelling the cylinders, where a part of the large deformations that developed at the early stage of a print were recovered. Leading to sometimes lower deformations at the end of a print than during a print. This is not in line with observations during the printing experiment. Recovery of deformations during a printing session were not observed. Therefore, this assumption is considered a flaw in the model.

Incorporating plasticity in the model, albeit approximated, does not mean that the elastic strains are not recovered anymore. It only means that some of the total strain will be permanent. As the plastic strains appeared to be small for the analysed prints, a lot of the total strains were still recovered. As recovery of deformations was not observed it in the experiments it might be possible that although the stress-strain relationship of fresh concrete behaves linearly until its yield point, it may not be elastic. Perhaps, a model that considers all deformations as permanent (plastic) will yield better results.

Due to the exponential growth of the Young's modulus, the effect of the recovery of deformations can become even more pronounced at later ages, meaning that the model accuracy might suffer at later ages and overestimate the stability of prints. The cylindrical and tubular prints that were investigated here, could still be modelled with high accuracy and capture the deformations occurring in reality.

For production purposes, the fact that deformations are partly recovered does not necessarily have to be a problem. One is only interested in prints that do not deform much during printing. As they do not deform much, the effect of recovery of deformations is less pronounced.

Introducing plasticity into the model increases the model complexity, which leads to increased computational effort and may cause convergence issues. Also, strains are likely to be plastic at the moment large deformations are present. These deformations would have also been noticed when assuming only elastic properties. Therefore, it is concluded that numerical modelling of the printing process can most efficiently be analysed with linear-elastic material properties.

By not only looking at results at the end of the print but by analysing the total printing process, the magnitude of the recovery of deformations can be determined. For instance, in cylinder C1 the print had already developed large deformations (~10 mm) after printing 50 layers. When it is known that these deformations are likely to be permanent, the print will have to be rejected. For this reason, a stop criterion is built into the script that runs ANSYS, based on deformations it encounters during the simulation. As soon as the deformation criterion is reached the simulation stops, meaning that the object is not printable.

In the end, the goal of the model is not to predict the final, highly distorted shape of a print. The goal of the model is to assess the printability of an object. Whether the deformations are caused by elastic strains, plastic strains or whether they are recovered is not of interest. The only thing that is important is that the print conforms to the intended geometry. It is therefore reasoned that small deformations occurring during printing therefore do not influence the precision of the model that much and the presented approach can give good results in predicting the stability of prints.

A numerical model that is able to predict the behaviour of concrete prints already exists in literature and the model that has been developed in this thesis is therefore not entirely new. The effects of recovery of deformations that occur during the simulation of prints of long time duration have however not been reported in literature. This is partly attributed to the fact that the concrete of Bruil develops at a much higher rate than any concrete used for printing found in literature. Because it develops at such a high rate, the effect of the weight of the added layers on the deformations is counteracted by the rapid development of the stiffness. When the stiffness remains relatively low during a printing sessions, the effects might not even be noticed in numerical models.

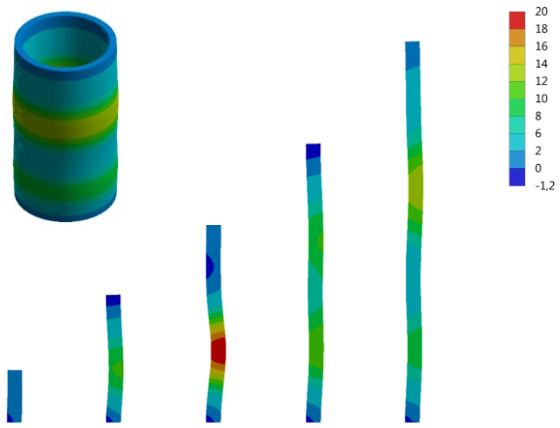

Figure 64: Radial deformations [mm] of cylinder C1 printed at 10.49 seconds per layer at 20, 50, 80, 120 and 150 layers and a 3D view at 150 layers. Deformations are plotted on true scale.

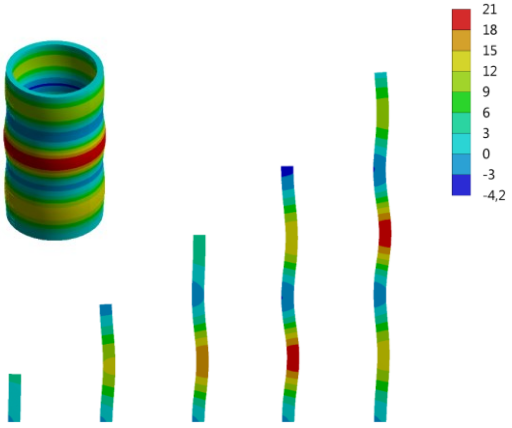

Figure 65: Radial deformations [mm] of cylinder C2 printed at 10.92 seconds per layer at 20, 50, 80, 120 and 150 layers and a 3D view at 150 layers. Deformations are plotted on true scale.

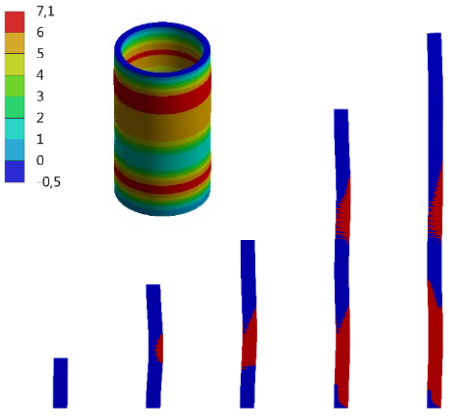

Figure 66: Plastic regions developing during printing of cylinder C1 at 16.70 seconds per layer indictated in red. Results are displayed at 20, 50, 80, 120 and 150 layers. Deformations are plotted on true scale.

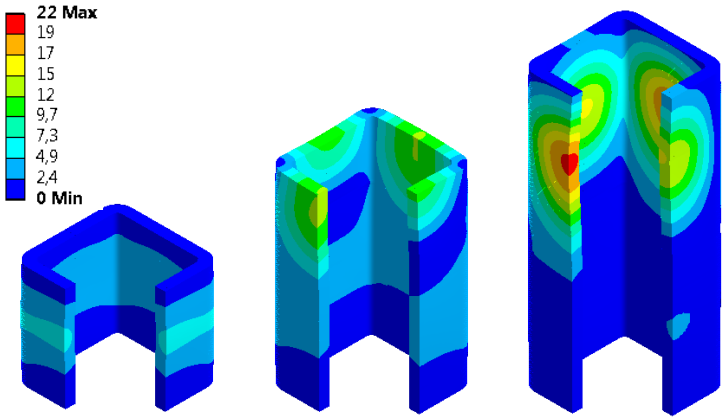

Figure 67: Radial deformations of square tube S1 printed at 14.70 s per layer at 82, 148 and 214 layers. Deformations are plotted in true scale.

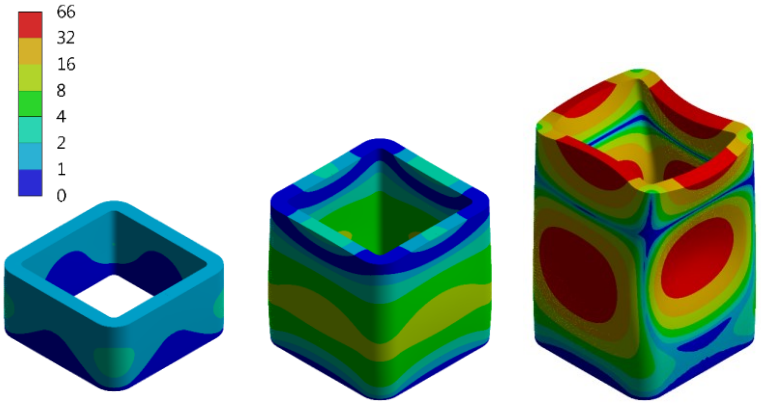

Figure 68: Radial deformations of square tube S1 printed at 8.4 seconds per layer at 60, 104 and 148 layers. Elastic buckling occurs at 148 layers. Deformations are plotted in true scale.

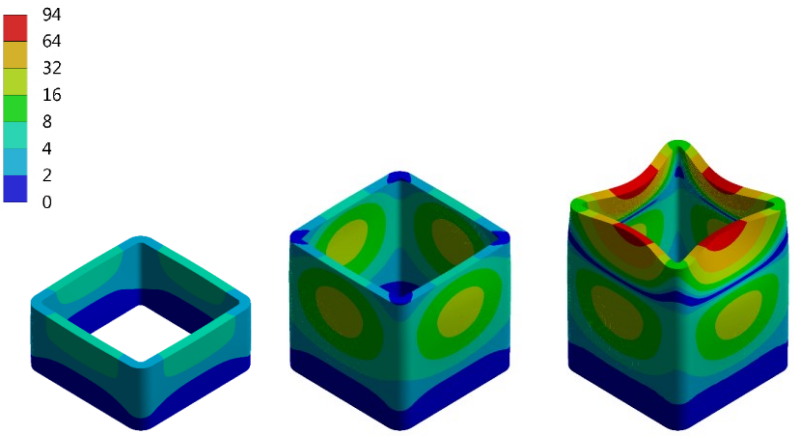

Figure 69: Radial deformation of square tube S3 printed at 18.03 seconds per layer at 52, 106 and 133 layers. The print collapses at 133 layers. Deformations are plotted in true scale.

7

Conclusions and recommendations

Based on experimental material research into the mechanical properties of freshly printed concrete a numerical model has been developed in ANSYS to predict the printability of arbitrary geometries specific for the printing process at Bruil. The model can be used to effectively explore design and process parameters to optimize printed objects. Moreover, the model can be used to improve the reliability of the printing process, reduce the number of failures during production and enhance the production capabilities complex geometries.

The research has contributed to the better understanding of the influence of temperature on the development of mechanical properties of concrete during printing. Also, a direct relation between measured material properties and printed objects has not yet been presented in literature. By extracting samples directly from printed concrete, the influence of the total printing process on the mechanical properties of the concrete over time was captured. By the knowledge of the writer this method of extracting samples has never been used before. The amount of compaction of concrete can greatly influence mechanical properties. With the presented procedure it is possible to transfer the amount of compaction that is present in printed concrete directly to a test sample.

A comprehensive experimental programme was designed in which uniaxial compression tests have been performed to determine the mechanical properties of the concrete during the printing process. To quantify the volatility of the measured properties, and produce reliable results, multiple samples have been tested at multiple concrete ages. By pushing cylindrical moulds into a small print that has just been finished, test samples could be extracted directly from printed concrete. This novel method proved to be very suitable to quantify the mechanical properties of fresh concrete.

The effect of temperature on the strength and stiffness of the concrete has been effectively explored during the test programme. The influence of elevated temperatures on the mechanical properties is negligible up to an age of 45 minutes, when concrete is stored at 35 C° before testing. After that, concrete at an elevated temperature will rapidly increase in strength and stiffness. At an age of 90 minutes, concrete stored at 35 C° may be three times stronger and nearly 2.5 times stiffer than concrete stored at room temperature. This can greatly enhance the stability of prints of longer duration. It is therefore extremely important that the temperature of the concrete is controlled during the printing process.

Along with testing the mechanical properties, printing experiments were conducted. With this part of the experimental programme the reliability of the printing process could be qualitatively explored. It is concluded that when printing on the edge of what is possible, the difference between a successful or unsuccessful print is very small. The need for predictive models and control over the printing parameters is emphasized by the outcomes of these printing experiments.

It was possible to directly relate tested material properties to failure of prints. Directly determining the mechanical properties of concrete by means of a uniaxial compression test during printing sessions has not been reported in literature. It has been demonstrated that there is a connection between the mechanical properties and the behaviour of printed object on a day to day basis and even during a day of printing. The uniaxial compression tests may therefore be suitable as a method to monitor the evolution of material properties during an actual printing process. Based on the evolution of material

properties during the printing process, process parameters may be automatically adjusted. When mechanical features of the material can be monitored during the printing process, the success rate of the printing process could be greatly improved.

The results of the experimental programme were successfully adopted in numerical simulations in ANSYS. The results of the simulations were compared to failure behaviour of cylindrical and square prints of the experimental research. The models capture the deformational behaviour of the print very well. From the numerical results it is concluded that the model underestimates the moment of buckling of prints and can therefore be considered as a conservative tool.

The experiments also showed that large deformations occurring during printing do not necessarily mean that a print will collapse. Although not collapsed, these prints should also be considered as failed objects. The numerical model can be used to not only determine the moment of collapse of a print, but also to determine the order of magnitude of deformations that are to be expected in a print. Based on deflection criteria agreed with the client or according to standards, it can be decided to alter either geometrical features and/or printing velocities to make the print conform to the intended geometry.

Based on the results of the numerical models it can be concluded that geometrical non-linear simulations based on purely elastic material properties are sufficient to analyse the behaviour of prints when one is interested in producing a stable structure. This is a different approach than trying to model failure behaviour of a print in which large deformations gradually develop. When extremely large deformations develop during a print, the accuracy of the model can be expected to reduce.

It is concluded that the numerical model can serve as a powerful tool to examine the structural behaviour of printed objects. In a first instance it can be used to define an operating window in terms of printing speed in which a particular object can be printed. Secondly, it may be used to explore the effect of altering geometrical features on the printability of objects. Thirdly, it might be used as a productional tool to optimize productivity.

7.1 Recommendations

The results of this thesis have proven that numerical models are suitable for analysing the structural behaviour of prints during the printing process. To further improve the model, it is recommended that additional research is conducted into the material behaviour at small strains. In the model it is assumed that small strains are elastic, and that when the material matures, these strains are partly recovered because of a higher Young's modulus. Based on the comparison between the numerical models and the experiments, it is expected that the material is not able to recover from these small strains as it matures and that even small strains are permanent, especially at the youngest ages where concrete is relatively soft.

The method of performing the uniaxial compression tests by extracting samples directly from printed concrete has proven to be suitable to determine the material properties. If the experiments are to be repeated in the future it is recommended to use steel moulds, which have tight geometrical tolerances, to improve the accuracy. Furthermore, the samples should be monitored by two camera's to more accurately measure the deformations. Additionally, a testing rig with a higher load capacity is advised to also measure properties of heated concrete after an age of 90 min. It is recommended to use a testing rig with a capacity of at least 10 kN to be sure the samples can be crushed. To be able to adopt a material model to accurately model plastic behaviour it is advised to adopt triaxial compression tests. With such a test all mechanical properties can be measured at once. It is however fairly difficult to conduct triaxial tests at specific ages as they take a lot more time and effort to perform. Besides that, they will not be useful for concrete with an age of over 60 min. The failure stress is already so high that it is highly unlikely that it will be reached during printing of an object. For ages under 60 min. they may be useful.

It is proposed to adopt techniques to monitor the strength and stiffness of fresh concrete during printing. However, the uniaxial compression tests performed in this thesis are very labour intensive and therefore less suitable to adopt in practice as a method of in-line measuring of the material properties. In literature, ultrasonic pulse velocity measurements on fresh concrete have however proven to be suitable to monitor the development of material properties during curing of concrete. It was shown that these measurements

can be corelated to the development of strength and stiffness of maturing concrete. It is recommended to investigate this technique to measure the development of mechanical properties during a printing process. Besides that, it can be used to qualitatively explore the effect of different process parameters or material compositions on the mechanical properties of the concrete.

The numerical model has proven to be adequate in assessing the performance of printed objects of moderate duration. It is recommended to also assess the accuracy of the model on prints of longer duration (> 60 min). At this age temperature effects start to play a major role in the development of the mechanical properties. By comparing numerical results to the printed objects, it can be explored whether material properties that were found at room temperature or material properties that were found at elevated temperatures represent the structural behaviour best.

To incorporate the high variability of the mechanical properties into the model it is recommended to adopt lower bound material properties in the numerical model. The 5^{th} percentile of a normal (or exponentially) distributed variable is commonly adopted in civil and building engineering practice to define material properties, and is referred to as the characteristic value. It is proposed to use a similar approach to define lower bound material properties for the numerical model. The 5^{th} percentile is however deemed to be too conservative for this manufacturing process. A value between the 10^{th} and 20^{th} percentile is considered a more suitable value. By adopting a lower bound approach, the reliability of the printing process can be greatly improved and limit the number of failed prints.

Furthermore, the sub-goal of this thesis was to optimize an object for 3D printing and provide optimal parameters as input for the printing process. This goal has not been achieved within the timeframe of this research. It is however still a great topic for further research, as the developed model in ANSYS might be used as a basis for an optimization strategy to find the optimal printing parameters for printing complex geometries.

Bibliography

[1] C. Llatas, “A model for quantifying construction waste in projects according to the European waste list,” *Waste Manag.*, vol. 31, no. 6, pp. 1261–1276, 2011.

[2] J. Lehne and F. Preston, “Making Concrete Change: Innovation in Low-carbon Cement and Concrete,” *Chatham House Rep.*, pp. 1–122, 2018.

[3] M. Lord, A. Jones, and K. Sharma, *Beyond Zero Emissions: Zero Carbon Industry Plan - Rethinking Cement*. 2017.

[4] C. Holt, L. Edwards, L. Keyte, F. Moghaddam, and B. Townsend, “Construction 3D Printing,” in *3D concrete printing technology*, J. G. Sanjayan, B. Nematollahi, and A. Nazari, Eds. Elsevier, 2016, pp. 349–370.

[5] T. A. M. Salet, Z. Y. Ahmed, F. P. Bos, and H. L. M. Laagland, “Design of a 3D printed concrete bridge by testing,” *Virtual Phys. Prototyp.*, vol. 13, no. 3, pp. 222–236, 2018.

[6] J. C. van Wolfswinkel *et al.*, “Design Process of a 3D-Printed Concrete Water Taxi Stop,” *High tech Concr. Where Technol. Eng. meet*, pp. 2702–2709, 2018.

[7] Musa Alawneh, Ph.D, P.E, Motasem Matarneh, B.S., M.S, and Sameh El-Ashri, B.S., M.S., “the World’S First 3D–Printed Office Building in Dubai,” *2018 PCI Conv.*, 2018.

[8] N. Gaudillière *et al.*, “Large-Scale Additive Manufacturing of Ultra-High-Performance Concrete of Integrated Formwork for Truss-Shaped Pillars,” *Robot. Fabr. Archit. Art Des. 2018*, no. May 2019, pp. 459–472, 2019.

[9] C. Borg Costanzi, Z. Y. Ahmed, H. R. Schipper, F. P. Bos, U. Knaack, and R. J. M. Wolfs, “3D Printing Concrete on temporary surfaces: The design and fabrication of a concrete shell structure,” *Autom. Constr.*, vol. 94, no. August 2017, pp. 395–404, 2018.

[10] A. S. J. Suiker, “Mechanical performance of wall structures in 3D printing processes: Theory, design tools and experiments,” *Int. J. Mech. Sci.*, vol. 137, no. January, pp. 145–170, 2018.

[11] R. J. M. Wolfs, F. P. Bos, and T. A. M. Salet, “Early age mechanical behaviour of 3D printed concrete: Numerical modelling and experimental testing,” *Cem. Concr. Res.*, vol. 106, no. January, pp. 103–116, 2018.

[12] N. Roussel, “Rheological requirements for printable concretes,” *Cem. Concr. Res.*, vol. 112, no. May, pp. 76–85, 2018.

[13] T. Lecompte and A. Perrot, “Non-linear modeling of yield stress increase due to SCC structural build-up at rest,” *Cem. Concr. Res.*, vol. 92, pp. 92–97, 2017.

[14] N. Roussel, G. Ovarlez, S. Garrault, and C. Brumaud, “The origins of thixotropy of fresh cement pastes,” *Cem. Concr. Res.*, vol. 42, no. 1, pp. 148–157, 2012.

[15] D. Marchon, S. Kawashima, H. Bessaies-Bey, S. Mantellato, and S. Ng, “Hydration and rheology control of concrete for digital fabrication: Potential admixtures and cement chemistry,” *Cem. Concr. Res.*, vol. 112, no. May, pp. 96–110, 2018.

[16] A. Perrot, D. Rangeard, and A. Pierre, “Structural built-up of cement-based materials used for 3D-printing extrusion techniques,” *Mater. Struct. Constr.*, vol. 49, no. 4, pp. 1213–1220, 2016.

[17] R. A. Buswell, W. R. Leal de Silva, S. Z. Jones, and J. Dirrenberger, “3D printing using concrete extrusion: A roadmap for research,” *Cem. Concr. Res.*, vol. 112, no. October 2017, pp. 37–49, 2018.

[18] D. Lootens, P. Jousset, L. Martinie, N. Roussel, and R. J. Flatt, “Yield stress during setting of cement pastes from penetration tests,” *Cem. Concr. Res.*, vol. 39, no. 5, pp. 401–408, 2009.

[19] A. F. Omran, S. Naji, and K. H. Khayat, “Portable vane test to assess structural buildup at rest

of self-consolidating concrete," *ACI Mater. J.*, vol. 108, no. 6, pp. 628–637, 2011.

[20] T. Di Carlo, "Experimental and Numerical Techniques To Characterize Structural Properties of Fresh Concrete Relevant To Contour Crafting," no. December, 2012.

[21] R. J. M. Wolfs, F. P. Bos, and T. A. M. Salet, "Correlation between destructive compression tests and non-destructive ultrasonic measurements on early age 3D printed concrete," *Constr. Build. Mater.*, vol. 181, pp. 447–454, 2018.

[22] J. Gołaszewski and J. Szwabowski, "Influence of superplasticizers on rheological behaviour of fresh cement mortars," *Cem. Concr. Res.*, vol. 34, no. 2, pp. 235–248, 2004.

[23] H. Huang, T. Huang, Q. Yuan, D. Zhou, D. Deng, and L. Zhang, "Temperature dependence of structural build-up and its relation with hydration kinetics of cement paste," *Constr. Build. Mater.*, vol. 201, pp. 553–562, 2019.

[24] L. J. Hermens, "Strength development of concrete used for 3D concrete printing," Eindhoven University of Technology, 2018.

[25] R. J. M. Wolfs, F. P. Bos, E. C. F. van Strien, and T. A. M. Salet, "A real-time height measurement and feedback system for 3D concrete printing," in *High Tech Concrete: Where Technology and Engineering Meet*, 2018, pp. 2474–2483.

[26] R. J. M. Wolfs, F. P. Bos, and T. A. M. Salet, "Hardened properties of 3D printed concrete : The influence of process parameters on interlayer adhesion," *Cem. Concr. Res.*, vol. 119, no. February, pp. 132–140, 2019.

[27] T. Wangler, N. Roussel, F. P. Bos, T. A. M. Salet, and R. J. Flatt, "Digital Concrete: A Review," *Cem. Concr. Res.*, vol. 123, no. May, 2019.

[28] T. T. Le *et al.*, "Hardened properties of high-performance printing concrete," *Cem. Concr. Res.*, vol. 42, no. 3, pp. 558–566, 2012.

[29] F. Bos, R. Wolfs, Z. Ahmed, and T. Salet, "Additive manufacturing of concrete in construction: potentials and challenges of 3D concrete printing," *Virtual Phys. Prototyp.*, vol. 11, no. 3, pp. 209–225, 2016.

[30] P. Wu, J. Wang, and X. Wang, "A critical review of the use of 3-D printing in the construction industry," *Autom. Constr.*, vol. 68, pp. 21–31, 2016.

[31] D. Asprone, F. Auricchio, C. Menna, and V. Mercuri, "3D printing of reinforced concrete elements: Technology and design approach," *Constr. Build. Mater.*, vol. 165, pp. 218–231, 2018.

[32] F. P. Bos, Z. Y. Ahmed, R. J. M. Wolfs, and T. A. M. Salet, "3D printing Concrete with Reinforcement," in *High tech concrete: Where technology and engineering meet*, vol. 1, D. A. Hordijk and M. Lukovic, Eds. Springer, 2017, pp. 2484–2493.

[33] S. Chaves Figueiredo *et al.*, "An approach to develop printable strain hardening cementitious composites," *Mater. Des.*, vol. 169, 2019.

[34] Y. Weng, M. Li, W. Lao, B. Lu, D. Zhang, and M. J. Tan, "Printability and fire performance of a developed 3D printable fibre reinforced cementitious composites under elevated temperatures," *Virtual Phys. Prototyp.*, vol. 0, no. 0, pp. 1–9, 2018.

[35] M. Hambach and D. Volkmer, "Properties of 3D-printed fiber-reinforced Portland cement paste," *Cem. Concr. Compos.*, vol. 79, pp. 62–70, 2017.

[36] J. Mink, "3D Concrete Printing," Delft University of Technology, 2019.

[37] ANSYS Inc., "Menetrey-Willam." [Online]. Available: ansyshelp.ansys.com.

[38] European Committee for Standardization, "Geotechnical investigation and testing - laboratory testing of soil - Part 7: Unconfined compression test (ISO 17892-7)." The Royal Netherlands Standardization Institute, Delft, 2018.

[39] K. Wille, S. El-Tawil, and A. E. Naaman, "Properties of strain hardening ultra high performance

fiber reinforced concrete (UHP-FRC) under direct tensile loading," *Cem. Concr. Compos.*, vol. 48, pp. 53–66, 2014.

[40] R. Weijermars, "Brittle failure," in *Principles of rock mechanics*, Alboran Science Publishing, 2011, pp. 79–101.

[41] A. G. Corkum, "A Model for Pore Pressure Response of a Claystone due to Liberated Residual Stress Dilation," *Rock Mech. Rock Eng.*, 2019.

[42] R. J. M. Wolfs, F. P. Bos, and T. A. M. Salet, "Triaxial compression testing on early age concrete for numerical analysis of 3D concrete printing," *Cem. Concr. Compos.*, vol. 104, no. May, p. 103344, 2019.

[43] R. J. M. Wolfs and A. S. J. Suiker, "Structural failure during extrusion-based 3D printing processes," *Int. J. Adv. Manuf. Technol.*, 2019.

[44] C. Gosselin, R. Duballet, P. Roux, N. Gaudillière, J. Dirrenberger, and P. Morel, "Large-scale 3D printing of ultra-high performance concrete - a new processing route for architects and builders," *Mater. Des. 100*, vol. 100, no. November 2017, pp. 102–109, 2016.

Appendix A: APDL script LBA

```
!LAYERS MUST BE ORDERED FROM BOTTOM TO TOP

n_layers = ARG1                             !Number of layers
time_per_layer = ARG2                       !Time in minutes

*DIM,E,,n_layers                            !Define empty array

*DO,i,1,n_layers,1
layer_age = time_per_layer*(n_layers+1-i)  !Define the age of a layer
E(i) = 0.0781+0.0012*layer_age              !Store the elastic modulus according to material law
*ENDDO

*CFOPEN,emodulus.txt                        !Write out a text file
*VWRITE, E(1)
(E20.5)
*CFCLOSE

*DO,i,1,n_layers,1                          !Assign elastic modulus to correct layer
MP,EX,i,E(i)
*ENDDO
```

Appendix B: APDL scripts GNLA

Command snippet 1

```
!This script is the first command snippet to be inserted in the Static Structural tree
!It will assign temperature values to each layer for each loadstep
!Temperature can be condidered as layer age in the analysis
!GEOMETRY MUST BE ORDERED FROM TOP TO BOTTOM IN WORKBENCH FOR THIS SCRIPT TO WORK
!Set 'Step Selection Mode' to 'First'
!Fill in the total number of layers in the field ARG1
!Fill in the time per layer (IN MINUTES) in the field ARG2
!Fill in the number of layers to be analysed per load step in the field ARG3
!TOTAL NUMBER OF LAYERS DIVIDED BY LAYERS TO BE ANALYSED PER LOAD STEP MUST BE INTEGER

/com,#########################################################
/com,####################START SCRIPT#########################
/com,#########################################################

n_layers =       ARG1                              !Total number of layers
time_per_layer = ARG2                              !Time to print a layer in MINUTES
layers_pl = ARG3                                   !Set number of layers to analyse per loadstep
n_lstp = NINT(n_layers/layers_pl+0.4999999999)     !Round of number of loadsteps to nearest integer above

!Calculate number of layers left in first loadstep
residual_layers = NINT((n_layers/layers_pl-NINT(n_layers/layers_pl-0.499999999))*layers_pl)

!Assign temperature to layers
*IF,residual_layers,EQ,0,THEN                      !Check if there are no residual layers
        *DO,i,1,n_layers,1
                esel,none                          !Deselect all elements
                nsel,none                          !Deselect all nodes
                esel,a,mat,,n_layers-i+1           !Select layer (from bottom to top)
                layer = n_layers-i+1               !Temporary store the layer number in a variable
                !Make a table with the length of number of layers
                *DIM,_loadvariable%layer%,TABLE,n_lstp+1,1,1,TIME
                *DO,j,0,n_lstp,1
                !Set the time values in starting from 0 to number of layers
                        _loadvariable%layer%(j+1,0,1) = j
                        *IF,j*layers_pl,GT,i-1,THEN
                        !Set the temperature values for the timesteps at the moment layer becomes active
                                _loadvariable%layer%(j+1,1,1) = time_per_layer*(j*layers_pl+1-i)
                        *ELSE
                        !Set the temperature to 0 before layer is active
                                _loadvariable%layer%(j+1,1,1) = 0.
                        *ENDIF
                *ENDDO
                nsle                               !Selects those nodes attached to the selected elements
                new_par = '_loadvariable%layer%'   !Temporary store parameter name of the table in variable
                !Make a string within %-signs for use in next command
                new_par2 = strcat(strcat('%',new_par),'%')
                BF,all,temp,new_par2               !Assign temperature table to the selected layer
        *ENDDO
*ELSE    !If there are residual layers do:
        *DO,i,1,n_layers,1
                esel,none                          !Deselect all elements
                nsel,none                          !Deselect all nodes
                esel,a,mat,,n_layers-i+1           !Select layer (from bottom to top)
                layer = n_layers-i+1               !Temporary store the layer number in a variable
                !Make a table with the length of number of steps. +1 for 0 step in table.
                *DIM,_loadvariable%layer%,TABLE,n_lstp+1,1,1,TIME
                *DO,j,0,n_lstp,1
                        !Set the time values starting from 0 to number of layers
                        _loadvariable%layer%(j+1,0,1) = j
                        *IF,i,GT,residual_layers,THEN
                        !Set the temperature values for the timesteps at the moment layer becomes active
                                _loadvariable%layer%(j+1,1,1) = time_per_layer*((j-1)*layers_pl+1-
i+residual_layers)
                        *ELSE
                                _loadvariable%layer%(j+1,1,1) = time_per_layer*((j-1)*layers_pl+1-
i+residual_layers)
                                _loadvariable%layer%(0,1,1) = 0
                                _loadvariable%layer%(1,1,1) = time_per_layer*(residual_layers-i+1)
                        *ENDIF
                *ENDDO
                *DO,j,0,n_lstp,1
                        *IF,_loadvariable%layer%(j+1,1,1),LT,0,THEN
                                !Set the negative values that were set before birth to 0
                                _loadvariable%layer%(j+1,1,1) = 0.
                        *ENDIF
                *ENDDO
                nsle               !Selects those nodes attached to the selected elements

                new_par = '_loadvariable%layer%'   !Temporary store parameter name of the table in variable
```

```
                !Make a string within %-signs for use in next command

                new_par2 = strcat(strcat('%',new_par),'%')
                BF,all,temp,new_par2      !Assign temperature table to the selected layer
        *ENDDO
*ENDIF

!Kill all layers above the first number of layers
!Residual number of layers is analysed first and are therefore not killed
*IF,residual_layers,EQ,0,THEN
        *DO,i,layers_pl+1,n_layers,1
                esel,none                       !Unselects full subset of elements.
                esel,a,mat,,(n_layers-i+1)      !Selects elements of a layer
                ekill,all                       !Kill layer
        *ENDDO
*ELSE
        *DO,i,residual_layers,n_layers,1
                esel,none                       !Unselects full subset of elements.
                esel,a,mat,,(n_layers-i)        !Selects elements of a layer
                ekill,all                       !Kill layer
        *ENDDO
*ENDIF
allsel                                          !Select everything to continue solve

/com,#########################################################
/com,#####################END SCRIPT##########################
/com,#########################################################
```

Command snippet 2

```
!This script is the second command snippet to be inserted in the Static Structural tree
!It will bring layers alive at each loadstep
!Set 'Step Selection Mode' to 'All'
!Script to stop solution when displacement criterium has been reached is included

/com,#########################################################
/com,####################START SCRIPT#########################
/com,#########################################################

criterium = ARG4

*GET,_stepnumber,ACTIVE,0,SET,LSTP              !Get current loadstep number
*IF,_stepnumber,GT,0,THEN
        nsel,s,u,x,criterium,criterium+5,,1     !Select nodes with displacement higher than criterium
        nsel,a,u,y,criterium,criterium+5,,1     !Select nodes with displacement higher than criterium
        *get,numnode,node,,count                !How many nodes with displacement higher than criterium
        *if,numnode,gt,0,then
                /EXIT,all
        *endif
nsel,none
        *IF,residual_layers,EQ,0,THEN
                *DO,i,0,layers_pl-1,1
                        esel,none               !Deselect everything
                        !Select the layer that needs to become active
                        esel,a,mat,,(n_layers-(_stepnumber*layers_pl+i))
                        ealive,all              !Make the selected element alive
                *ENDDO
                *ELSE
                *DO,i,0,layers_pl-1,1
                        esel,none               !Deselect everything
                        !Select the layer that needs to become active
                        esel,a,mat,,(n_layers+(layers_pl-residual_layers)-(_stepnumber*layers_pl+i))
                        ealive,all              !Make the selected element alive
                *ENDDO
        *ENDIF
*ENDIF
allsel                                          !select everything to continue solve

/com,#########################################################
/com,#####################END SCRIPT##########################
/com,#########################################################
```

Appendix C: Forms used during experiments

Labels are used to define each printed sample and are of the form: B#-T#-P#. Where the hashtags are replaced by the batch number (B), aimed age (T) and sample number (P). For example: a sample tested in batch 1 at an age of 15 min. and sample number 2 will get the label “B1-T15-P2”. As there are only two samples at each time the sample number can only have the value 1 or 2. The same counts for the batches, as there are only two batches on a single test day. The forms can be found on the next three pages.

C1. Meetdata drukproeven: batch 1

Naam :_____

Datum :_____

Tijdstip start print batch 1:_____

	W/C ratio	Lucht gehalte [%]	Druk leiding [bar]	Druk printkop [bar]	Temp. water [°C]	Temp. menger [°C]	Temp. print [°C]
batch 1							

Malnummer	Gewicht [g]	Temp. Proefstk. [°C]	Temp. hal [°C]	Luchtvocht. hal [%]	Start test [uu:mm]
B1-T0-P1					
B1-T0-P2					
B1-T15-P1					
B1-T15-P2					
B1-T30-P1					
B1-T30-P2					
B1-T60-P1					
B1-T60-P2					
B1-T90-P1					
B1-T90-P2					
B1-T120-P1					
B1-T120-P2					
B1-T180-P1					
B1-T180-P2					

Opmerkingen:

_____
_____
_____
_____
_____
_____
_____
_____
_____

C2. Meetdata drukproeven: batch 2

Naam :_____

Datum :_____

Tijdstip start print batch 2:_____

	W/C ratio	Lucht gehalte [%]	Druk leiding [bar]	Druk printkop [bar]	Temp. water [°C]	Temp. menger [°C]	Temp. print [°C]
batch 2	-	-					

Malnummer	Gewicht [g]	Temp. Proefstk. [°C]	Temp. hal [°C]	Luchtvocht. hal [%]	Start test [uu:mm]
B2-T0-P1					
B2-T0-P2					
B2-T15-P1					
B2-T15-P2					
B2-T30-P1					
B2-T30-P2					
B2-T60-P1					
B2-T60-P2					
B2-T90-P1					
B2-T90-P2					
B2-T120-P1					
B2-T120-P2					
B2-T180-P1					
B2-T180-P2					

Opmerkingen:

C3. Meetdata print

Naam :_____

Datum :_____

Printnr. :_____

Tijd [min.]	Temp. print [°C]	Temp. water [°C]	Temp. menger [°C]	Druk leiding [bar]	Druk kop [bar]
5					
10					
20					
30					
40					
50					
60					

Opmerkingen:

Appendix D: Gantt-charts

D1. Gantt-chart of testing samples at room temperature

Task Name	Start time	End time	Duration (minutes)
Printer, mallen en testopstelling klaarmaken	8:00	8:45	0:45
W/C ratio en luchtgehalte meten	8:45	8:55	0:10
Muurtje printen	8:59	9:02	0:03
Proefstukken steken	9:02	9:05	0:03
Printer print objecten en en wordt opgenomen	9:05	11:10	2:05
Test B1-T0-P1 & B1-T0-P2	9:05	9:11	0:06
Test B1-T15-P1 & B1-T15-P2	9:11	9:17	0:06
Test B1-T30-P1 & B1-T30-P2	9:26	9:32	0:06
Test B1-T60-P1 & B1-T60-P2	9:56	10:02	0:06
Test B1-T90-P1 & B1-T90-P2	10:26	10:32	0:06
Test B1-T120-P1 & B1-T120-P2	10:56	11:02	0:06
Test B1-T180-P1 & B1-T180-P2	11:56	12:02	0:06
Muurtje printen	11:11	11:14	0:03
Proefstukken steken	11:14	11:17	0:03
Printer print objecten en wordt opgenomen	11:17	13:17	2:00
Test B2-T0-P1 & B2-T0-P2	11:17	11:23	0:06
Test B2-T15-P1 & B2-T15-P2	11:23	11:29	0:06
Test B2-T30-P1 & B2-T30-P2	11:38	11:44	0:06
Test B2-T60-P1 & B2-T60-P2	12:08	12:14	0:06
Test B2-T90-P1 & B2-T90-P2	12:38	12:44	0:06
Test B2-T120-P1 & B2-T120-P2	13:08	13:14	0:06
Test B2-T180-P1 & B2-T180-P2	14:08	14:14	0:06
Schoonmaken printer en tafels leeghalen	13:17	14:47	1:30
Opruimen testopstelling	14:14	14:44	0:30

* The orange cells can be changed on per test day to have the correct testing and printing times.

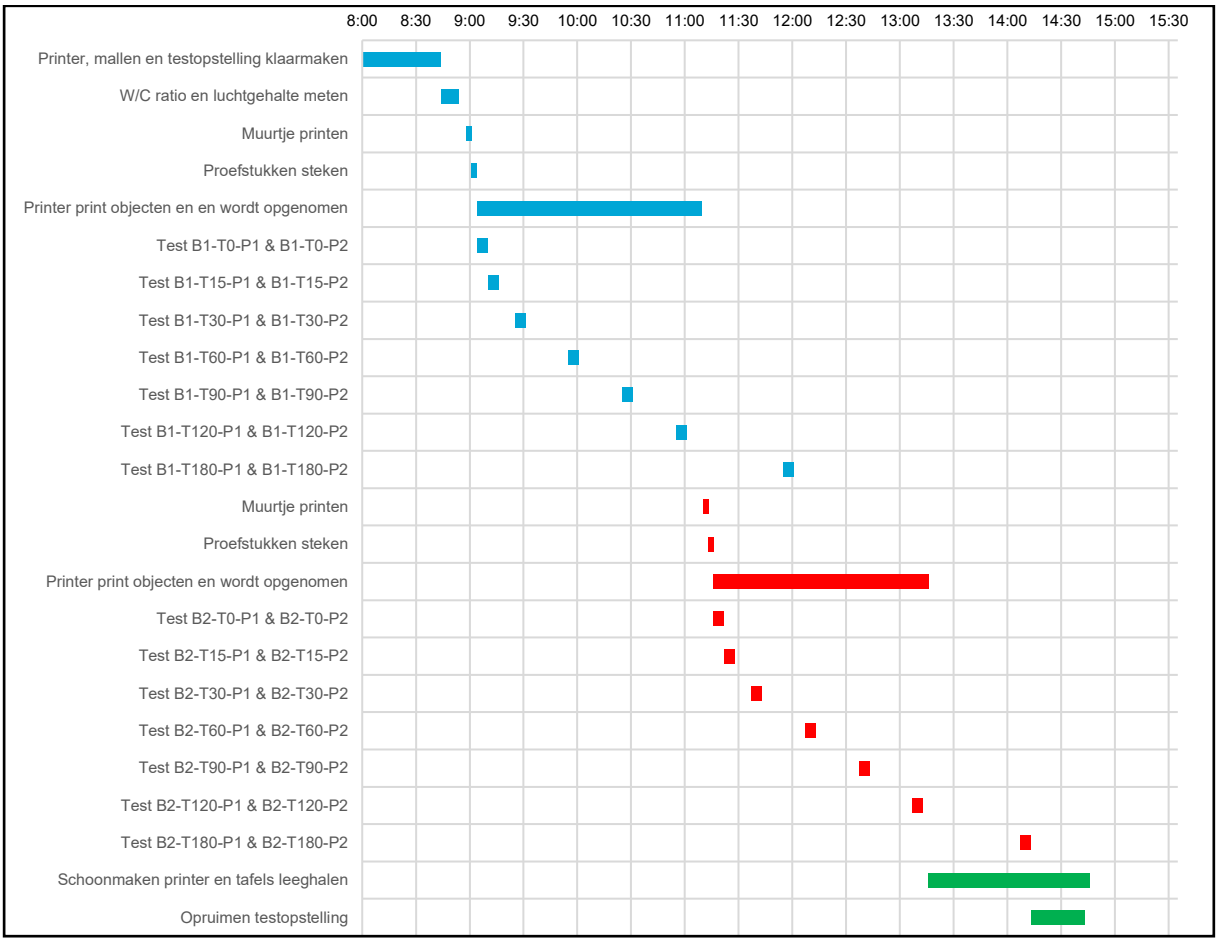

D2. Gantt-chart of testing samples at room temperature

Task Name	Start time	End time	Duration (minutes)
Printer, mallen en testopstelling klaarmaken	8:00	8:45	0:45
W/C ratio en luchtgehalte meten	8:45	8:55	0:10
Muurtje printen	8:16	8:19	0:03
Proefstukken steken	8:19	8:22	0:03
Printer print objecten en wordt opgenomen	8:22	9:47	1:25
Test B1-T15-P1 & B1-T15-P2	8:28	8:34	0:06
Test B1-T30-P1 & B1-T30-P2	8:43	8:49	0:06
Test B1-T45-P1 & B1-T45-P2	8:58	9:04	0:06
Test B1-T60-P1 & B1-T60-P2	9:13	9:19	0:06
Test B1-T75-P1 & B1-T75-P2	9:28	9:34	0:06
Test B1-T90-P1 & B1-T90-P2	9:43	9:49	0:06
Muurtje printen	10:01	10:04	0:03
Proefstukken steken	10:04	10:07	0:03
Printer print objecten en wordt opgenomen	10:07	11:37	1:30
Test B2-T15-P1 & B2-T15-P2	10:13	10:19	0:06
Test B2-T30-P1 & B2-T30-P2	10:28	10:34	0:06
Test B2-T45-P1 & B2-T45-P2	10:43	10:49	0:06
Test B2-T60-P1 & B2-T60-P2	10:58	11:04	0:06
Test B2-T75-P1 & B2-T75-P2	11:13	11:19	0:06
Test B2-T90-P1 & B2-T90-P2	11:28	11:34	0:06
Schoonmaken printer en tafels leeghalen	11:37	13:07	1:30
Opruimen testopstelling	11:34	12:04	0:30

* The orange cells can be changed on per test day to have the correct testing and printing times.